UNIVERSITY OF CALIFORNIA,
IRVINE

Methionine Metabolism and Cell Cycle Control

DISSERTATION

submitted in partial satisfaction of the requirements
for the degree of

DOCTOR OF PHILOSOPHY

in Biomedical Sciences

by

Stacey Borrego

Dissertation Committee:
Professor Peter Kaiser, Chair
Professor Aimee Edinger
Professor Suzanne B. Sandmeyer
Professor Paolo Sassone-Corsi
Professor Marian L. Waterman

2016

DEDICATION

This dissertation is dedicated to

my parents,
Vivian and Andrew Borrego

in recognition of their constant love, support, and encouragement

TABLE OF CONTENTS

LIST OF FIGURES

Page

ACKNOWLEDGEMENTS

I would like to acknowledge all of the people in my life who have contributed to making this thesis possible. I am eternally grateful to have the wonderful support system that is my family. My parents, Vivian and Andrew, and sisters, Shannon and Gail, have provided unconditional love and support throughout this journey. I can always count on their encouragement and participation, near or far, to help me bring my big ideas to fruition. I thank my husband, Michael, for his absolute love and support. He has been with me since the beginning; first as a friend, then as a collaborator, and now as a husband and father-to-be. He has always been available to celebrate good experimental results and listen to my struggles when the data was not making sense. I would like to thank you all for always being there for me morning, noon, and night.

I am particularly grateful to my advisor, Dr. Peter Kaiser, for bearing with me for all these years. I could not imagine navigating through this academic experience without his patience, guidance, mentorship, and support. He has entertained my scientific theories with thoughtful discussion, supported my efforts outside the lab, and dedicated time to answer my questions about the inner workings of the academic system. He is an exemplary scientist and understanding advisor when life brings on the unexpected. I am forever indebted to Dr. Kaiser for his mentorship that has extends well beyond the bench.

I would also like express my gratitude to my collaborators for their shared time and talents. The metabolic aspect of this thesis was performed in partnership with Dr. Oliver Fiehn and Dr. Johannes Fahrmann at the West Coast Metabolomics Center. Dr. Fahrmann performed mass spectroscopy assays, preliminary data analyses, and provided insightful discussions in

regards to metabolism and data interpretation. FLIM analyses were performed by the Laboratory of Fluorescence Dynamics in collaboration with Dr. Enrico Gratton, Dr. Chiara Stringari, and Rupsa Datta. Data analysis on both metabolism and RNA methyl cap projects was performed by Dr. Michael Zeller and Yu Liu from Dr. Pierre Baldi's group. In addition to these major collaborations, I would also like to thank all of the graduate students and senior scientist that have taken the time to help me by troubleshooting and teaching me new techniques.

Futhermore, I would like to thank the members of my dissertation committee: Dr. Aimee Edinger, Dr. Suzanne Sandmeyer, Dr. Paolo Sassone-Corsi, and Dr. Marian Waterman. I am lucky to have had such a passionate group of successful scientists to discuss my project with over the years; their critical advice and support in regards to my research and other aspects of graduate life have been invaluable. Thank you for taking the time to get to know me, contributing to my development as a critical scientist, and supporting my efforts towards research outreach beyond the lab.

While pursuing my Ph.D. at UCI, I have had the opportunity to lead two groups that are important to me and I would like to thank everyone that has participated in one way or another. Forming the UC Irvine Tumor Suppressors Relay for Life team has been an amazing experience, not only in the success of our efforts but in the dedication of my peers and friends to contribute to the cause and support the team. Likewise, the support I have received for the School of Medicine Roundtable discussion group has been overwhelming. With the combination of Dr. Kaiser's encouragement to initiate this group, Dr. Hertel's support, guest speaker participation, and my peers and friends attending every other week to learn something new and engage in scientific discussion, this group has been become so much more than I initially envisioned.

I would also like to thank my labmates and friends for being such a large part of my life these past few years. I have been lucky to be part of a lab with such warm hearted people and I am especially thankful for the friendships of Dr. Da-Wei Lin, Dr. An Tyrrell, Dr. Geetha Durairaj, Dr. Karin Flick, and Linda Hall. Furthermore, this journey through graduate school would have been completely different without my friends, Selma Alkafeef and James Yu, just down the hall to grab a cup of coffee with or share a pitcher of beer with at the pub. Although now across the country, I am grateful to have had Betsy Meyers work across the hall so that we could become the friends we are today. I am thankful to have such a great addition to my support system and look forward to our continued friendships.

Lastly, I would like to thank the journal Cancer and Metabolism for allowing reprinting of published materials. This work was funded by NSF IGERT DGE 0549479, NIH F31 GM105321-01 to Stacey Borrego, NIH GM-066164-10, and pilot project funding by the West Coast Metabolomics Center as part of NIH-DK097154.

CURRICULUM VITAE

Stacey Borrego

Education

2010 - 2016 University of California, Irvine, CA
Graduate student, doctoral program in Biological Chemistry

2004 - 2008 University of Arizona, Tucson, CA
Bachelor of Science in Molecular and Cellular Biology, Biochemistry Minor
Undergraduate Thesis Title: Characterization of Mosquito Iron Regulatory Protein 1 in the *Aedes aegypti* Mosquito.

Research Experience

2010 - Present Graduate Student
Dr. Peter Kaiser, Ph.D.
Department of Biological Chemistry
University of California, Irvine, Irvine, CA

2009 - 2010 Research Technician II
Dr. Lucio Comai, Ph.D.
Department of Molecular Microbiology and Immunology
University of Southern California, Los Angeles, CA

2006 - 2008 Undergraduate Student Research Assistant
Dr. Joy Winzerling, Ph.D.
Nutritional Sciences Department
University of Arizona, Tucson, AZ

Scientific Conferences

2016 Abcam West Coast Epigenetics Day, UC Irvine, CA

2015 Abcam Cancer and Metabolism, Cambridge, UK

2015 Metabolomics Society Conference, San Francisco, CA

2015 UCI Center for Epigenetics and Metabolism: Epigenetics and Gene Expression, Irvine, CA

2014 Abcam Crossing Boundaries: Linking Metabolism to Epigenetics, Cambridge, MA

2013 UCI – INSERM 2nd International Symposium: Epigenetic Control and Cellular Plasticity, Irvine, CA

2013 Metabolic Signaling and Disease: From Cell to Organism, Cold Spring Harbor, NY

2011 UCI – INSERM 1st International Symposium: Epigenetic Control and Cellular Plasticity, Irvine, CA

2008 Experimental Biology, San Diego, CA

Oral Presentations

2015 Borrego, S. and Kaiser, P. Metabolic changes associated with methionine stress in MDA-MB-468 breast cancer cells.
Presented at UC Irvine, Department of Biological Chemistry, Student Seminar Series

2014 Borrego, S. and Kaiser, P. Integration of S-adenosylmethionine metabolism with epigenetics and cell cycle.
Presented at Crossing Boundaries: Linking Metabolism to Epigenetics, Cambridge, MA

2014 Borrego, S. and Kaiser, P. Integration of S-adenosylmethionine metabolism with epigenetics and cell cycle.
Presented at UC Irvine, Department of Biological Chemistry, Student Seminar Series

2014 Borrego, S. and Kaiser, P. Integration of S-adenosylmethionine metabolism with epigenetics and cell cycle.
Presented at UC Irvine, Cancer Biology Research in Progress Series

Poster Presentations

2015 Borrego, S., Fahrmann, J., Stringari, C., Datta, R., Zeller, M., Baldi, P., Gratton, E., Fiehn, O., Kaiser, P. Metabolite changes associated with methionine stress sensitivity in cancer.
Presented at Abcam Cancer and Metabolism Conference 2015, Cambridge, UK

2015 Borrego, S., Fahrmann, J., Stringari, C., Datta, R., Zeller, M., Baldi, P., Gratton, E., Fiehn, O., Kaiser, P. Metabolite changes associated with methionine stress sensitivity in cancer.
Presented at Chao Family Comprehensive Cancer Center Retreat, Palm Springs, CA.

2015 Borrego, S., Fahrmann, J., Stringari, C., Datta, R., Zeller, M., Baldi, P., Gratton, E., Fiehn, O., Kaiser, P. Metabolite changes associated with methionine stress sensitivity in cancer.
Presented at 2015 Metabolomics Society Conference, San Francisco, CA

2014 Borrego, S., Fahrmann, J., Stringari, C., Gratton, E., Fiehn, O., Kaiser, P. Metabolite changes associated with methionine stress sensitivity in cancer.
Presented at West Coast Metabolomics Center Pilot Project Retreat, UC Davis, CA

2013 Borrego, S., Booher, K., Lin, DW., Kaiser, P. Integration of S-adenosylmethionine metabolism with epigenetics and cell cycle.
Presented at Metabolic Signaling and Disease: From Cell to Organism, Cold Spring Harbor, NY

2012 Borrego, S., Booher, K., Kaiser, P. Integration of metabolic pathways and cell function.
Presented at Cancer Research Institute Symposium on Basic Cancer Research, UC Irvine, CA

2012 Borrego, S., Booher, K., Kaiser, P. Integration of metabolic pathways and cell function.
Presented at The 3rd International Symposium on LifeChips, UC Irvine, CA

2011 Booher K., Lin D., Borrego S., Kaiser P. Downregulation of Cdc6 and pre-replication complexes in response to methionine stress in breast cancer cells.
Presented at Chao Family Comprehensive Cancer Center Retreat, Palm Springs, CA.

2008 Borrego, S., Mayo J., Geiser D., Winzerling J. Characterization of mosquito iron regulatory protein 1 in the *Aedes aegypti* mosquito. *FASEB J.* 2008 22:1048.2.
Presented at Experimental Biology 2008, San Diego, CA.

Publications

2016 Borrego, SL.*, Fahrmann, J.*, Datta, R., Stringari, C., Grapov, D., Zeller, M., Chen, Y., Wang, P., Baldi, P., Gratton, E., Fiehn, O., Kaiser, P. Metabolic changes associated with methionine stress sensitivity in MDA-MB-468 breast cancer cells. *Cancer Metab* 2016, 4:9.
*authors contributed equally to this work

2012 Booher, K., Lin, DW., Borrego, SL., Kaiser, P. Downregulation of cdc6 and pre-replication complexes in response to methionine stress in breast cancer cells. *Cell Cycle* 2012, 11:4414-23.

2011	Candelario J., Borrego S., Reddy S., Comai L. Accumulation of distinct prelamin A variants in human diploid fibroblasts differentially affects cell homeostasis. *Exp Cell Res* 2011 317:319-29.

Scientific Awards and Fellowships

2016	John Wasmuth Graduate Student Research Seminar Award
2014	John Wasmuth Graduate Student Research Seminar Award
2013	UC Irvine – School of Medicine Individual Fellowship Bonus
2012	NIH Ruth L. Kirschstein NRSA Predoctoral Fellowship Award
2012	NSF Graduate Research Fellowship (honorable mention)
2010	LifeChips NSF Integrative Graduate Education and Research Traineeship
2010	NIH Minority Biomedical Research Support (declined)
2008	University of Arizona Undergraduate Biology Research Program
2008	ASBMB Undergraduate Student Competitive Award (declined)
2008	FASEB MARC Undergraduate Travel Award
2007	University of Arizona Honor's College Undergraduate Research Grant

Leadership

2014 - Current	UCI School of Medicine Research Roundtable Founder and Group Leader
2014 - 2015	UCI School of Medicine Student Advisory Council – Social Committee
2014	UCI Department of Biological Chemistry Student Representative

Mentoring

2014 - 2015	Matthew Low, UCI Undergraduate Researcher
2013	UCI Mathematical, Computational, and Systems Biology Boot Camp Mentor
2010 - 2013	Jane Chang, UCI Undergraduate Researcher

Community Service

2016	Relay for Life Team Captain for Chao Family Comprehensive Cancer Center, American Cancer Society, Irvine, California
2015	Relay for Life Team Captain for Chao Family Comprehensive Cancer Center, American Cancer Society, Irvine, California

2014	Ask-A-Scientist/Engineer Night, Rancho San Joaquin Middle School, Irvine, California
2014	Relay for Life Team Captain, American Cancer Society, Irvine, California
2009 – 2011	Health Fair Staff, American Cancer Society, Orange County, California
2009 – 2010	Youth Mentor, Orange County On Track, Orange County, California
2009	Relay for Life Event Staff, American Cancer Society, Orange County, California
2007	Science Fair Mentor, University of Arizona, Tucson, Arizona

ABSTRACT OF THE DISSERTATION

Methionine Metabolism and Cell Cycle Control

By

Stacey Borrego

Doctor of Philosophy in Biomedical Sciences

University of California, Irvine, 2016

Professor Peter Kaiser, Chair

The majority of cancer cells have a unique metabolic addiction to methionine in contrast to normal cells. This "methionine-dependent" phenotype describes the inability of cancer cells to proliferate in methionine stress conditions, where methionine has been replaced with its metabolic precursor, homocysteine, in the growth media. Methionine-dependence is implicated as a signature of cancer and upon spontaneous reversion to a methionine-independent phenotype, cells lose anchorage independent growth, a hallmark of tumorigenicity. Comparing methionine-dependent and -independent cell lines is critical for a clear interpretation of our results as we investigate the molecular mechanisms behind methionine-dependence and malignancy. For this purpose, we use the methionine-dependent, triple negative, breast cancer cell line MDA-MB-468 and derived a methionine-independent variant, MDA-MB-468res-R8. With this breast cancer cell pair we are able to compare cancer and normal-like cells due to their similar genetic backgrounds, proliferation rates, and media requirements.

Previous studies on methionine-dependence identified a reduction in the synthesis of S-adenosylmethionine (SAM) during methionine stress. SAM is the principal methyl donor in the

cell and, interestingly, cancer cells have been shown to have higher methylation activity as compared to normal cells. Therefore, the studies presented in this thesis focus on the early response to methionine stress and how the resultant decrease in SAM is communicated throughout the cell. We used mass spectroscopy methods to understand the metabolic response to methionine stress in both cell lines over a 24 hour period. We observed methionine stress induced oxidative stress in both cell types resulting in a redirection of homocysteine metabolism toward synthesis of the antioxidant glutathione. Additionally, lipidomic analyses indicated a complete reprogramming of lipid synthesis in the methionine-dependent cell line that may be caused by irreversible oxidative damage and limited SAM availability for the synthesis of SAM-dependent lipids such as phospho- and sphingolipids.

To further understand how SAM levels are communicated to initiate a cellular response for protection of cell integrity, we focused on SAM as a co-factor for substrate methylation. SAM is a universal methyl donor and can serve as a co-factor for protein, lipid, chromatin, and RNA methylation events. Particularly, we focus on mRNA 5' cap methylation and it's influence on protein translation as a possible mechanism to communicate SAM levels. We employed both human cell lines and yeast strains to develop a methyl cap purification method for use in high-throughput RNA sequencing and have thus far identified unique, gene-specific responses to SAM depletion in regards to methyl cap stability. Continuing our efforts to fully understand this unique, metabolic requirement of cancer will allow us to shed light on an undefined molecular area essential for the development and use for cancer therapeutics in methionine-dependent cancers.

CHAPTER ONE

Introduction

In contrast to normal differentiated cells, cancer cells rely on aerobic glycolysis despite the presence of fully functional mitochondria (Hanahan and Weinberg, 2011a; Vander Heiden et al., 2009; Hsu and Sabatini, 2008). Although glycolysis is an inefficient provider for cellular energy, this type of metabolism provides metabolic components such as nucleotides, amino acids, and lipids for proliferating cells. These observations of cancer metabolism were first recorded in the 1920's by Dr. Otto Warburg and thus termed the Warburg effect (Warburg, 1956). In addition to this well-known cancer specific use of glycolysis, reprogramming of several established metabolic pathways are proving to be key factors in the transformation and progression of cancer cells (Locasale, 2013). One pathway that is particularly important to cancer is the methionine, or remethylation, pathway. Methionine and folate metabolic cycles form an interconnected network called the one-carbon cycle, which integrates cellular nutrients for synthesis of macromolecules, redox status maintenance, methylation of substrates, and more (Figure 1.1) (Locasale, 2013). Although the one-carbon cycle was originally thought to maintain

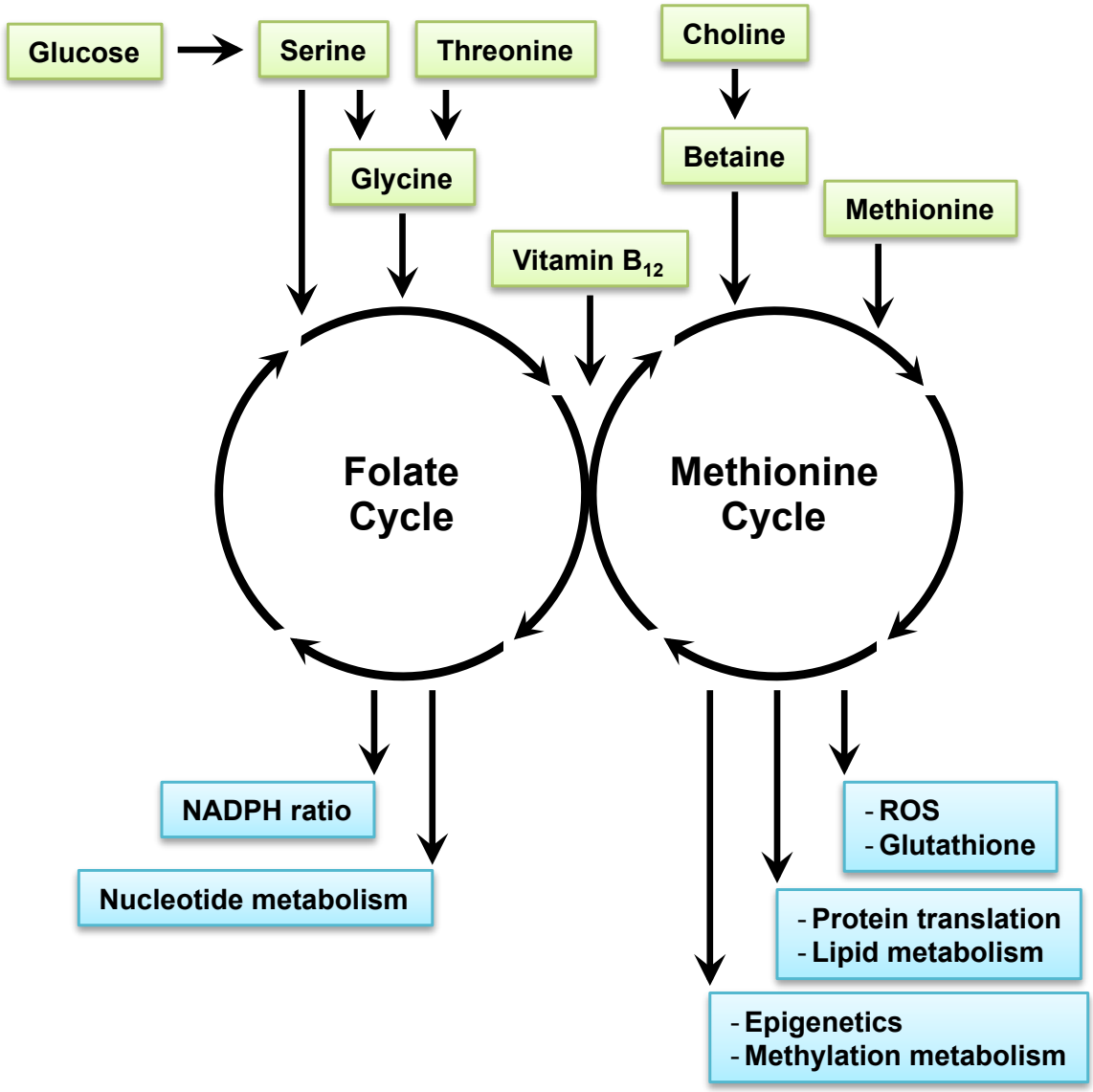

Figure 1.1 *The one-carbon cycle and cellular nutrient sensing*
Nutrient sources are imported or synthesized by the cell before entering the one carbon cycle (shown in *green*). The one-carbon cycle is defined as the network comprised of the folate and methionine cycles. These pathways provide critical metabolic factors for nucleotide metabolism, protein and lipid synthesis, glutathione production, and methylation events (shown in *blue*).

upkeep of basic cellular functions, a more critical connection to fundamental processes such as pluripotency, epigenetic remodeling, and cancer malignancy is becoming more clear (Booher et al., 2012; Locasale, 2013; Shyh-Chang et al., 2013).

In the context of cancer, the importance of methionine metabolism in cancer cell proliferation has been known and studied for over fifty years. Initial studies connecting metabolism and tumor malignancy investigated the effects of removing essential amino acids from the diets of healthy and tumor burdened rats. A notable decrease in tumor size was observed in methionine deprived mice as compared to controls and little health consequences were present in methionine deprived healthy rats (Sugimura et al., 1959). Later research applied an *in vitro* approach to these studies by substituting methionine for its metabolic precursor, homocysteine, in the growth media of cancer cell lines from different origins (Halpern et al., 1974; Mecham et al., 1983). While the majority of cancer cells were unable to survive under such growth conditions, normal cell proliferation was unaffected. This unique metabolic requirement for methionine became known as the "methionine dependency of cancer" and remains the only general metabolic defect common among most malignant cells (Stern et al., 1984).

With the potential to selectively target malignant cells and leave normal cells unharmed, exploiting methionine restriction in cancer therapies is an ongoing effort. Early clinical trials tested methionine restriction and possible toxicity as a result of nutrient deprivation; although patients consistently exhibited weight loss, the modified diet was generally well tolerated (Epner et al., 2002). Methionine is in all dietary proteins but is generally highest in fish, beef, dairy, eggs, nuts, and grains and therefore a long term methionine restrictive diet is, for the most part, of a vegan nature. Short term studies can easily control and restrict methionine rich foods from

patients' diets, and thus the majority of clinical studies have yet to investigate the long term benefit of methionine restriction in cancer treatment. Methionine restriction alone is challenging as a long term therapy due to patient non-compliance; however, combining a slightly modified diet with chemotherapeutics presents a more feasible and flexible avenue for treatment. Combining methionine restriction with some chemotherapeutics, such as the tumor growth inhibitor cystemustine, did not improve patient outcome (Thivat et al., 2009). However, despite limited patient sampling, methionine restriction alongside the combination chemotherapy FOLFOX (5-fluorouracil, leucovorin, and oxaliplatin) demonstrated partial patient responses and thus an encouraging result for further study of methionine restriction in cancer therapeutics (Durando et al., 2010). While patient studies continue to identify the right chemotherapy combination, the mechanistic reasoning for methionine dependency is still largely unknown.

Understanding the source of methionine dependency has been complicated and debated. Early studies focused on the methionine cycle and regeneration of methionine for clues into the cancer specific methionine-dependent phenotype. Homocysteine metabolism is of particular interest as it can be remethylated to regenerate methionine by either methionine synthase (MS) or betaine homocysteine methyltransferase (BHMT), converted to its metabolic precursor S-adenoyslhomocystiene (SAH), or enter the transsulfuration pathway toward cysteine metabolism and glutathione synthesis (Figure 1.2) (Grzelakowska-sztabert and Balinska, 1980; Kamely et al., 1973; Turner et al., 2000). Suggestions of defective methionine biosynthesis programs as the focal point for methionine dependence were countered with several studies proving otherwise. In normal methionine media (Met+), cancer cells synthesized more methionine than normal cells, indicating no MS defect in cancer (Hoffman and Erbe, 1976). Additionally, methionine stress does not increase methionine abundance in either methionine-dependent or

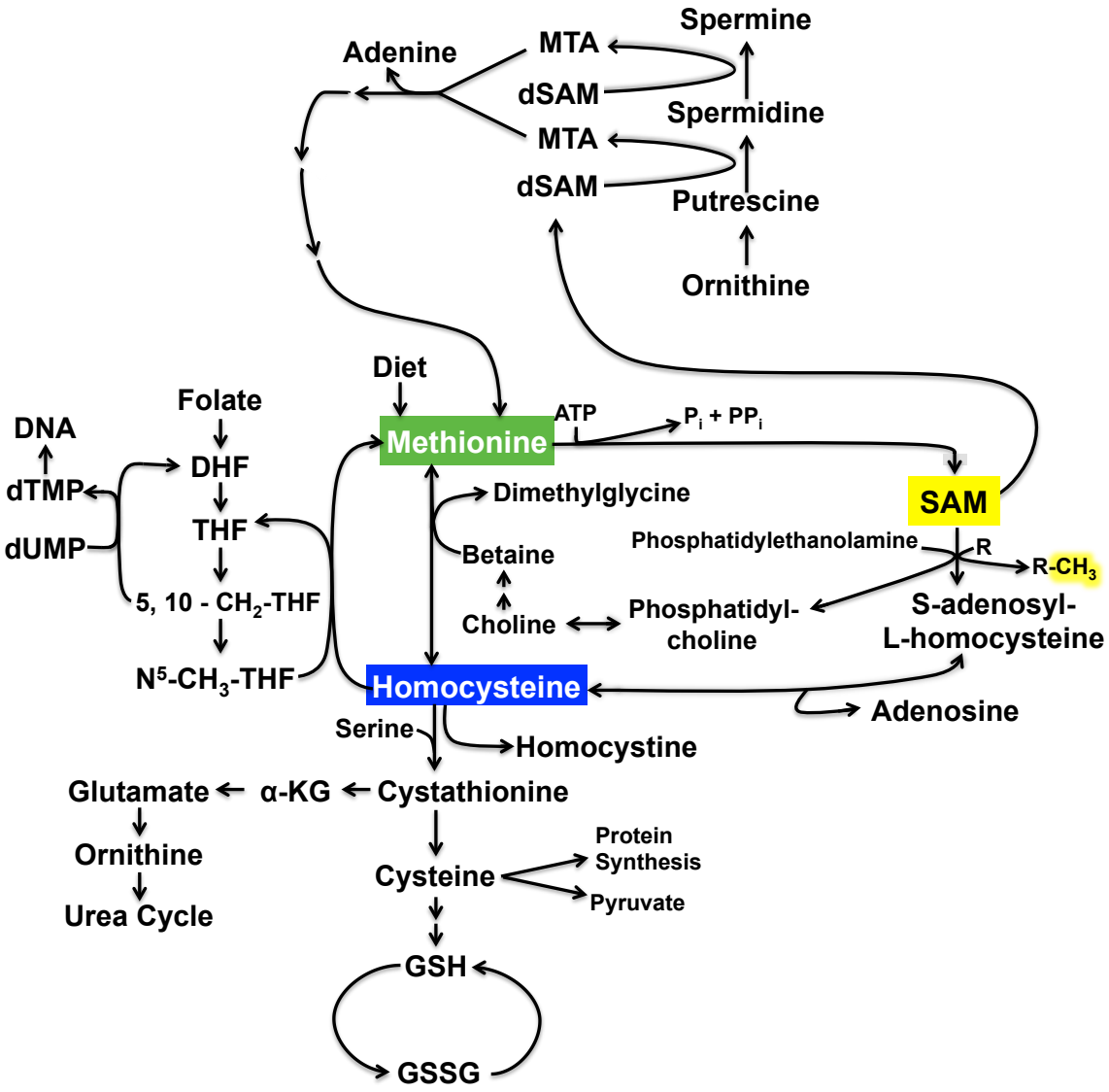

Figure 1.2 *The mammalian one-carbon cycle*
Homocysteine can be processed in four different ways: remethylated to regenerate methionine by either methionine synthase (MS) or betaine homocysteine methyltransferase (BHMT), converted to its metabolic prescursor S-adenoyslhomocystiene (SAH), or enter the transsulfuration pathway toward cysteine metabolism and glutathione synthesis. Regeneration of methionine from homocysteine is essential for the production of S-adenosylmethionine (SAM), the principal methyl donor in the cell. SAM is involved in the majority of methylation reactions in the cells including those on chromatin, RNA, proteins, and lipids.

-independent cells, indicating that upregulation of methionine synthesis is not a requirement for methionine independence (Hoffman and Erbe, 1976; Hoffman et al., 1979). Despite normal methionine synthesis, methionine utilization for SAM production was reduced (Coalson et al., 1982). Free methionine, however, is lower in methionine-dependent cell cultures grown in homocysteine media (Met-Hcy+) as compared to normal cells (Stern et al., 1983). With a higher demand for exogenous methionine and reduced SAM synthesis in cancer cells, it may be possible that metabolic pathways feeding into the one-carbon cycle, such as the methionine salvage pathway, may be contributing to the prevention of methionine use in SAM production but exogenous methionine can be used for cellular functions such as protein synthesis.

Alternatively, the consequence of reduced SAM production may be the key factor in methionine dependence and not methionine itself. SAM is a universal methyl donor in the cell and the ratio of SAM to SAH, the byproduct of any methylation reaction, indicates the methylation potential of the cell. Not only is reduced SAM problematic for methylation of substrates but the accumulation of SAH inhibits methyltransferases and the SAM/SAH ratio is considered an indicator for intracellular methylation potential (Tehlivets et al., 2013). In normal Met+ media, both methionine-dependent and -independent cells demonstrate normal SAM/SAH ratios. However, when cultured in Met-Hcy+ media, SAM is reduced and SAH increases resulting in a reduced SAM/SAH ratio in the methionine-dependent cell line (Coalson et al., 1982). Since malignant cells have been shown to have a higher demand for methylation of substrates and thus the methylation co-factor SAM, it is easy to see why a reduced SAM and SAM/SAH ratio can selectively impact cancer cells.

Methionine dependence is likely linked to SAM for it's essential role as the principal methyl donor in the cell; however, it is unlikely that simply adjusting the SAM/SAH ratio would

result in cell death without stimulating some type of survival response. Monitoring nutrient availability is vital for cell survival and metabolic check-points such as the "restriction point" and mTORC1 signaling (mammalian target of rapamycin complex 1) are well-know gatekeepers of proliferation during nutrient limitation. The "restriction point" prevents normal cells from entering S-phase in suboptimal nutrient conditions. Malignant cells, however, lose this survival sensory mechanism and their growth during nutrient deprivation results in cell death (Pardee, 1974). Similarly, low glucose and low amino acid levels inactivate the mTORC1 nutrient sensory pathway and protein synthesis is downregulated. In yeast, studies have identified a SAM monitoring program mediated by the ubiquitin ligase SCF^{Met30}. When SAM levels are reduced, SCF^{Met30} no longer binds to the transcription factor Met4 resulting in increased levels of the cell cycle inhibitor Met32 (Ouni et al., 2010; Yen et al., 2012). As the yeast cells undergo a cell cycle arrest their metabolic and transcription landscape is modified by Met4-induced upregulation of sulfur metabolism genes. As a cell cycle regulator in response to cellular SAM concentrations this phenomenon has been thus termed the SAM-checkpoint (Figure 1.3) (Kaiser et al., 2006a).

The molecular mechanism connecting cellular SAM abundance and cell cycle progression have not been as well defined in mammals as it has in yeast. In both human breast cancer and mouse leukemic cell lines, methionine stress induced by Met-Hcy+ media or reduction of SAM results in the G_1 cell cycle arrest known as the SAM-checkpoint (Booher et al., 2012; Lin et al., 2013). In breast cancer cells this arrest is in part due to pre-replication complex instability as a result of downregulation of the cell division cycle 6 (Cdc6) protein (Booher et al., 2012). In both breast and leukemic cell lines, reduced activation of cyclin-dependent kinase 2 (Cdk2) contributes to this robust cell cycle arrest. Furthermore, mTORC1 activity is not significantly affected during SAM limitation, indicating that the SAM-checkpoint

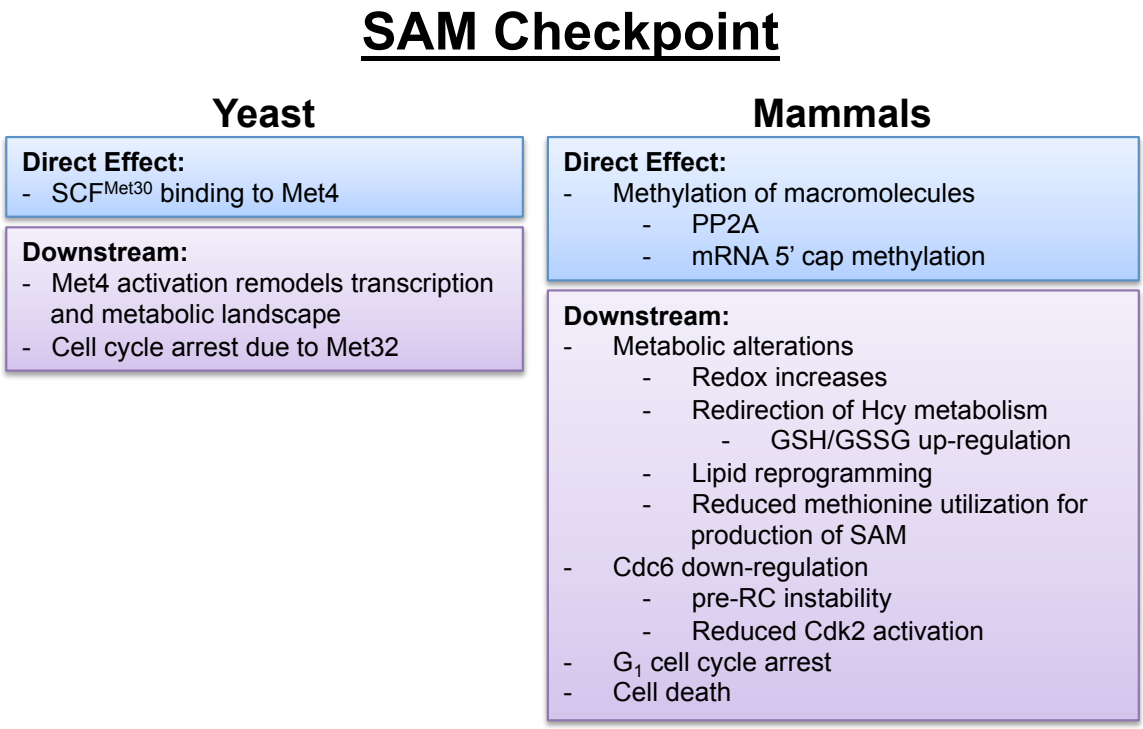

Figure 1.3 *The SAM-checkpoint in yeast and mammals*
The molecular mechanism of SAM-checkpoint induction is well defined in yeast. Low SAM levels prevent SCF^{Met30} binding to the transcription factor Met4 resulting in up-regulation of transcription of sulfur metabolism genes and a Met32 induced cell cycle arrest. In mammals, low SAM levels affect substrate methylation on macromolecules include protein phosphatase 2A (PP2A) and mRNAs. Downstream effects include global metabolic alterations, Cdc6 protein down-regulation, G_1 cell cycle arrest, and eventually cell death in cancer cells.

is specific for sensing SAM levels, which can be communicated to other cellular processes to initiate arrest in suboptimal SAM conditions.

The work presented in this thesis addresses the early response of methionine stress in methionine-dependent and –independent breast cancer cells in order to understand how SAM levels are communicated to other cellular processes. To do this, we approached the question of what metabolic changes occur during methionine stress in methionine-dependent cells as compared to methionine-independent cells using mass spectroscopy analyses over the course of 24 hours. We observed that methionine stress induced oxidative stress in both cell types resulting in a redirection of homocysteine metabolism toward synthesis of the antioxidant glutathione. The timing to address the Met-Hcy+ induced oxidative stress by glutathione upregulation is severely delayed in methionine-dependent cells. Lipidomic analyses indicate a complete reprogramming of lipid synthesis in the methionine-dependent cell line that may be caused by unrecoverable oxidative stress damage and limited SAM availability for the synthesis of phospholipids. Additionally, we asked how SAM abundances can be communicated by substrate methylation, particularly in respect to mRNA 5' cap methylation and regulation of potential key sensory genes such as Cdc6 (Figure 1.3). We employed both human cell lines and mutant yeast strains to develop a methyl cap purification method for use in high-throughput RNA sequencing. We have thus far identified unique, gene-specific responses to SAM depletion in regards to methyl cap stability in yeast. With these techniques and our results thus far, defining the molecular mechanism behind the SAM-checkpoint and its importance to methionine dependency in cancer is within grasp. Understanding this cancer specific phenotype will be invaluable for the development of cancer therapeutics and key to combination therapies already responsive to dietary methionine restrictive approaches.

CHAPTER TWO

A methionine dependent and independent breast cancer cell pair

INTRODUCTION

Methionine metabolism is an essential metabolic pathway in mammals. Cellular methionine can be generated through the methionine salvage pathway from 5'-methylthioadenosine or by remethylation of homocysteine (Figure 1.2). Early studies of methionine metabolism identified a strict metabolic requirement for the methionine in transformed, cancer cell lines, a phenotype later known as "the methionine dependency of cancer". Cancer cells cannot grow or survive in growth media where methionine has been replaced with its metabolic precursor, homocysteine (Chello and Bertino, 1973; Halpern et al., 1974; Hoffman and Erbe, 1976). In contrast, normal non-transformed cell proliferation is mostly unaffected by the metabolite replacement (Mecham et al., 1983). Biosynthesis of methionine in both cancer and normal cells is not affected when cells are cultured in homocysteine media; however, S-adenosylmethionine (SAM) synthesis is downregulated and the proliferation defects associated with methionine dependency can be rescued by SAM supplementation (Booher et al., 2012; Hoffman and Erbe, 1976).

Reversion of transformed cells to methionine independence is a rare event, it occurs approximately once in every 10,000 cells. Hoffman and colleagues determined that transformed cells that reverted to methionine independence are able to grow in homocysteine media and exhibit normal-like properties such as increased anchorage dependence, altered morphologies, and decreased serum usage (Hoffman et al., 1979). Interestingly, reversion produces a heterogeneous group of untransformed cells, each with varying degrees of normal-like properties. Since methionine dependence results in decreased SAM in homocysteine media, transformation and reversion may be a result of SAM sensitivity and maintenance of epigenetic markers essential for transformation (Kokkinakis et al., 2004).

Our studies investigate the cellular response to methionine stress induced by homocysteine media in the triple negative breast cancer cell line MDA-MB-468 (shortened to MB468). As a control, we have derived rare clones from MB468 cells (referred to as MB468res) that are methionine independent and have lost their tumorigenic ability for anchorage independent growth. The MB468 and MB468res cell line pair is an ideal model to identify unique metabolic signatures linking methionine dependence and tumorigenicity.

RESULTS

Methionine independent clones derived from the breast cancer cell line MB468

Previous studies by Hoffman and colleagues demonstrated that transformed and carcinoma cells exposed to homocysteine media (Met-Hcy+) for a prolonged period of time resulted in methionine independent revertants (Hoffman et al., 1979). While not all cells lines are capable of reversion, the triple negative breast cancer cell line MB468 is among the few cell lines that can. We generated our own methionine independent cell lines by culturing MB468

cells in Met-Hcy+ media for a minimum of two weeks (Figure 2.1A). The vast majority of transformed cells did not survive the prolonged methionine stress conditions; however, a few small colonies began to form and continued to grow in Met-Hcy+ media. Three methionine stress resistant cell lines, MB468res-R8, -R21, and –R28, were generated using this method and compared to the parental MB48 cell line.

The ability to grow in semisolid medium is characteristic of transformed and carcinogenic cells. To compare the transformed phenotype of the methionine stress resistant cell lines to the parent MB468 cell line, anchorage independence assays were performed by culturing cells in soft agar with methionine media (Met+) (Figure 2.1B). As expected for a tumorigenic cell line, MB468 cells grew numerous colonies in a great range of sizes. The three methionine stress resistant cell lines formed fewer and smaller colonies as compared to MB468 cells indicating a loss of the transformed phenotype. Consistent with previous reports of the heterogeneity of revertant cell properties, each of the resistant lines formed colonies in a unique manner (Hoffman et al., 1979). MB468res-R8 cells overall formed fewer and smaller colonies than MB468, MB468res-R21 had no colony formation, and MB468res-R28 formed far more colonies than MB468 cells but small enough to be scarcely visible to the naked eye. The varied growth of each resistant cell line indicates that reversion is a spontaneous event and likely one induced by epigenetic alterations.

Methionine dependent cells cannot grow during methionine stress

Using the same background cell line to compare transformed and non-transformed properties provides a tremendous benefit to any cancer based study. Previous research has compared transformed, metastatic cells to normal cell lines such as fibroblasts. Interpretation of

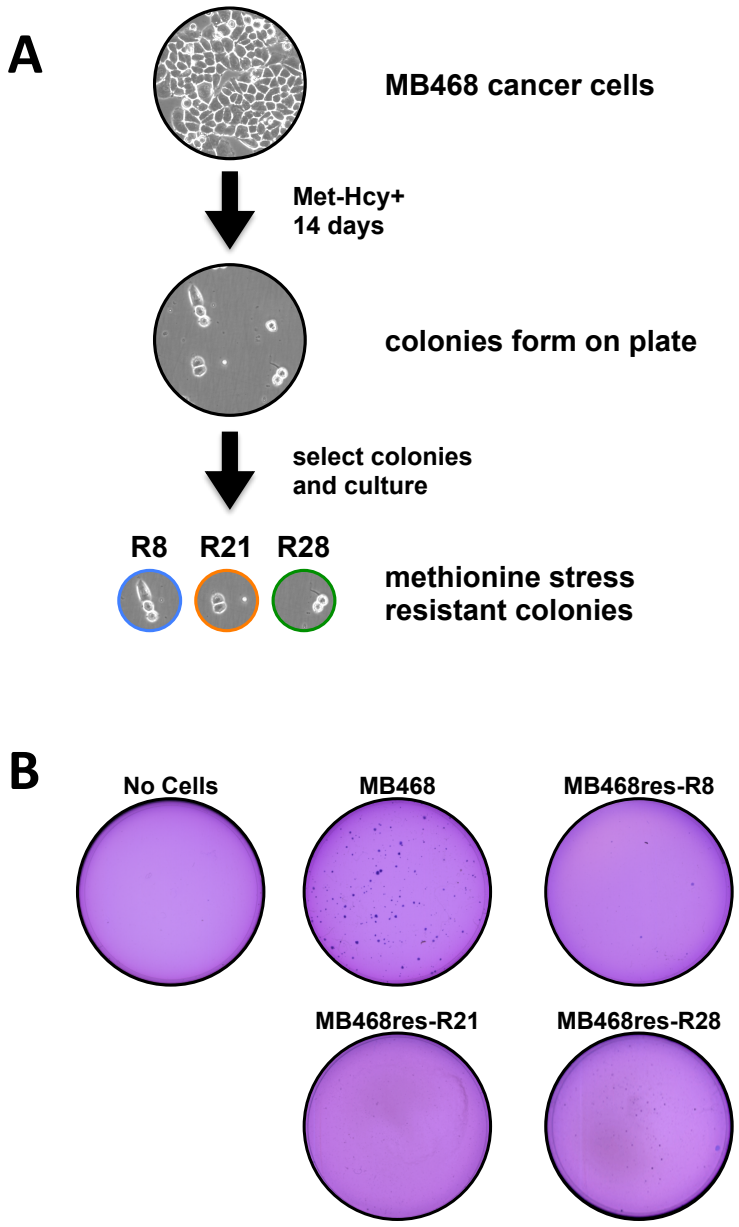

Figure 2.1 *Methionine stress resistant cells derived from MB468 breast cancer cells*
A) An example schematic of the method used to generate methionine stress resistant clones. B) Methionine stress resistant clones MB468res-R8, -R21, and -28 form fewer and smaller clones in soft agar as compared to the parental MB468 cell line. Control plate does not contain cells.

results in such studies can become problematic as they need to consider different proliferation rates, media requirements, and innate genetic differences between the two cell lines. By deriving methionine stress resistant clones, these issues can be avoided and comparisons more easily interpreted. Therefore, we employ our methionine resistant clones as a control in our studies to better understand methionine stress.

In addition to the loss of anchorage independent growth, the methionine stress resistant cell line MB468res-R8 have a similar proliferation rate as MB468 cells in Met+ media and continue to grow in Met-Hcy+ media (Booher et al., 2012; Borrego et al., 2016). The proliferation defect in cancer cells during methionine stress has been associated with a cell cycle arrest in G_1, called the SAM-checkpoint, as a result of cell division cycle 6 (Cdc6) protein downregulation (Booher et al., 2012). Cdc6 is an essential component for cell cycle progression as it forms the pre-replication complex (pre-RC) on DNA for initiation of DNA replication and activates cyclin-dependent kinase 2 (Cdk2). During methionine stress in MB468 as compared to MB468res-R8 cells, downregulation of Cdc6 results in pre-RC instability and reduced activation of Cdk2, which is consistent with the cell's inability to progress from G_1 to S-phase. This cell cycle arrest is common among cancer cells cultured in Met-Hcy+ media, indicating a possible cancer specific cell cycle checkpoint during metabolite deprivation.

Methionine stress induces a cell line specific metabolic response

Identifying the cause for the G_1 cell cycle arrest during methionine stress provides insight into the molecular mechanisms activated specifically in cancer. However, how this message is initially transmitted from a metabolic signal to other molecular machinery is still unknown. Using the MB468 and MB468res-R8 cell pair, we investigate the metabolic response to

methionine stress over the course of 24 hours. Global metabolite analyses and stable-isotope tracing studies indicate a cancer specific response to methionine stress that is further discussed in Chapter 3. Furthermore, Chapter 4 discusses the immediate changes in lipids associated with methionine stress in the form of oxidative damage and lipid biosynthesis reprogramming.

DISCUSSION

Using a methionine-dependent and -independent cell pair is essential to understanding the role of methionine metabolism in cancer. While our studies focus on the different responses to methionine stress in these two cells types, the emergence of methionine stress resistant cell lines is as equally interesting. How does reversion directly connect with methionine stress and what makes the cells that revert insensitive to it? We hypothesize that two situations are likely, one starting with a homogenous cancer cell population and another that is heterogeneous with cells continuously reverting between normal and transformed phenotypes (Figure 2.2). In the scenario that a homogenous cancer cell population exposed to prolonged methionine stress results in methionine-independent clones, an epigenetic program depending on SAM levels is likely the cause. Shyh-Chang and colleagues have shown a SAM dependent effect on histone methylation in mice, indicating SAM as a possible modulator of cell fate (Shyh-Chang et al., 2013). Interestingly, we observe reversion back to a transformed phenotype in methionine resistant cell lines after prolonged culturing in Met+ media. For this reason, resistant cell lines must be frequently "cleaned" by culturing the cells in Met-Hcy+ media and removing the transformed population. This observation suggests a dynamic conversion between transformed and untransformed cells and prolonged exposure to homocysteine media may only remove the transformed cell population leaving the already present normal-like cells to thrive in methionine

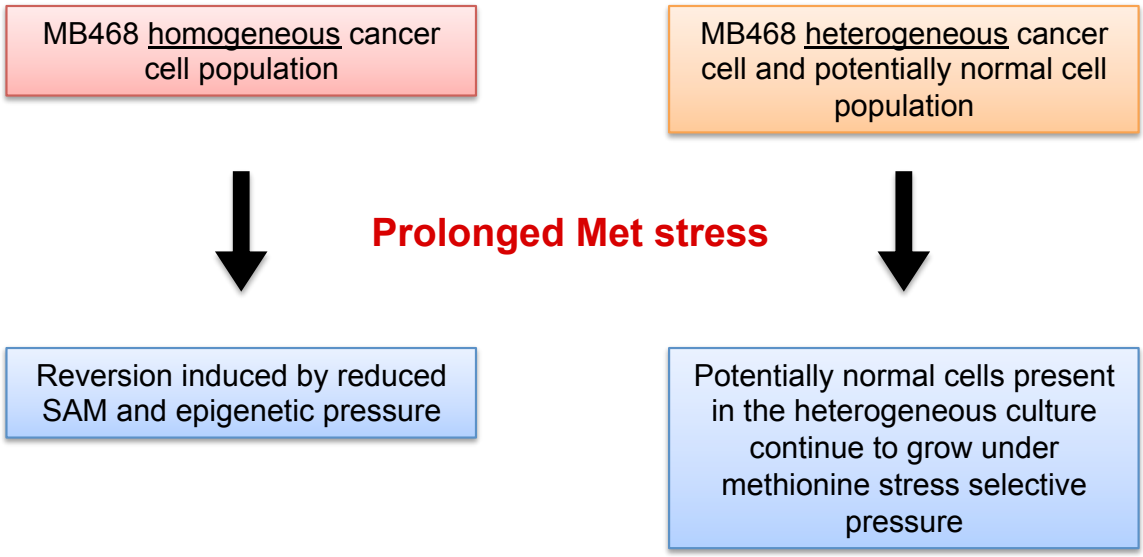

Figure 2.2 *Methionine stress induced reversion to an untransformed phenotype*
Two potential scenarios are suggested for reversion of transformed, cancer cells to an untransformed phenotype. In the first scenario, the MB468 culture is a homogeneous cancer cell population. Prolonged methionine stress decreases SAM levels and results in an epigenetic pressure that modifies chromatin methylation to better suite a low SAM environment. In the second scenario, the MB468 culture is a heterogeneous mixture of cancer and untransformed cells. Loss of transformation occurs spontaneously in Met+ media and prolonged methionine stress removes the transformed population leaving the revertant cells to thrive.

stress conditions. The ability of cancer cells to convert back and forth to an untransformed phenotype is likely a result of dynamic epigenetic modifications.

Although exact epigenetic modifications on DNA and histones have not been identified in the context of methionine stress, understanding the (epi)genetic changes between cancer cells and their revertant clones will provide invaluable insight to the vulnerabilities of cancer. Mainly, why are cancer cells sensitive to methionine stress? If normal cells can cope with methionine stress is it possible that essential cell survival factors necessary for growth in homocysteine medium are defective in cancer? In early studies, Hoffman and colleagues demonstrated that methionine synthesis from homocysteine is unaffected in both cancer and normal cells during methionine stress (Hoffman and Erbe, 1976). This result is consistent with the stable-isotope labeling study performed in MB468 and MB468res-R8 cells and also indicates reduced SAM levels despite methionine availability and upregulated methionine adenosyltransferase expression (Borrego et al., 2016). Additionally, SAM reduction is a common consequence of culturing in homocysteine media and supplementation of SAM during methionine stress rescues the proliferation defect observed in cancer cells (Booher et al., 2012; Obeid and Herrmann, 2009). Evidence suggests that SAM availability is the key factor of methionine dependence and the ability of normal cells to survive in low SAM conditions indicates an extremely high dependence on SAM in cancer (Barak et al., 1993). It is possible that the demand for SAM is higher in cancer cells than normal cells for use in lipid synthesis, duplication of epigenetic marks during replication, and protein and RNA methylation. To understand the differences in demand for SAM it is imperative to employ a methionine-dependent and –independent cell pair to tease apart the most essential molecular responses during methionine stress. Identifying key metabolic

vulnerabilities in cancer will provide one more tool that can be applied in cancer therapeutics either on its own or in combination with currently available therapies.

CHAPTER THREE

Metabolic changes associated with methionine stress sensitivity in MDA-MB-468 breast cancer cells

INTRODUCTION

Reprogrammed metabolism in cancer has gained greater attention in recent years, beyond the well known Warburg effect (Hanahan and Weinberg, 2011b). While mechanistic insights into the metabolic changes in cancer are limited, the importance of methionine metabolism in cancer cell proliferation has been known for over fifty years (Figure 3.1A) (Sugimura et al., 1959). Early studies describe a unique metabolic requirement of cancer for methionine known as the "methionine dependence phenotype". The vast majority of malignant cells experience methionine dependence and cannot proliferate in growth media in which methionine is replaced by its metabolic precursor, homocysteine. In contrast, most normal non-tumorigenic cells are unaffected by culturing in homocysteine media (Figure 3.1B) (Halpern et al., 1974).

Methionine is an essential amino acid necessary for normal growth and cell function. It contributes to protein synthesis and is the precursor to S-adenosylmethionine (SAM), the

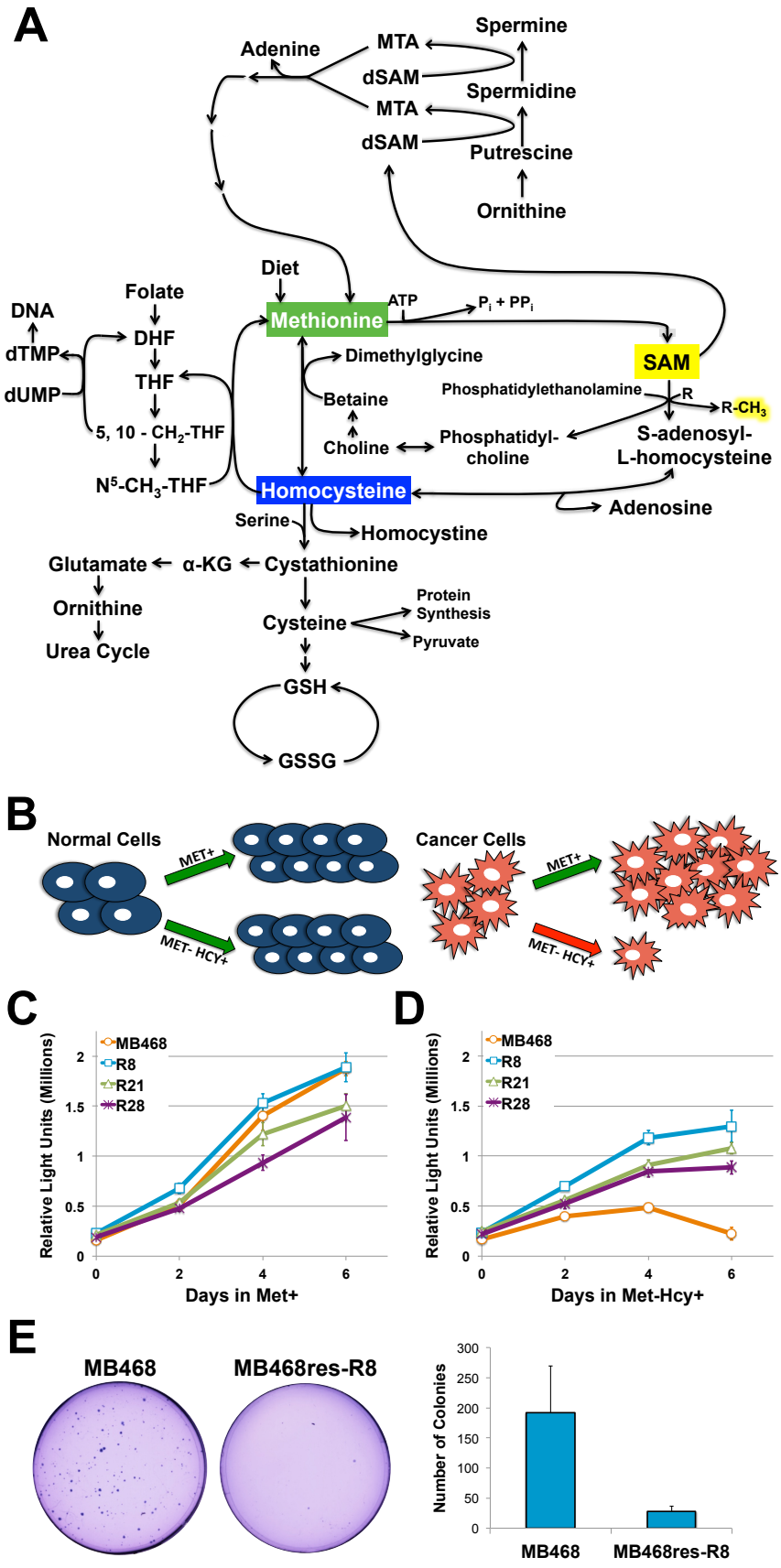
A
Adenine
MTA
dSAM
MTA
dSAM
Spermine
Spermidine
Putrescine
Ornithine
Diet
Folate
DNA
dTMP
dUMP
DHF
THF
5, 10 - CH2-THF
N5-CH3-THF
Methionine
ATP
Pi + PPi
Dimethylglycine
Betaine
Choline
Phosphatidyl-
choline
Phosphatidylethanolamine
SAM
R
R-CH3
S-adenosyl-
L-homocysteine
Adenosine
Homocysteine
Serine
Homocystine
Glutamate
α-KG
Cystathionine
Ornithine
Urea Cycle
Cysteine
Protein
Synthesis
Pyruvate
GSH
GSSG
B
Normal Cells
MET+
MET- HCY+
Cancer Cells
MET+
MET- HCY+
C
MB468
R8
R21
R28
Relative Light Units (Millions)
Days in Met+
D
MB468
R8
R21
R28
Relative Light Units (Millions)
Days in Met-Hcy+
E
MB468
MB468res-R8
Number of Colonies
MB468
MB468res-R8

Figure 3.1 *Methionine dependency of cancer cells*
(A) Methionine metabolism in mammals: the one-carbon cycle is essential to regenerate methionine and S-adenosylmethionine (SAM). SAM is the major methyl donor in the cell and is involved in reactions for phospholipid synthesis, chromatin, RNA, and protein methylation, and one-carbon donor pool homeostasis. (B) Illustration depicting the methionine dependency of cancer. Most cancer cells (*red*) do not grow in homocysteine growth medium (Met-Hcy+), whereas normal cells (*blue*) are unaffected. Green arrows indicate positive proliferation rates, red arrows indicate reduced or no proliferation. (C) MB468 and MB468res cells proliferate in methionine growth media (Met+) at similar rates, (D) but only the resistant cells (MB468res: R8, R21, R28) maintain proliferation in Met-Hcy+ media. Proliferation rates were quantified by luminescent cell viability assay. Error bars represent standard deviation. (E) Methionine-stress resistant clone MB468res-R8 forms fewer colonies in soft agar than the parental MB468 cell line. Cells were plated in 0.3% agar, cultured for 30 days, and stained with crystal violet. Colony values are the average of three independent experiments. Error bars indicate standard deviation.

principal methyl donor in the cell. SAM is a versatile molecule required for methylation of DNA, RNA, proteins, and lipids by a variety of methyltransferases. In addition SAM is critical for the formation of 1-methylnicotinamide, a primary factor involved in stem cell pluripotency (Sperber et al., 2015), polyamine biosynthesis (Hu et al., 2004), and the methionine salvage pathway (Tang et al., 2000). As SAM donates its activated methyl group in methylation reactions, it is converted to S-adenosylhomocysteine, which is further hydrolyzed to homocysteine in a reversible reaction (Figure 3.1A) (de la Haba and Cantoni, 1958). Homocysteine is a junction metabolite and its metabolism can be either directed towards the remethylation pathway to regenerate methionine by receiving a methyl group from betaine or N_5-methyltetrahydrofolic acid, or toward cysteine and glutathione synthesis in the transsulfuration pathway (Finkelstein and Mudd, 1967). Homocysteine inhabits a critical position where, depending on demand, metabolic flux can be redirected to increase methylation potential or produce antioxidants.

Although initial studies suggested methionine limitation to be responsible for the "methionine dependence phenotype", limited availability of SAM is the actual culprit. Work by Coalson and colleagues has shown that methionine dependent cells endogenously synthesize methionine at normal levels in homocysteine media (Met-Hcy+), but show reduced SAM synthesis (Coalson et al., 1982). Accordingly, by supplementing homocysteine growth medium with SAM, cell proliferation of methionine-dependent breast cancer cells can be restored, suggesting SAM limitation as the cause for methionine dependence (Booher et al., 2012). Furthermore, SAM limitation induced by knock-down of methionine adenosyltransferase (MAT), the enzyme responsible for synthesis of SAM from methionine and ATP, mimics the cell cycle arrest induced by replacing methionine with homocysteine in the growth media (Booher et al., 2012; Lin et al., 2013). The specific cell cycle arrest in the G_1 phase induced by

homocysteine medium or MAT knock-down is reminiscent of an evolutionary conserved metabolite responsive cell cycle checkpoint first described in yeast. This "SAM-checkpoint" was proposed to protect cellular integrity and maintain epigenetic stability as it halts cell cycle progression before intracellular SAM concentrations get too low to support the various methylation reactions necessary for normal cell physiology. Cancer cells have a highly responsive SAM-checkpoint, likely because of their higher demand on SAM (Booher et al., 2012). Details of why cancer cells depend on high levels of SAM remain to be discovered, but their increased proliferation rate requires constant duplication of chromatin methylation marks, methylation of RNAs, and SAM-dependent synthesis of membrane lipids. In addition, many cancer cells are characterized by hyperactive polyamine synthesis (Giardiello et al., 1998), which consumes SAM. A decarboxylated form of SAM reacts with the polyamine putrescine to form spermidine and spermine, generating the byproduct 5'-deoxy-5'-methylthioadenosine (MTA). Further processing of MTA generates adenine and replenishes the methionine pool (Pegg et al., 1982). Although polyamine synthesis clearly contributes to SAM usage in cancer cells and modified polyamines, specifically diacetylspermine, have been shown as clear biomarkers in lung (Wikoff et al., 2015) and colon cancer (Johnson et al., 2015), SAM limitation or growth in homocysteine media do not imitate effects of polyamine depletion and cannot be rescued by spermidine supplementation (Lin et al., 2013; Seidenfeld et al., 1986).

While some progress has been made by linking methionine-dependency of cancer to SAM limitation and induction of a specific cell cycle arrest, our understanding of this striking metabolic dependence of cancer remains minimal. Here we characterized the dynamics of metabolic changes in breast cancer cells when they are shifted to homocysteine-based growth

media, using untargeted metabolomics as well as stable isotope-labeled tracer studies to follow the metabolic fate of homocysteine.

RESULTS AND DISCUSSION

A methionine dependent and independent breast cancer cell line pair

The majority of malignant cells exhibit the methionine-dependent phenotype as indicated by cell cycle arrest and apoptosis when cultured in media where methionine (methionine media, Met+) is replaced with the immediate metabolic precursor homocysteine (homocysteine medium, Met-HCY+) (Cavuoto and Fenech, 2012; Halpern et al., 1974; Kreis and Goodenow, 1978). Although methionine dependence is specific for cancer cells and non-tumorigenic cells proliferate well in homocysteine medium, long term culturing of malignant cell lines in Met-Hcy+ can select methionine-independent, methionine stress resistant clones (Booher et al., 2012; Hoffman et al., 1978). The data presented in this study focuses on the triple negative breast cancer cell line MDA-MB-468 (shortened to MB468) due to our ability to derive multiple methionine-stress resistant clones (MB468res) as controls (Booher et al., 2012). These methionine-stress resistant cells propagate at similar rates as the parental MB468 cell line when cultured in methionine growth medium, however, MB468res cells continue to proliferate in Met-Hcy+ medium unlike MB468 cells (Figure 3.1C and 3.1D). Spontaneous reversion to methionine independence has been associated with loss of transformation-specific properties such as anchorage independence (Cassingena et al., 1990). We therefore tested whether phenotypes associated with tumorigenicity are also lost in MB468res cells. When cultured in soft agar with Met+ growth media, MB468 cells efficiently formed colonies consistent with their tumorigenic phenotype. In contrast, MB468res-R8 cells formed only few or very small colonies (Figure

3.1E), indicating a loss of the transformation phenotype. Similar results were obtained with the MB468res-R21 and R28 lines. However, whereas R8 and R21 did not form colonies, the R28 line formed numerous tiny colonies scarcely visible with the naked eye. We continued our studies with the MB468res-R8 cell line as their proliferation rate in Met+ medium is closest to the parental MB468 cell line, which eliminates potential effects on metabolite demand due to growth rate differences. MB468res-R8 cells provide an excellent control for our investigation of methionine dependence because cell morphology, proliferation rate, growth medium requirements, and genetic background resemble those of methionine stress sensitive MB468 cells. The molecular mechanism of reversion to methionine independence is unknown. Reversion is an extremely rare event and stable for several generations. However, after several generations MB468res-R8 cultures can revert back to methionine dependence, suggesting epigenetic mechanisms behind this phenomenon.

Homocysteine media induces a metabolic down-regulation of oxidative phosphorylation

To monitor metabolic states in MB468 cells and their methionine-independent derivatives, MB468res-R8, we employed fluorescence lifetime imaging microscopy (FLIM). Using two-photon excitation at 740 nm we measured the intrinsically fluorescent molecule reduced nicotinamide adenine dinucleotide (NADH) in live cells (Figure 3.2A). NADH is a powerful biomarker for the metabolic state of the cell as it is the principal electron donor in glycolysis and electron acceptor in oxidative phosphorylation (Heikal, 2010). Phasor analysis of NADH FLIM data gives spatial distribution of free to protein-bound NADH (Figure 3.2B) (Bird et al., 2005; Stringari et al., 2011, 2012a). Importantly, FLIM analysis is different from the intensity ratio at two different emission wavelengths, which is commonly used to correlate with

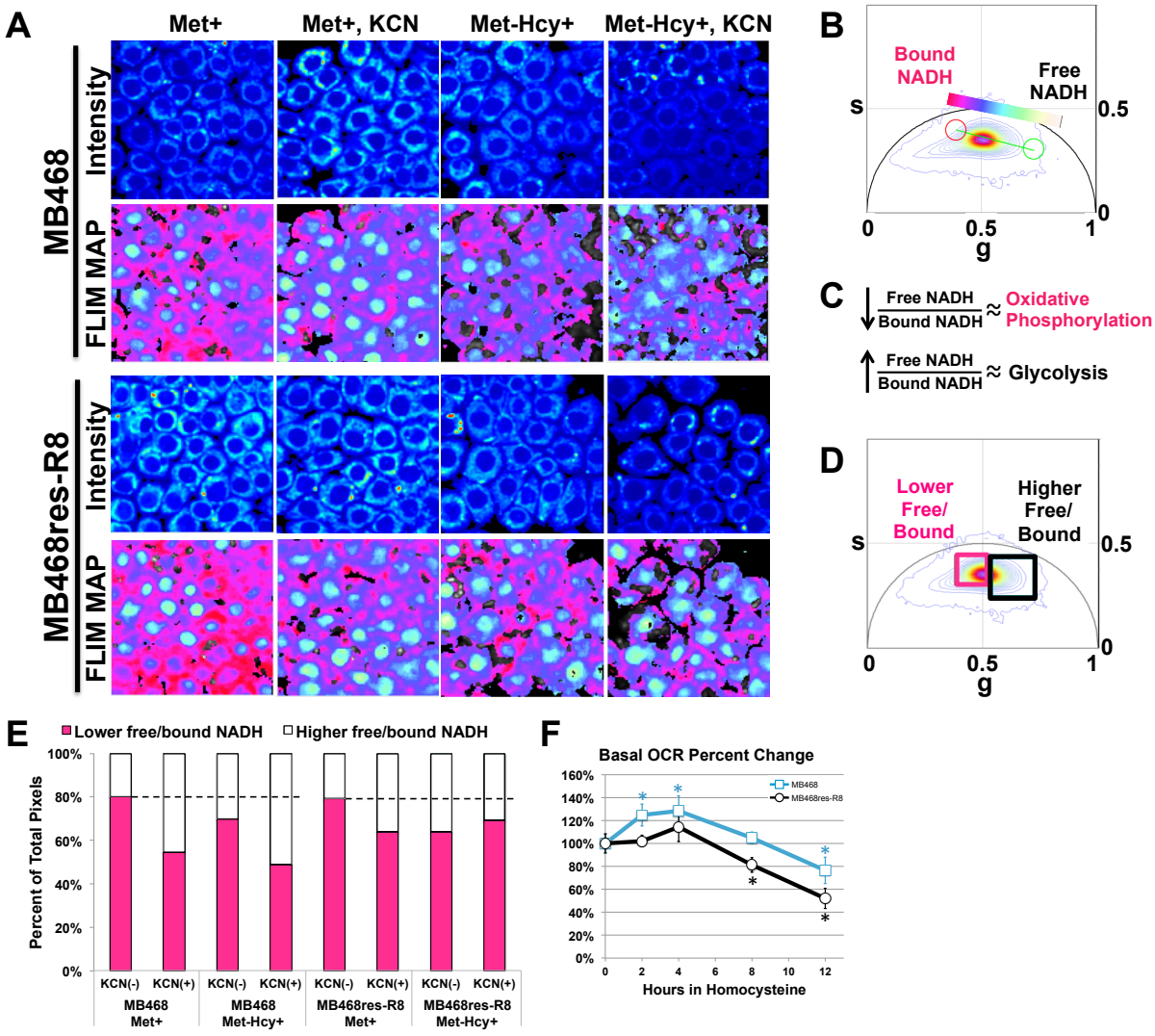
A
Met+
Met+, KCN
Met-Hcy+
Met-Hcy+, KCN
MB468
Intensity
FLIM MAP
MB468res-R8
Intensity
FLIM MAP
B
Bound NADH
Free NADH
s
0.5
0
0
0.5
1
g
C
Free NADH / Bound NADH ≈ Oxidative Phosphorylation
Free NADH / Bound NADH ≈ Glycolysis
D
Lower Free/ Bound
Higher Free/ Bound
s
0.5
0
0
0.5
1
g
E
Lower free/bound NADH
Higher free/bound NADH
Percent of Total Pixels
100%
80%
60%
40%
20%
0%
KCN(-) KCN(+) KCN(-) KCN(+) KCN(-) KCN(+) KCN(-) KCN(+)
MB468 Met+
MB468 Met-Hcy+
MB468res-R8 Met+
MB468res-R8 Met-Hcy+
F
Basal OCR Percent Change
MB468
MB468res-R8
160%
140%
120%
100%
80%
60%
40%
20%
0%
0 2 4 6 8 10 12
Hours in Homocysteine

Figure 3.2 *Homocysteine media induces a metabolic shift from oxidative phosphorylation to glycolysis*
(A) MB468 and MB468res-R8 cells cultured in Met+ or Met-Hcy+ growth media for 48 hours with or without 4 mM KCN were imaged using two-photon microscopy at 740 nm. NADH free/bound fluorescence lifetime imaging microscopy (FLIM) maps of cells are shown using the color spectrum in the FLIM phasor histogram (B). (C) The phasor histogram represents relative fractions of free NADH (*cyan-white*) and protein-bound NADH (*red-purple*). (D) Cluster analysis using the phasor histogram to separate signals of high free/bound (*black square*) and low free/bound (*pink square*) NADH ratios. (E) Quantitation of NADH ratios from cells in (A) are shown. Two fields for each sample with a minimum of 15 cells per field were analyzed by cluster analysis and normalized to total pixels measured. The black dotted line indicates the average percentage of lower free/bound NADH ratios of MB468 (80%) and MB468res-R8 (79%) cells cultured in in Met+, KCN(-). (F) MB468 and MB468res-R8 cells cultured in Met+ media for 12 hours or Met-Hcy+ media for 2, 4, 8, and 12 hours were analyzed by Seahorse Bioscience XF analyzer. MB468 (*blue line with squares*) and MB468res-R8 (*black line with circles*) basal oxygen consumption rates (OCR) are shown normalized to the Met+ treated sample. Error bars represent normalized standard deviation, n = 4 replicates, statistical differences between Met+ media and Met-Hcy+ media are indicated by (*) where $p \leq 5.0 \times 10^{-7}$.

metabolism. In the FLIM analysis only NADH in the bound and free form is measured by proper selection of excitation and emission wavelengths. More importantly, the FLIM technique is based on fluorescence lifetime, which is independent of the total concentration of NADH, contrary to the common dual wavelength emission ratio. In our analysis we determine directly the free to bound (to proteins) ratio. Protein-bound NADH is characterized by longer fluorescence lifetimes, influenced by binding to various enzymes. In contrast, shorter fluorescence lifetimes of NADH indicate a higher fraction of NADH that is not bound to proteins (Lakowicz et al., 1992). By measuring the NADH phasor distribution along the metabolic trajectory on the phasor plot, we can calculate the free/bound NADH ratio (Stringari et al., 2012b). A series of previous experiments have shown that low free/bound NADH ratios are characteristic for cells actively engaged in oxidative phosphorylation, whereas higher free/bound ratios indicate increased dependence on glycolysis for energy production (Figure 3.2C) (Pate et al., 2014; Stringari et al., 2011, 2012a).

We compared fluorescence lifetimes of NADH from both MB468 and MB468res-R8 cells cultured in Met+ and Met-Hcy+ media. We used phasor cluster analysis to quantify the signals of higher and lower free/bound NADH ratios of both cell lines (Figure 3.2D). In Met+ media, both cell lines had similar profiles with approximately 80% of the signal representing a lower free/bound ratio providing a baseline for oxidative phosphorylation activity in these cell types (Figure 3.2E). 48 hours after cells were transferred to Met-Hcy+ media, 70% of the MB468 and 67% of the MB468res-R8 signal represented the lower free/bound NADH ratio and thus a reduction in cellular respiration. Importantly, the addition of potassium cyanide, a potent inhibitor of mitochondrial respiration, resulted in a decrease in the signal of the lower free/bound ratio, similar to culturing in Met-Hcy+ media alone (Figure 3.2A and 3.2E). The similar

metabolic trajectories of potassium cyanide treated cells and Met-Hcy+ cultures suggest that methionine stress may affect mitochondria function or force cells to reduce oxidative phosphorylation.

We further analyzed mitochondrial function using an extracellular flux (XF) analyzer, which measures oxygen consumption rates (OCR) as an indicator for mitochondrial respiration. Both MB468 and MB468res-R8 cells were cultured in either Met+ media for 12 hours or Met-Hcy+ media for 2, 4, 8, and 12 hours prior to measuring basal levels of OCR (Figure 3.2F). Within 4 hours in Met-Hcy+ media, both MB468 and MB468res-R8 cell lines respond by transiently increasing OCR. However, after 8 hours both cell lines showed decreased respiration, which continued to decline. Interestingly, we observed the MB468res-R8 cells to have a faster decline in respiration as compared to MB468 cells. In additional analyses with the XF analyzer, spare respiration capacity was measured in MB468 and MB468res-R8 cells cultured in Met+ media and treated with the electron transport chain accelerator carbonyl cyanide-4-phenylhydrazone (FCCP). MB468 cells can maximize OCR 1.9 times that of basal levels when stressed with FCCP, whereas MB468res-R8 cells have a maximum 1.5 fold increase of OCR under the same conditions. We hypothesize that the faster decline in mitochondrial respiration in Met-Hcy+ media (Figure 3.2F) and the reduced effect of KCN in the FLIM analysis (Figure 3.2E) as compared to MB468 cells may be due to an innate lower capacity for respiration. With a smaller reserved respiration capacity, MB468res-R8 cells may feel the effects of a dysfunctional mitochondria sooner but may not be as reliant on oxidative phosphorylation resulting in improved tolerance of metabolic stress as compared to MB468 cells. Regardless of these differences the general response of both cell lines to Met-Hcy+ media and KCN is comparable,

indicating reduced mitochondrial respiration during culture in Met-Hcy+ media as determined by both FLIM and XF analyses.

Metabolite changes associated with culturing in homocysteine media

FLIM and XF analyses indicated that cells change their metabolism in response to homocysteine medium. These results prompted us to investigate the immediate metabolic response to homocysteine media. Both MB468 and MB468re-R8 were cultured in Met+ media or transitioned to Met-Hcy+ media for 2, 4, 8, 12, and 24 hours and metabolites were analyzed by an untargeted metabolomics approach using gas chromatography/time of flight mass spectrometry (Figure 3.3A). Immediate changes in select metabolites are observed for both cell lines, albeit with distinct trends. Interpretation of differential changes of metabolite concentrations between the two cell lines at the later time points is complicated by the fact that MB468 cells respond with cell cycle arrest whereas MB468re-R8 continue to proliferate. It is thus difficult to distinguish between changes due to homocysteine growth media and changes caused by the block in proliferation. However, metabolite concentration changes at the early time points cannot be indirect consequences of cell cycle arrest as the time frame for cell cycle arrest is substantially longer (Booher et al., 2012). Interestingly, the general trends of metabolite concentration changes between the cell lines seem to project into different directions. In MB468 cells, several metabolites responded within 4 hours with a general decrease in abundance as compared to Met+ cultured cells. In contrast the majority of metabolites in MB468res-R8 cells that responded within 4 hours increased in their abundance. Pathway analysis using the web server Metabolite Biological Role showed that within 4 hours of culturing in Met-Hcy+ media,

fewer pathways are affected in MB468 cells as compared to MB468res-R8 (Figure 3.3B and 3.3C) (Baldi and Long, 2001; Chagoyen and Pazos, 2011; Kayala and Baldi, 2012).

Metabolites connected to methionine

We next looked at individual metabolic pathways in more detail. Changes in metabolite levels associated with methionine stress are evident in both MB468 and MB468res-R8 cell lines as early as two hours after switching to Met-Hcy+ media. Several metabolite concentration changes occurred in both the methionine dependent (MB468) and independent (MB468res-R8) cell lines and reflect a general response to homocysteine becoming the primary source of sulfur amino acid. Metabolite responses with distinct patterns in the two cell lines were particularly evident for metabolites connected to the methionine salvage pathway and purine/pyrimidine synthesis (Figure 3.4). We found a striking response in levels of 5'-deoxy-5'-methylthioadenosine (MTA) and adenine, the two SAM-derived metabolites in the methionine salvage pathway. Both MTA and adenine decreased rapidly in MB468 cells but not in MB468res-R8 (Figure 3.4A). MTA is the byproduct of polyamine synthesis and adenine is released as MTA is recycled into methionine (Figure 3.4B). MTA and adenine concentrations decreased to about one-fifth of the starting concentration within 2 hours after MB468 cells were shifted to Met-Hcy+ medium, and recovered somewhat to about 60% of starting levels after 24 hours. Surprisingly, even though the rapid and dramatic reduction in MTA and adenine levels suggest repression of polyamine synthesis, the levels of putrescine and spermidine remained largely unchanged over the time course (Figure 3.4B). It is possible that the amount of polyamines synthesized over the 24 hour period we monitored does not significantly contribute to the total polyamine pool in cells. However, the decrease in MTA production clearly reflects a

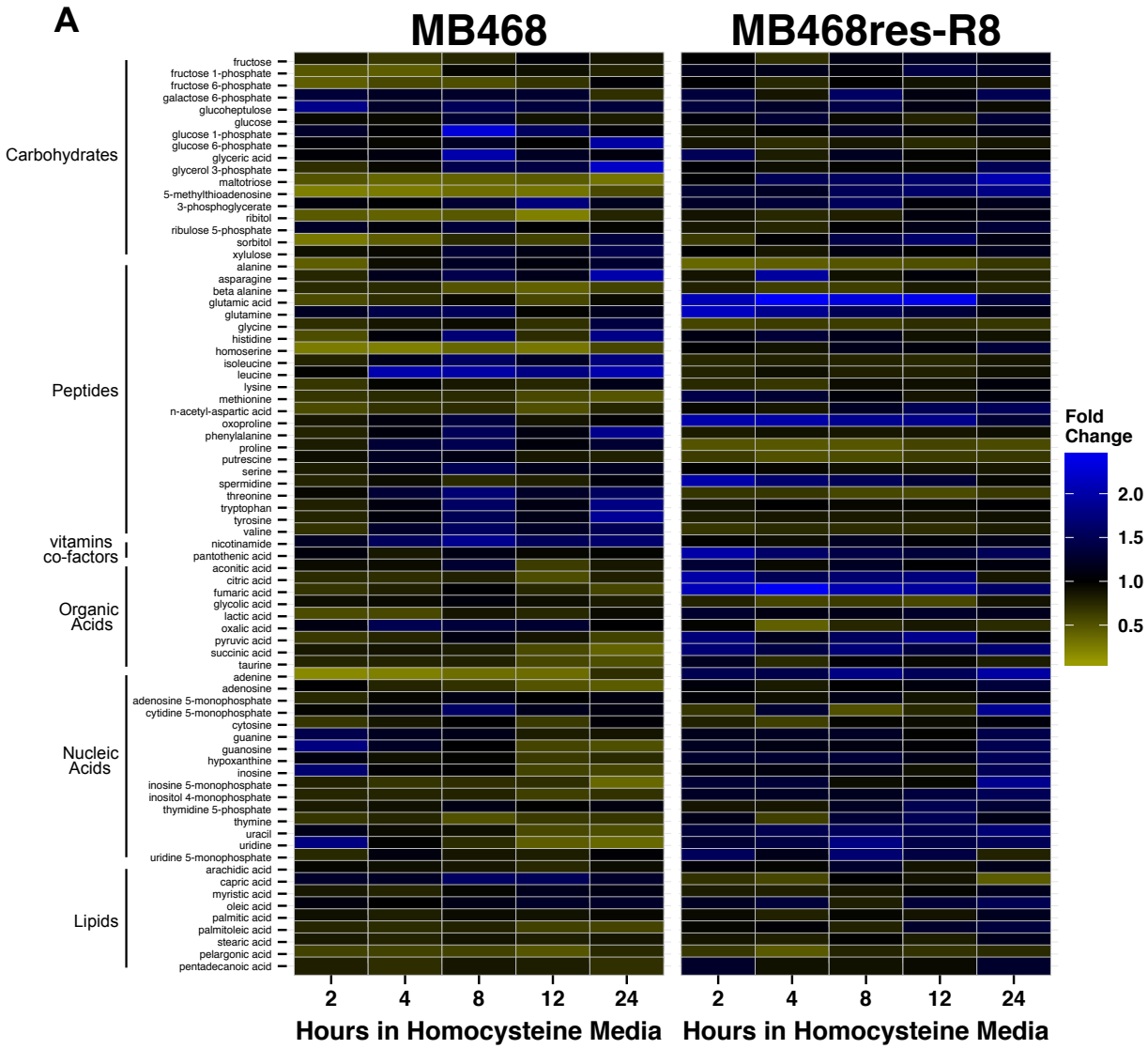

B

MB468

D-glutamine and D-glutamate metabolism
Purine metabolism
Nitrogen metabolism
Glutathione metabolism
Cysteine and methionine metabolism

C

MB468res-R8

D-glutamine and D-glutamate metabolism
Nitrogen metabolism
Glutathione metabolism
Cysteine and methionine metabolism
Oxidative phosphorylation
Pantothenate and CoA biosynthesis
Aminoacyl-tRNA biosynthesis
Glycerolipid metabolism
Biosynthesis of unsaturated fatty acids

Figure 3.3 *Homocysteine media induces a metabolic response in MB468 and MB468res-R8 cells*

MB468 and MB468res-R8 cells were cultured in Met+ or Met-Hcy+ media over the course of 24 hours and analyzed by untargeted UHPLC and GCMS based methodologies (see methods). (A) Heatmaps representing metabolites measured in both MB468 and MB468res-R8 cells. Metabolites are color filled based on fold change to the Met+, time-zero sample. *Yellow* indicates a decrease in metabolite abundance and *blue* indicates an increase as compared to time-zero control. (B and C) Pathways enriched within 4 hours of culturing in Met-Hcy+ media. Metabolites with significantly different abundance at 2 and 4 hours as compared to time zero were determined using the Bayesian t-test, Cyber-T (Baldi and Long, 2001; Kayala and Baldi, 2012), with a Benjamini-Hochberg $p \leq 0.05$. Enriched pathways were determined using the web server Metabolite Biological Role (MBRole) with a raw p-value cutoff at $p \leq 0.1$ (Chagoyen and Pazos, 2011).

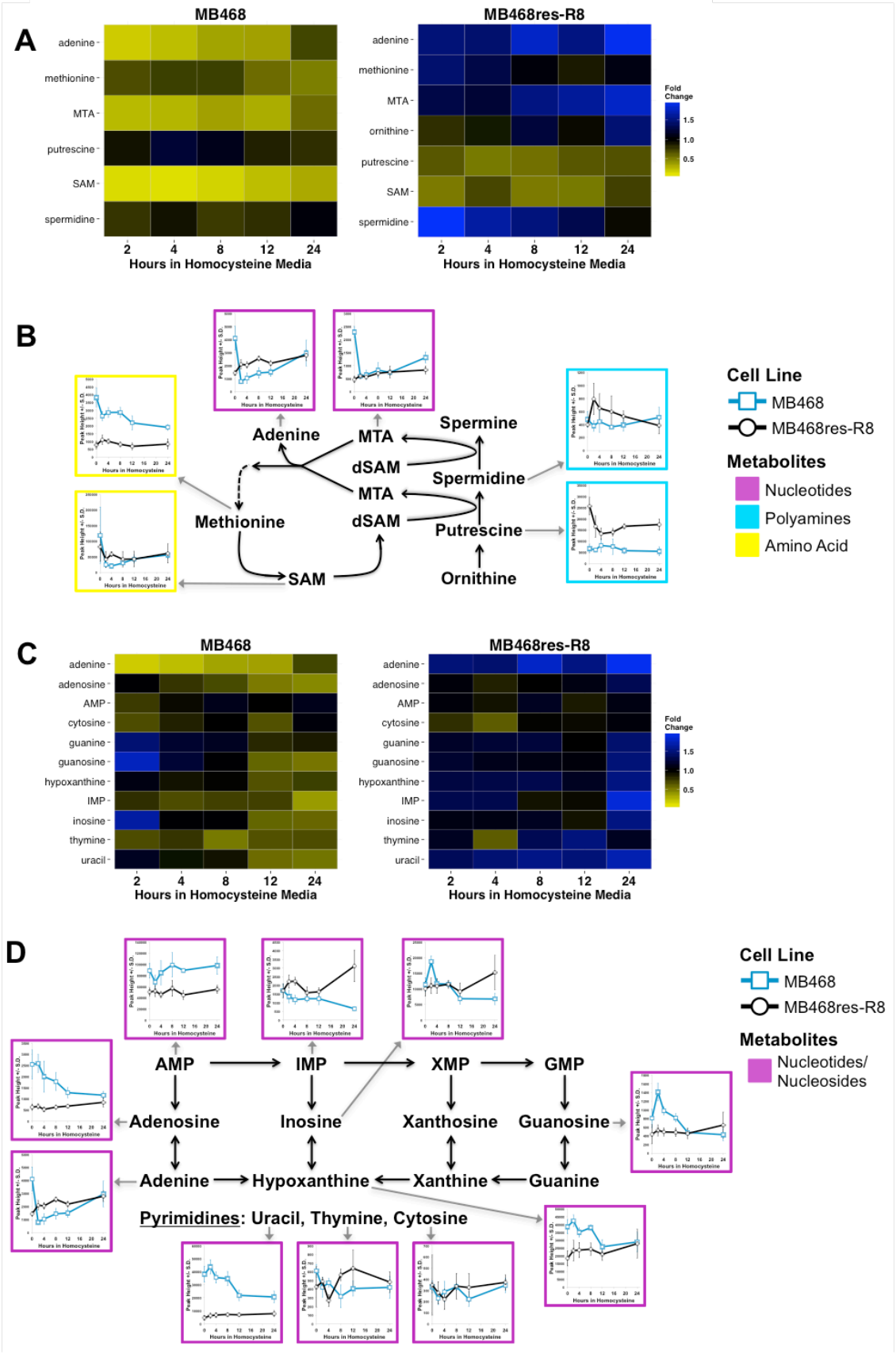
A
MB468
MB468res-R8
adenine
methionine
MTA
putrescine
SAM
spermidine
ornithine
2 4 8 12 24
Hours in Homocysteine Media
Fold Change
1.5
1.0
0.5
B
Adenine
MTA
Spermine
dSAM
Spermidine
MTA
Methionine
dSAM
Putrescine
SAM
Ornithine
Cell Line
MB468
MB468res-R8
Metabolites
Nucleotides
Polyamines
Amino Acid
C
MB468
MB468res-R8
adenine
adenosine
AMP
cytosine
guanine
guanosine
hypoxanthine
IMP
inosine
thymine
uracil
2 4 8 12 24
Hours in Homocysteine Media
Fold Change
1.5
1.0
0.5
D
AMP
IMP
XMP
GMP
Adenosine
Inosine
Xanthosine
Guanosine
Adenine
Hypoxanthine
Xanthine
Guanine
Pyrimidines: Uracil, Thymine, Cytosine
Cell Line
MB468
MB468res-R8
Metabolites
Nucleotides/
Nucleosides

Figure 3.4 *Metabolite changes linked to methionine and nucleoside metabolism*
(A) MB468 and MB468res-R8 cells were cultured in Met+ or Met-Hcy+ media over the course of 24 hours and analyzed by untargeted GCTOFMS and HILIC-UHPLC-qTOFMS-based metabolomics. Heatmaps represent fold changes of metabolites in the purine salvage as compared to the Met+, time-zero sample. Metabolites are color filled by fold change: *yellow* indicates a decrease in metabolite abundance and *blue* indicates an increase as compared to time-zero control. (B) Schematic of polyamine synthesis and methionine regeneration by way of the methionine salvage pathway. Metabolites with gray arrows are pointing to line graphs of the corresponding metabolite abundances in MB468 (*blue line with squares*) and MB468res-R8 (*black line with circles*) cells. Peak height reflecting relative metabolite abundance is marked on the y-axis and hours in homocysteine are marked on the x-axis. Error bars represent standard deviation. (C) Heatmaps represent fold changes of metabolites involved in purine/pyrimidine synthesis. Color fill is the same as (A). (D) Schematic of purine synthesis and pyrimidines with corresponding metabolite abundances, same as (B).

physiological response of MB468 cells to methionine stress and suggests that cells attempt to preserve SAM concentrations by repression of polyamine synthesis. In contrast, MB468res-R8 cells appear to up-regulate polyamine synthesis indicated by doubling of spermidine abundance within 2 hours and a correction to starting levels after 24 hours. MTA and adenine levels show a similar increase in abundance over 2 hours and continue to increase after 24 hours to almost twice the starting levels.

The differences in the levels of MTA may contribute to the difference in methionine levels between the two cell lines. MB468 cells have a slight decrease in methionine starting at 2 hours, staying around 0.7 fold abundance until 24 hours when the levels decrease to half the starting quantity (Figure 3.4B). MB468res-R8 cells increase in methionine levels as early as 2 hours but return to normal after 8 hours. It is important to note, that the MB468res-R8 cells continue to proliferate in Met-Hcy+ media unlike the MB468 cells, which may affect the use of metabolites in each cell line after 24 hours, the approximate doubling time of these cells. However, the early changes we observed can be attributed to a metabolic response to the switch from methionine to homocysteine in the growth medium.

Purines and pyrimidines

Both adenine and adenosine are byproducts of the methionine salvage and remethylation pathways and are essential components in purine synthesis. With few exceptions, changes in purine as well as pyrimidine concentrations were not evident until 12 to 24 hours after cells were shifted (Figure 3.4C). In MB468res-R8 cells only adenine increased to approximately 1.5 fold of the starting quantity within 2 hours. After 12 and 24 hours inosine, inosine monophosphate, and hypoxanthine were significantly increased (Figure 3.4D). In contrast, MB468 cells respond to

Met-Hcy+ medium with a delayed decrease in inosine, guanine, and guanosine, as well as an immediate steep decrease in adenine levels as described above. Unlike the overall increase in purines in MB468res-R8 cells, many purines in MB468 cells decrease to half the starting quantity by 24 hours. Interestingly the changes in components of the purine synthesis pathway are not observed for the pyrimidines thymine and cytosine. In both MB468 and MB468res-R8 cells, thymine and cytosine abundance indicate a minimal response to methionine stress. Uracil, the pyrimidine derivative found in RNA, showed a comparable trend as the purine response in both cell lines as levels decrease in MB468 cells and increase in MB468res-R8 cells over the course of 24 hours (Figure 3.4D).

Glycolysis and citric acid cycle

Despite major changes in other biochemical pathways, Met-Hcy+ media had minimal effects on the abundances of metabolites involved in glycolysis (Figure 3.5A). Both MB468 and MB468res-R8 cells indicate only slightly decreased abundances in glucose and glucose 6-phosphate. More noticeable differences between the two cell lines were observed in fructose 6-phosphate and pyruvate. Unlike MB468res-R8, abundances of fructose 6-phosphate and pyruvate in MB468 indicated initial reductions post media switch followed by partial equilibration back towards baseline levels (Figure 3.5B). Using the XF analyzer to further evaluate glycolysis, we treated MB468 and MB468res-R8 cells in Met+ media for 12 hours or Met-Hcy+ media for 2, 4, 8, and 12 hours and measured the extracellular acidification rate (ECAR), an indicator of glycolysis (Figure 3.5C). Similar to many of the metabolite profiles, an initial decrease in glycolysis occurs within 2 hours post media switch followed by partial recovery to baseline. MB468 cells decrease glycolysis at 2 hours to 75% baseline with an average partial recovery to

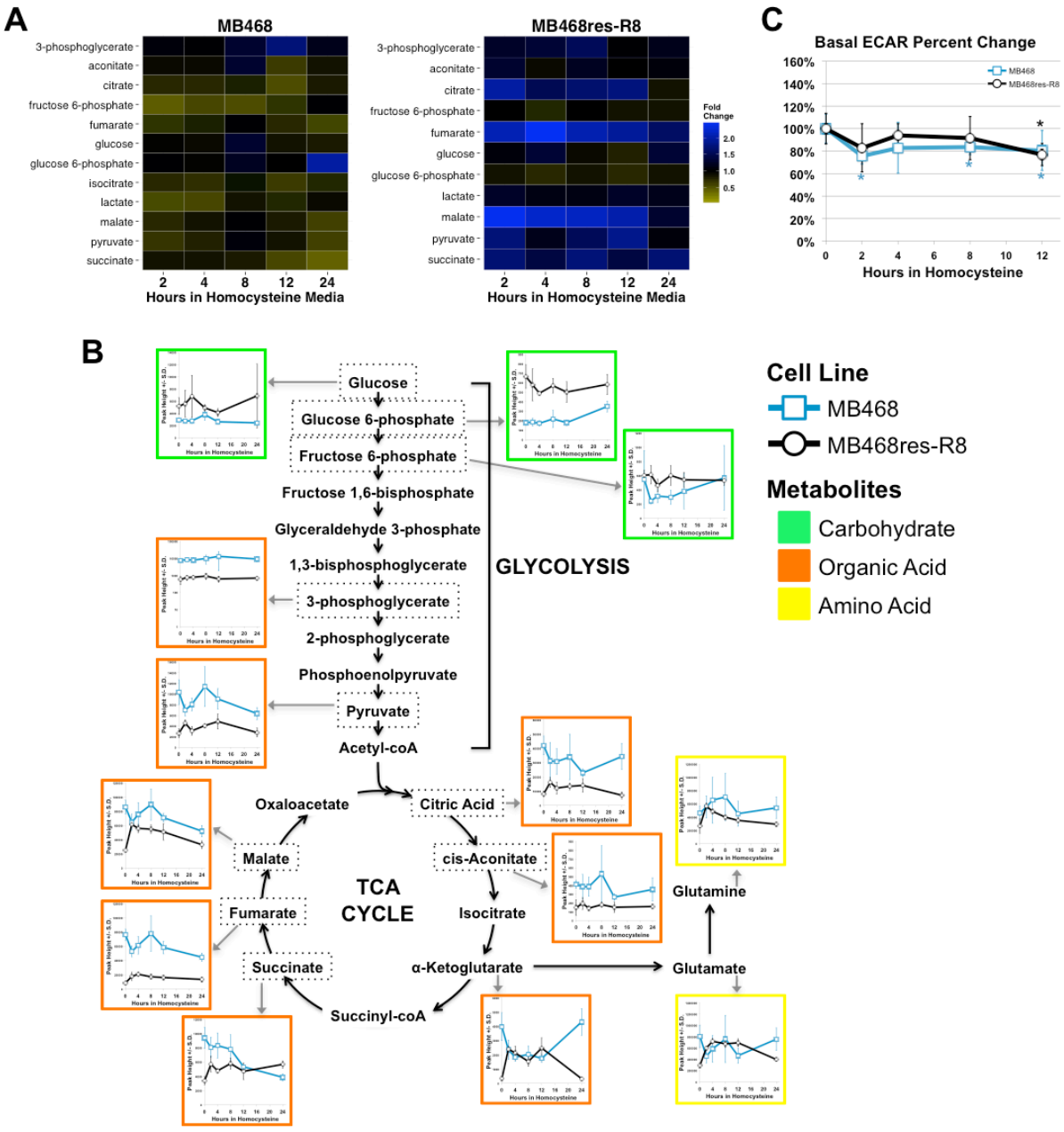
A
MB468
MB468res-R8
3-phosphoglycerate
aconitate
citrate
fructose 6-phosphate
fumarate
glucose
glucose 6-phosphate
isocitrate
lactate
malate
pyruvate
succinate
2 4 8 12 24
Hours in Homocysteine Media
Fold Change
2.0
1.5
1.0
0.5
C
Basal ECAR Percent Change
MB468
MB468res-R8
160%
140%
120%
100%
80%
60%
40%
20%
0%
0 2 4 6 8 10 12
Hours in Homocysteine
B
Glucose
Glucose 6-phosphate
Fructose 6-phosphate
Fructose 1,6-bisphosphate
Glyceraldehyde 3-phosphate
1,3-bisphosphoglycerate
3-phosphoglycerate
2-phosphoglycerate
Phosphoenolpyruvate
Pyruvate
Acetyl-coA
GLYCOLYSIS
Oxaloacetate
Citric Acid
cis-Aconitate
Isocitrate
α-Ketoglutarate
Succinyl-coA
Succinate
Fumarate
Malate
TCA CYCLE
Glutamine
Glutamate
Cell Line
MB468
MB468res-R8
Metabolites
Carbohydrate
Organic Acid
Amino Acid

Figure 3.5 *Metabolite changes in glycolysis and the TCA cycle associated with methionine stress*

(A) MB468 and MB468res-R8 cells were cultured in Met+ or Met-Hcy+ media over the course of 24 hours and analyzed by untargeted metabolomics as described for figure 4. Heatmaps represent fold changes of metabolites in glycolysis and the tricarboxylic acid (TCA) cycle as compared to the Met+, time-zero sample. Metabolites are color filled by fold change: *yellow* indicates a decrease in metabolite abundance and *blue* indicates an increase as compared to time-zero control. (B) Schematic of glycolysis and the TCA cycle. Metabolites with gray arrows are pointing to line graphs of the corresponding metabolite abundances in MB468 (*blue line with squares*) and MB468res-R8 (*black line with circles*) cells. Peak height reflecting relative metabolite abundance is indicated on the y-axis and hours in homocysteine are indicated on the x-axis. Error bars represent standard deviation. Metabolites included in the heatmaps (A) are outlined. (C) MB468 and MB468res-R8 cells cultured in Met+ media for 12 hours or Met-Hcy+ media for 2, 4, 8, and 12 hours were analyzed by the Seahorse Bioscience XF analyzer. MB468 (*blue line with squares*) and MB468res-R8 (*black line with circles*) basal extracellular acidification rates (ECAR) are shown normalized to the Met+ treated sample. Error bars represent normalized standard deviation, n = 4 replicates, statistical differences between Met+ media and Met-Hcy+ media treatments are indicated by (*) where $p \leq 0.002$.

82% over the next 10 hours. MB468res-R8 cells follow a similar trend with a decrease in glycolysis to 83% baseline at 2 hours and average recovery of 87% thereafter. These subtle changes in glycolysis suggest early partitioning of glucose towards the pentose phosphate pathway for generation of NADPH (not detected) following the switch to Met-Hcy+ media.

Similar to our earlier observations of decreased mitochondrial respiration in Met-Hcy+ media (Figure 3.2), the TCA-related metabolites succinate, fumarate, and malate indicate general reductions in MB468 cells. In contrast, MB468res-R8 cells show a two-fold increase in malate and fumarate with less striking increases in other TCA cycle components including citrate, succinate, and aconitate (Figure 3.5B). The reduction in MB468-dependent TCA intermediates corroborates with decreased oxidative phosphorylation; however, the difference in response of MB468res-R8 may be a result of their lower respiration capacity and thus their reduced dependence on respiration in these cells.

Homocysteine metabolism is redirected during HCY culturing

The changes in steady state levels of metabolites are informative and indicate a significant rewiring of metabolic pathways in response to methionine stress and highlight different metabolic responses in methionine dependent and independent cell lines. However, interpretations of steady state level changes are complicated by reversibility of reactions, such that pathway activities or flux changes can only be inferred in some situations. The methionine dependence of cancer is closely linked to the availability of SAM as a co-factor for methylation, which is also illustrated by the complete suppression of growth inhibition of MB468 cells cultured in Met-Hcy+ supplemented with SAM (Booher et al., 2012). We therefore asked how homocysteine is used in cells over time with particular focus on remethylation and

transsulfuration (Figure 3.6A). To this end we used deuterium labeled homocysteine ($_{d4}$Hcy = Hcy-$_{d4}$(3,3,4,4)) to replace methionine in the cell growth media (Figure 3.6B). Both MB468 and MB468res-R8 cells accumulated $_{d4}$Hcy to about the same extent confirming that uptake of homocysteine cannot account for methionine stress sensitivity (Figure 3.6C). Methionine flux analyses have shown that generally homocysteine remethylation and entry into the transsulfuration pathway each account for approximately 50% (Turner et al., 2000), (Storch et al., 1990). Surprisingly, post Met-$_{d4}$Hcy+ media switch, the majority of homocysteine metabolism in both MB468 and MB468res-R8 is predominantly directed towards the transsulfuration pathway as indicated by the almost complete dominance of deuterated cystathionine (transsulfuration) after 24 hours and underrepresentation of deuterated methionine (Figure 3.6D and 3.6E). However, this effect was significantly delayed in MB468 cells. The methionine stress resistant MB468res-R8 cells showed a complete shift to deuterated cystathionine within 4 hours of the media switch, whereas methionine stress sensitive MB468 cells required at least 24 hours in Met-$_{d4}$Hcy+ medium to show a comparable transition to deuterated cystathionine. These studies also revealed that MB468res-R8 cells use homocysteine to remethylate an average of 13% more methionine molecules as compared to MB468 cells, a difference that is reflected in labeled SAM levels as well (Figure 3.6F).

It is interesting to note that while MB468res-R8 cells process homocysteine forward through the remethylation pathway, MB468 cells process an average of 6% more homocysteine through the reversible hydrolytic activity of S-adenosylhomocysteine hydrolase (Figure 3.6G). S-adenosylhomocysteine (SAH) is the byproduct of all biological transmethylation reactions requiring SAM and is also generated from homocysteine and adenosine. This reverse processing of homocysteine in MB468 cells may partially contribute to the decrease in adenosine abundance

(Figure 3.6H). Comparing the relative concentration of SAM and SAH can indicate the methylation potential of the cell. However, it has been shown that a reduced ratio bares little consequence without a corresponding increase in SAH (Caudill et al., 2001; Hoffman et al., 1980). In both MB468 and MB468res-R8 cells, SAM and SAH were measured over a 24 hour period in Met-Hcy+ media (Figure 3.6I). For both cell lines the SAM:SAH ratio decreased within 2 hours of the media switch. In MB468 cells this decrease in SAM:SAH is a result of a simultaneous decrease in SAM to less than one-fifth starting quantity and increase in SAH to 1.5 times the starting quantity. After 12 hours, however, both SAH and SAM begin to recover toward starting levels. In contrast, the SAM:SAH decrease observed in MB468res-R8 cells are a result of SAM levels declining to half the starting quantity with minimal perturbations in SAH. Considering SAM levels are two fold greater in MB468 cells in Met+ media as compared to MB468res-R8 cells, the consequences of an altered SAM:SAH ratio and elevated SAH levels in MB468 cells on the methylation potential of the cell may play an important role in methionine sensitivity. Clearly, both cell lines experience limited methylation potential as indicated by feedback upregulation of methionine adenosyltransferase (MAT), the enzyme that produces SAM from methionine and ATP (Figure 3.6J). Although labeled methionine levels are higher in MB468res-R8 cells, in both cell lines it appears that the catalytic MAT2A subunit is, for unknown reasons, unable to use the available methionine for SAM synthesis and therefore protein levels increase to compensate this deficiency. Interestingly, MAT2B, the regulatory subunit of the enzyme, is unaffected by methionine perturbations.

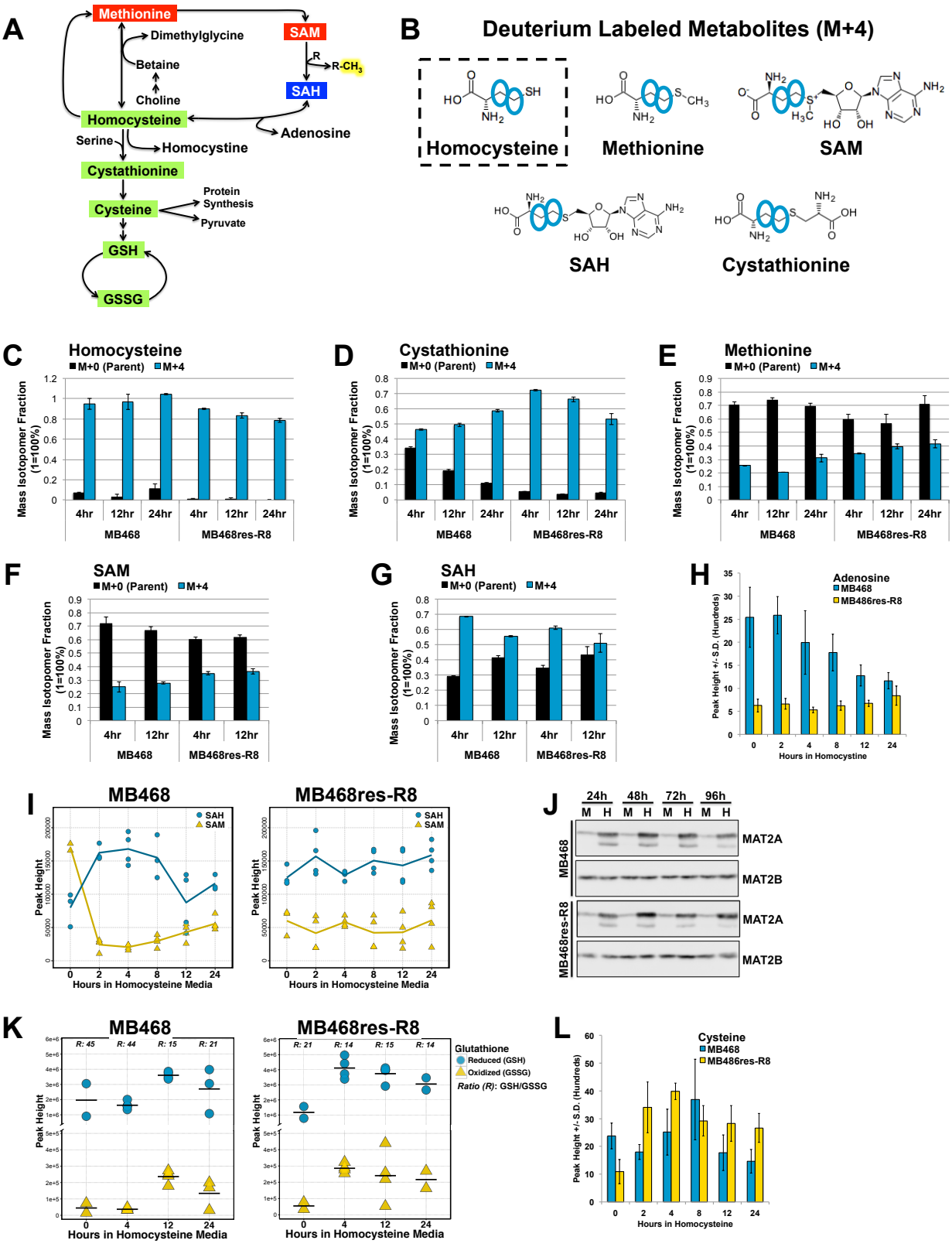
A
Methionine
Dimethylglycine
SAM
R
R-CH3
Betaine
SAH
Choline
Homocysteine
Adenosine
Serine
Homocystine
Cystathionine
Protein Synthesis
Cysteine
Pyruvate
GSH
GSSG
B
Deuterium Labeled Metabolites (M+4)
Homocysteine
Methionine
SAM
SAH
Cystathionine
C
Homocysteine
D
Cystathionine
E
Methionine
M+0 (Parent)
M+4
Mass Isotopomer Fraction (1=100%)
4hr
12hr
24hr
MB468
MB468res-R8
F
SAM
G
SAH
H
Adenosine
MB468
MB486res-R8
Peak Height +/- S.D. (Hundreds)
Hours in Homocystine
I
MB468
MB468res-R8
SAH
SAM
Peak Height
Hours in Homocysteine Media
J
24h
48h
72h
96h
M
H
MB468
MB468res-R8
MAT2A
MAT2B
K
MB468
MB468res-R8
R: 45
R: 44
R: 15
R: 21
R: 14
Glutathione
Reduced (GSH)
Oxidized (GSSG)
Ratio (R): GSH/GSSG
Peak Height
Hours in Homocysteine Media
L
Cysteine
MB468
MB486res-R8
Peak Height +/- S.D. (Hundreds)
Hours in Homocysteine

Figure 3.6 *Homocysteine metabolism is redirected towards the transsulfuration pathway during methionine stress*

(A) A schematic summarizing isotope tracer results. The majority of deuterium atoms labeled homocysteine and cystathionine, indicating a greater flux towards glutathione synthesis (*green*). Methionine and SAM synthesis and abundance decrease (*red*) in both cell lines. SAH levels increase (*blue*) in MB468 cells only. The activated methyl group of SAM is highlighted *yellow*. (B) Deuterated homocysteine (Hcy-$_{d4}$(3,3,4,4), dashed square) was used to prepare Met-Hcy+ media for isotope tracer analysis. Metabolite structures with blue circles indicate the expected location of the deuterium atoms. Mass isotopomer distributions (MID) were calculated using the Fiehnlab MID Analyzer and validated by comparing spectra of enriched molecules to non-labeled spectra. MIDs for M+0 (*black*) non-labeled parent molecule and M+4 (*blue*), corresponding to a mass shift resulting from 4-deuterium atoms, are plotted for (C) homocysteine, (D) cystathionine, (E) methionine, (F) S-adenosylmethionine (SAM), and (G) S–adenosylhomocysteine (SAH) for MB468 and MB468res-R8 cells. (H) Adenosine levels for MB468 (*blue*) and MB468res-R8 (*yellow*) cells were measured by GCTOFMS. Error bars represent standard deviation. (I) SAM (*yellow triangles*) and SAH (*blue circles*) levels were measured by HILIC-UHPLC-qTOFMS in MB468 and MB468res-R8 cells. Scatterplots represent peak heights for individual replicates. The overlaid line graph (SAM- *yellow*, SAH- *blue*) indicates average peak heights. A minimum of two replicates were measured per sample. (J) MB468 and MB468res-R8 cells cultured in Met+ ("M") or Met-Hcy+ ("H") media were analyzed for methionine adenosyltransferase 2A and 2B (MAT2A, MAT2B) by immunoblot. (K) Glutathione pools are shown for MB468 and MB468res-R8 cells. Reduced (GSH, *blue circles*) and oxidized (GSSG, *yellow triangles*) glutathione species are plotted for each time point post Met-Hcy+ media switch, horizontal bars indicate averages for each replica set. Ratios of GSH/GSSG are listed above each time point. (L) Cysteine levels for MB468 (*blue*) and MB468res-R8 (*yellow*) cells were measured by GCTOFMS. Error bars represent standard deviation.

Homocysteine and its relationship to ROS, mitochondria, and oxidative stress

Transsulfuration is critical to maintain the cellular redox balance as this metabolic pathway leads directly to glutathione synthesis (Figure 3.6A). Interestingly, signaling pathways in yeast that are activated by methionine or SAM limitation induce a massive increase in glutathione synthesis suggesting a common physiological response to methionine stress in yeast and mammals (Kaiser et al., 2006b; Lee et al., 2010; Wheeler et al., 2002, 2003). Accordingly, the redirection of homocysteine metabolism to the transsulfuration pathway suggests the activation of a protective mechanism in response to Met-Hcy+ media. Under normal culturing conditions, the majority of cellular glutathione exists in its reduced form (GSH). As an antioxidant, glutathione protects the cell from oxidative stress by reducing the disulfide bonds of cytoplasmic proteins and in the process is oxidized to form glutathione disulfide (GSSG) (Liou and Storz, 2010). Interestingly, in Met+ media the abundance of GSH is twice as much in MB468 as compared to MB468res-R8 despite similar levels of GSSG (Figure 3.6K). After culturing in Met-Hcy+ media, both cell lines experience oxidative stress as indicated by increasing levels of GSSG and a steep increase in GSH, presumably to combat oxidative pressure. The timing of this transition to the transsulfuration pathway and glutathione synthesis occurred within 4 hours post media switch in MB468res-R8 cells and by 12 hours in MB468 cells. This timing mirrors the increases of labeled cystathionine in both cell lines (Figure 3.6D), supporting the hypothesis that redirection of homocysteine metabolism to transsulfuration is due to the cellular need to balance redox potentials. Cysteine abundances could not be analyzed by stable isotope tracer studies because metabolic processing of cystathionine results in an unlabeled molecule of cysteine and a deuterium labeled alpha-ketobutyrate molecule. However, using an untargeted approach, cysteine levels indicate a similar increase as compared to both

glutathione and cystathionine with peak abundances at 8 hours in MB468 and 4 hours in MB468res-R8 cells post media switch (Figure 3.6L).

The oxidative stress associated with Met-Hcy+ media is not unexpected as studies on atherosclerosis have identified a relationship between elevated homocysteine levels in plasma and oxidative stress in tissue (Olszewski and S., 1993). The observed stress may be attributed to auto-oxidation of homocysteine, which generates hydrogen peroxide and reactive oxygen species (ROS). Alternatively, the source of stress may be related to inhibition of ATP synthesis in the mitochondria. N-methyl-D-aspartate (NMDA) receptors are glutamate and glycine activated calcium channels that are largely found in neurons. Recent studies have identified active NMDA receptors in human neuroblastoma cells, small-cell lung cancer cells, and breast cancer cells and tumors, but not normal tissues (North et al., 2010a, 2010b). Free and reduced homocysteine molecules can bind to NMDA receptors at the glutamate binding location and activate an influx of calcium ions resulting in reduced ATP synthesis, reduced oxidative phosphorylation, and an accumulation of ROS (McCully, 2009). Although this is a suggested mechanism for Met-Hcy+ induced oxidative stress, the loss of oxidative phosphorylation activity is evident in both cell lines (Figure 3.2) and the response to counter an oxidative insult by increasing glutathione abundance supports this scenario (Figure 3.6K).

In addition to reduced glutathione ratios, the presence of oxidized lipids becomes more prevalent upon Met-Hcy+ media switch. The FLIM approach can effectively visualize and measure oxidized lipids at the single cell and sub-cellular level. Oxidized lipids are detected by a long fluorescence lifetime (LLS) and serve as biomarkers for oxidative stress (Figure 3.7A) (Datta et al., 2015). To quantify the LLS fraction in each field we used phasor cluster analysis of MB468 and MB468res-R8 cells cultured in Met-Hcy+ media over the course of 48 hours (Figure

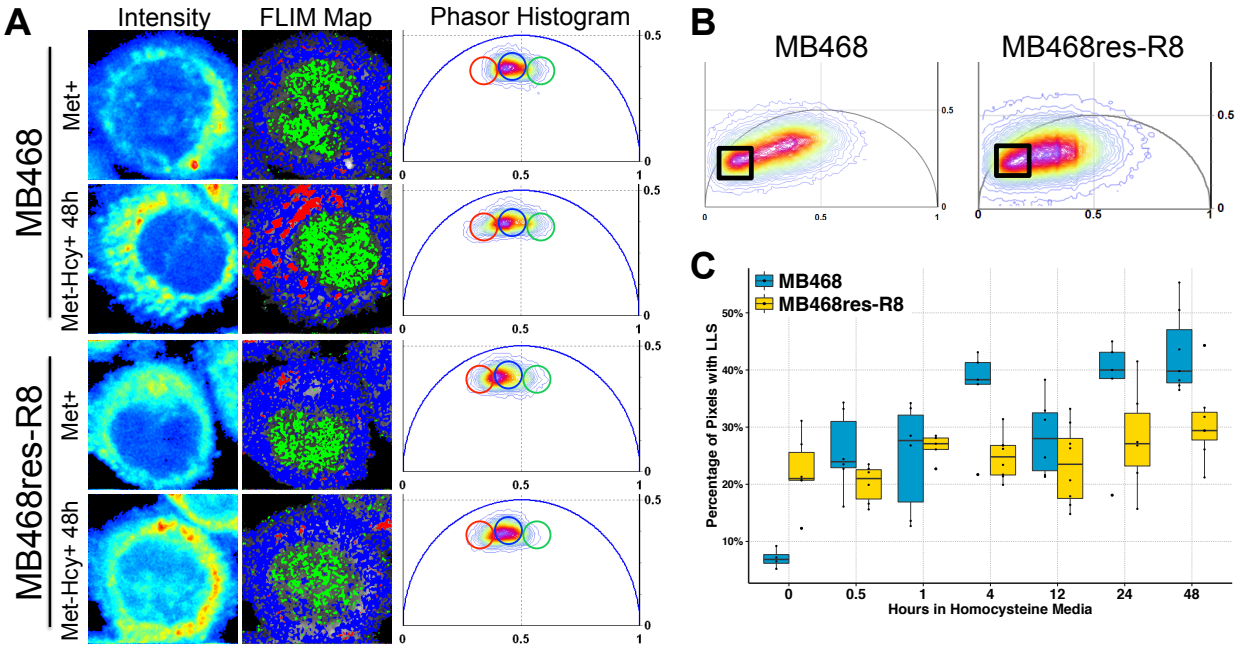

Figure 3.7 *Methionine stress induces an increase in oxidative stress*
(A) Two-photon fluorescence intensity images of individual MB468 and MB468res-R8 cells in Met+ or Met-Hcy+ media (48 h). Pixels within three groups in the phasor histogram have been isolated and colored accordingly in the FLIM map image. Higher free/bound NADH ratios are highlighted in *green*, indicating a more reduced state in the nucleus. Lower free/bound NADH ratios are highlighted in *blue*, indicating higher ratios of oxidative phosphorylation versus glycolysis in the mitochondria/cytoplasm. Long lifetime species (LLS) are highlighted in *red*, indicating the presence of oxidized lipids in the cell. (B) Phasor histograms of MB468 and MB468res-R8 cells. The black box selects the phasors with LLS signature. (C) A boxplot representing the percentage of pixels with the LLS (oxidized lipids) signature in MB468 (*blue*) and MB468res-R8 (*yellow*) in in Met-Hcy+ over a 48 hour time course.

3.7B). In normal Met+ culturing conditions, the average fraction of LLS in MB468 cells is 7% and 22% in MB468res-R8 cells (Figure 3.7C). Immediately after media switch to Met-Hcy+ the fraction of LLS increases in MB468 to 25% at 30 minutes and continues to increase over time to an average of 36% at 48 hours. In contrast, MB468res-R8 cells respond to the media shift with a 5% average increase to 27% LLS after 48 hours. It is interesting to note the higher level of oxidized lipids in MB468res-R8 cells in Met+ as compared to MB468 cells and yet the striking increase observed in the MB468 cells over time in Met-Hcy+. The biological function of these LLS species are not known, but are speculated to serve a protective function that shields cells from oxidative damage due to the sequestering of oxidized lipid in vesicles.

CONCLUSIONS

In conclusion, the present study reveals dynamic changes in the metabolic phenotype associated with methionine-dependency of breast cancer and further highlights the importance of SAM as a major regulator of tumorigenesis. Importantly, using a labeled precursor we discovered that in both MB468 and MB468res-R8 cell types, homocysteine does not significantly contribute to formation of methionine, and ultimately S-adenosylmethionine. Our study indicates that SAM metabolism, which is required for all methylation reactions, depends on availability of methionine in the cancer cell lines investigated and cannot be substituted for by homocysteine-forming pathways. Moreover, these findings shed light on the metabolic reprogramming, which accompanies methionine stress beyond methylation potential. Such knowledge is instrumental for elucidating novel targets of therapeutic intervention, which can be exploited in future studies. Given the importance of SAM in lipid biogenesis and our observed

changes in LLS, assessing impact of methionine-stress on lipid composition and synthesis is of considerable interest and warrants further investigation.

CHAPTER FOUR

Lipid remodeling associated with methionine stress sensitivity in MDA-MB-468 breast cancer cells

INTRODUCTION

Methionine metabolism is an integral aspect in cellular function and is particularly important in cancer. Cancer cells that cannot proliferate in growth medium when methionine is replaced with its metabolic precursor, homocysteine, have been characterized as being "methionine dependent" or "methionine sensitive". Previous studies indicate that cancer cells that become resistant to methionine stress or "methionine independent", lose their transformed phenotype (Borrego et al., 2016; Hoffman et al., 1978, 1979). Just as other metabolic alterations have been recognized as signatures of transformed cells, methionine metabolism is a unique metabolic requirement of cancer (Hanahan and Weinberg, 2011a).

Methionine is an essential metabolite for cell growth and function and is the precursor to S-adenosylmethionine (SAM), the principal methyl donor in the cell (FIGURE 4.1). SAM serves as a co-factor for a variety of methyltransferases and methylation events on DNA, RNA,

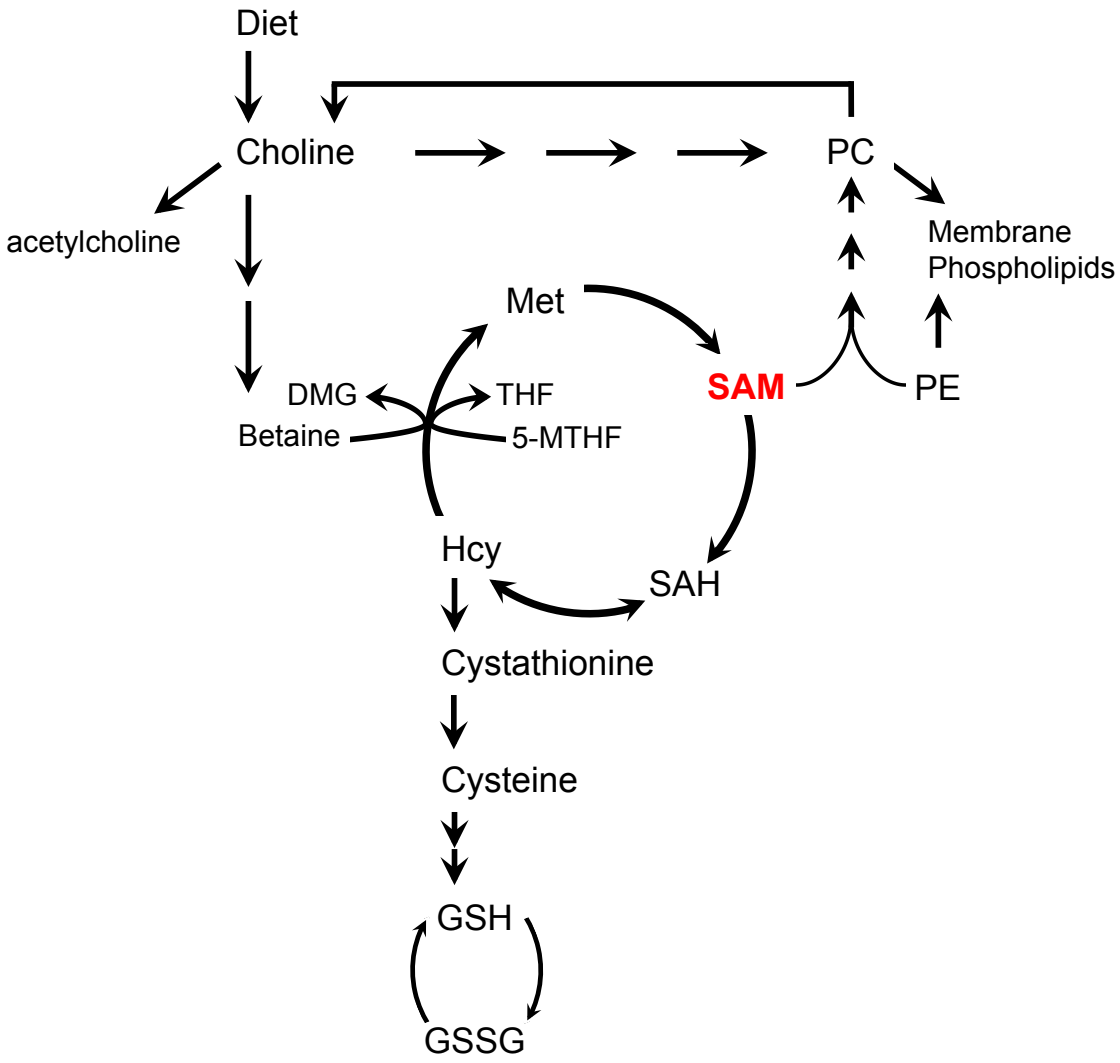

Figure 4.1 *Methionine metabolism and its connection to phospholipid synthesis*
A schematic of homocysteine metabolism indicating the connection of SAM and choline in phospholipid synthesis. Three methylation reactions on PE using SAM as a co-factor are necessary to synthesize PC through the phosphatidylethanolamine N-methyltransferase (PEMT) pathway. Choline is used as a precursor to PC in the Kennedy pathway. PC contributes to free choline through the enzyme phospholipase D. Abbreviations: DMG - dimethylglycine, GSH - reduced glutathione, GSSG - oxidized glutathione, Hcy - homocysteine, Met - methionine, 5-MTHF - 5-methyltetrahydrofolate, PC - phosphatidylcholine, PE - phosphatidylethanolamine, SAH - S-adenohomocysteine, SAM - S-adenosylmethionine, THF - tetrahydrofolate

proteins, and lipids (Finkelstein and Martin, 1984). After donating its methyl group, SAM is converted into S-adenosylhomocysteine (SAH) and further processed to homocysteine (Hcy). At this point, Hcy can be catabolized in the transsulfuration pathway or methylated to regenerate methionine by way of methionine synthase (MS) and 5-methyltetrahydrafolate or betaine homocysteine methyltransferase (BHMT) and betaine, a product of choline (FIGURE 1.2). Both SAM and betaine are direct components of methionine metabolism and closely linked to phospholipid processing (FIGURE 4.1).

Phosphatidylcholine (PC) and phosphatidylethanolamine (PE) are the two most abundant lipid species in the cell and play an important structural role in cell membranes. Both PC and PE can be synthesized *de novo* through the two branches of the Kennedy pathway referred to as the CDP-choline and CDP-ethanolamine pathways, respectively (DeLong et al., 1999; Gibellini and Smith, 2010). In normal cells, the majority of PC is synthesized through the CDP-choline pathway. Choline links methionine and PE metabolism as it is a precursor of betaine, which can regenerate methionine by way of BHMT, and it can be regenerated by PC catabolism by the enzyme phospholipase D (PLD) (Banno, 2002). Interestingly, both choline and PC levels have been shown to be aberrantly upregulated in cancer along with many of their associated enzymes including PLD (Cao et al., 2012; Glunde et al., 2004, 2011; Xu et al., 2008). However, the influence of choline upregulation on methionine remethylation is still unknown. In a less prominent pathway for PC synthesis, SAM is necessary for three sequential methylations on PE by phosphatidylethanolamine N-methyltransferase (PEMT) (Daum et al., 1998; Watkins et al., 2003). In both human and yeast studies, atypical Hcy or SAH levels lead to deregulation of phospholipid and triglyceride lipid metabolism (Malanovic et al., 2008; Tehlivets et al., 2013).

The level in which these two pathways can influence each other indicate a tight balance between methionine metabolism components and lipid synthesis.

The connection between methionine and lipid metabolic pathways have been extensively researched in in the context of liver dysfunction and heart disease in the presence of high homocysteine levels. Recent work has extended these studies to different types of cancers of varying malignancy and thus the role of lipid metabolism and its connection to the methionine pathway is becoming more clear in tumor progression and metastasis (Breillout et al., 1990; Cao et al., 2012; Glunde et al., 2011). In a continued effort to understand the metabolic response during methionine stress, we performed lipidomic analyses in parallel to the untargeted metabolic and stable isotope-tracing study previously reported (Borrego et al., 2016). Using the methionine-dependent breast cancer cell line MB468 and its methionine-independent derived clone MB468res-R8, we have characterized the dynamic lipid response when cells were cultured in homocysteine media (Met-Hcy+), a methionine stress inducing condition.

RESULTS

Lipid changes associated with culturing in homocysteine media

Our previous report indicated immediate metabolic changes in MB468 and MB468res-R8 in a cell line specific manner in response to homocysteine media (Met-Hcy+). In our continued study, we look beyond our untargeted metabolomics data and delve into lipidomics. Both MB468 and MB468res-R8 cells were cultured in normal methionine media (Met+) or transitioned to Met-Hcy+ media for 2, 4, 8, 12, and 24 hours, and lipids were measured by UHPLC-QTOF (Figure 4.2). We focus on the early time points to avoid cell cycle effects imposed by the arrested growth of MB468 and continued proliferation of MB468res-R8 in

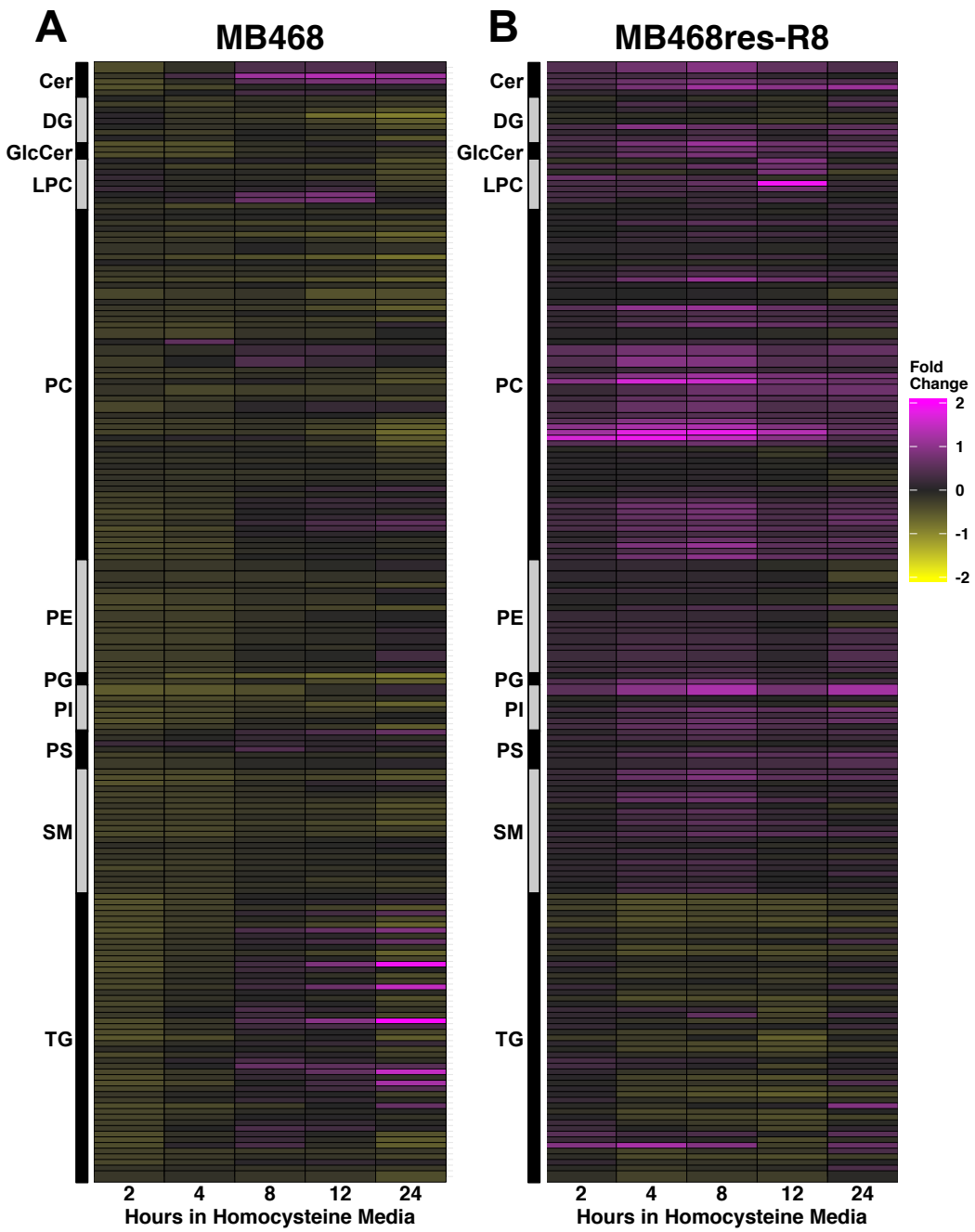

Figure 4.2 *Homocysteine media induces a lipid response in MB468 and MB468res-R8 cells* A) MB468 and B) MB468res-R8 cells were cultured in Met+ or Met-Hcy+ media over the course of 24 hours, measured by UHPLC-QTOF, and normalized to dry cell weight. Heatmaps indicating lipid classes are color filled based on fold change to the Met+, time-zero sample. *Yellow* indicates a decrease in metabolite abundance and *magenta* indicates an increase as compared to time-zero control. Abbreviations: Cer - ceramide, DG - diglyceride, GlcCer - glucosylceramide, LPC - lysophosphatidylcholine, PC - phosphatidylcholine, PE - phophatidylethanolamine, PG - phosphatidylglycerol, PI - phosphatidylinositol, PS - phosphatidylserine, SM - sphingomyelin, TG - triglyceride

Met-Hcy+ media (Booher et al., 2012; Borrego et al., 2016). Within two hours of exposure to Met-Hcy+ media, we observe a remarkable decrease in all lipid classes in MB468 cells (FIGURE 4.2A). In contrast, MB468res-R8 results indicate a global increase in lipid abundance with the exception of triglycerides (FIGURE 4.2B). The decline in MB468res-R8 triglyceride levels is not as immediate as observed in MB468 cells, it takes up to 4 hours in Met-Hcy+ media to observe a decline in the majority of triglycerides species. The stark contrast in global lipid behavior between the two cell lines could suggest either a differential coping mechanism to Met-Hcy+ induced methionine stress or differential damages occurring.

Lipid peroxidation induced by homocysteine media

The immediate decrease in global lipid abundances in response to Met-Hcy+ media suggests that lipid damage is likely the cause. Lipid peroxidation, a process that targets unsaturated lipids in the presence of free radicals or prooxidants, is one potential route for lipid damage when cells are cultured in Met-Hcy+ media (FIGURE 4.3A). In the presence of oxidative stress, prooxidants attack unsaturated lipids resulting in lipid radicals. Lipid peroxy radicals are produced when oxygen reacts with the lipid radical and these reactive lipid species propagate damage by reacting with more unsaturated lipids. Neither lipid radicals nor lipid peroxyl radicals are identified by mass spectrometry methods as the original lipid species since the mass (m/z) is altered and therefore a new spectrum is generated. As a consequence, the immediate decrease in lipid abundance is likely due to an increase in lipid radicals with a new mass that is no longer interpreted as the original lipid species. The lipid peroxidation reaction can be terminated in the presence of an antioxidant such as reduced glutathione (Ayala et al., 2014;

Halliwell and Chirico, 1993). Glutathione is a major cellular antioxidant and mainly exists in its reduced form, readily available to neutralize casualties of oxidation.

MB468 and MB468res-R8 cells were cultured in Met+ or Met-Hcy+ media for 4, 8, 12, and 24 hours and glutathione levels were measured. Interestingly, both reduced (GSH) and oxidized (GSSG) glutathione abundances increased when cultured in Met-Hcy+ media, although with different timing between the two cell lines. MB468 cells indicate an increase in both GSH and GSSG within 12 hours post Met-Hcy+ media switch (FIGURE 4.3B), whereas MB468res-R8 glutathione levels increase within 4 hours (FIGURE 4.3C). The need for both cell lines to increase their glutathione abundance strongly indicates that Met-Hcy+ induces oxidative stress, which in turn can result in lipid peroxidation in addition to other cellular injuries. Furthermore, fluorescence lifetime imaging microscopy (FLIM) was used to visualize and quantify oxidized lipids, which serve as a biomarker for oxidative stress (Datta et al., 2015). Both MB468 and MB468res-R8 cells were cultured in Met-Hcy+ media for 48 hours and oxidized lipids were measured by FLIM at 0, 0.5, 1, 4, 12, 24, and 48 hours. We observed a 36% overall increase in oxidized lipids in MB468 cells with a major 20% increase from starting levels as early as 30 minutes post media switch (FIGURE 3.7C). In contrast, steady-state levels of oxidized lipids in MB468res-R8 cells were three times higher than MB468 cells but only increase an average of 5% over 48 hours when cultured in Met-Hcy+ media (Borrego et al., 2016). These results corroborate with the immediate lipid response in MB468 cells (FIGURE 4.2A) and confirm a Met-Hcy+ induced oxidative stress assault that is not tolerated as well in MB468 cells as in the MB468res-R8 cell line.

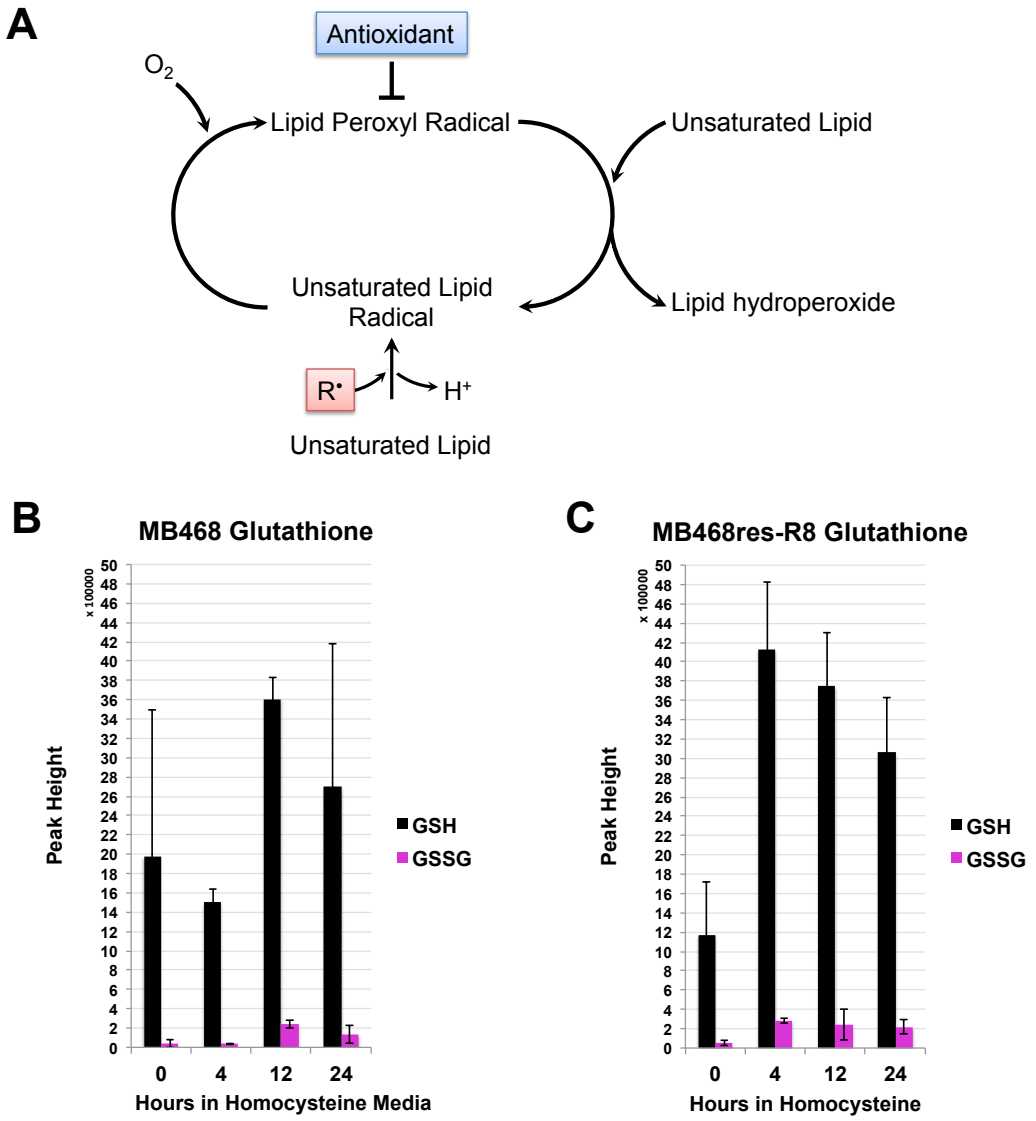

Figure 4.3 *Lipid peroxidation as a result of oxidative stress induced by homocysteine media* A) A schematic of lipid peroxidation. Three steps occur during lipid peroxidation: initiation, propagation, and termination. The reaction is initiated by a prooxidant targeting lipids, usually unsaturated lipids, resulting in lipid radicals. The reaction is propagated as the lipid radical reacts with oxygen to form a lipid peroxy radical and further reacts with other lipid molecules generating new lipid radicals and lipid peroxy radicals. The reaction is terminated in the presence of antioxidants that reduce the lipid radicals to non-radical products. Glutathione pools are shown for B) MB468 and C) MB468res-R8 cells. Reduced (*GSH, black*) and oxidized (*GSSG, magenta*) glutathione species are plotted for each time point post homocysteine (Met-Hcy+) media switch. Error bars represent standard deviation of peak heights.

Phospholipids are connected to methionine metabolism

Phospholipids are the largest class of lipids in the cell and are well-known targets of lipid peroxidation. We were particularly interested in phosphatidylcholine (PC) and phosphatidylethanolamine (PE) lipid species in response to Met-Hcy+ media due to their close connection with methionine metabolism (FIGURE 4.1). Both PC and PE are synthesized *de novo* through the Kennedy pathway from choline and ethanolamine, respectively (FIGURE 4.4A) (DeLong et al., 1999). Choline not only serves as a precursor to PC, but provides cellular betaine that can remethylate homocysteine for methionine regeneration. To gain a better understanding of how different lipid classes responded to Met-Hcy+ media, lipidomic analyses were performed on MB468 and MB468res-R8 cells cultured in Met+ or Met-Hcy+ media for 2, 4, 8, 12, and 24 hours. As indicated by the global analysis (FIGURE 4.2), MB468 and MB468res-R8 levels of PE (FIGURE 4.4B and 4.4C) and PC (FIGURE 4.4D AND 4.4E) respond to Met-Hcy+ in distinct fashions. Both PE and PC lipid types in MB468 cells have a steep drop in abundance within 2 hours post media switch, whereas, lipid abundances in MB468res-R8 cells indicate a gradual increase. The opposing trends between the two cell lines may be a result of oxidative stress and the different timing of the glutathione response (FIGURE 4.3B and 4.3C). The delayed increase of glutathione at 12 hours in MB468 cells may result in greater damage and loss of lipids as compared to the 4 hour response observed in MB468res-R8.

Both diacyglycerol and choline are necessary for biosynthesis of PC in the Kennedy pathway. With a completely different response to Met-Hcy+ media, diacylglycerols in MB468 cells (FIGURE 4.4F) indicate a gradual decrease in abundance over time whereas little change is observed in MB468res-R8 cells (FIGURE 4.4G). Interestingly, choline levels have a similar response to Met-Hcy+ media as glutathione (FIGURE 4.4H). Choline, GSH, and GSSG

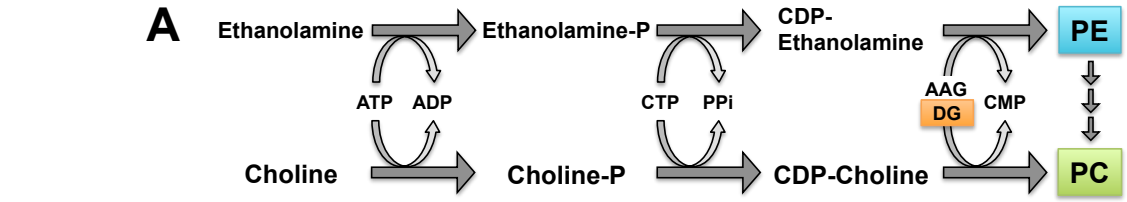
A
Ethanolamine
Ethanolamine-P
CDP-
Ethanolamine
PE
ATP
ADP
CTP
PPi
AAG
DG
CMP
Choline
Choline-P
CDP-Choline
PC

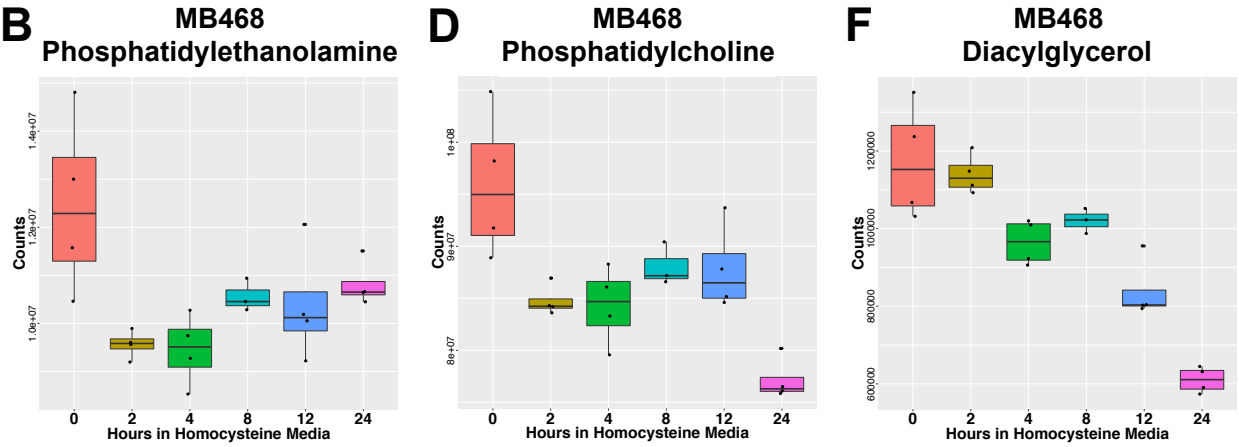
B
MB468
Phosphatidylethanolamine
D
MB468
Phosphatidylcholine
F
MB468
Diacylglycerol
Counts
Hours in Homocysteine Media
0
2
4
8
12
24

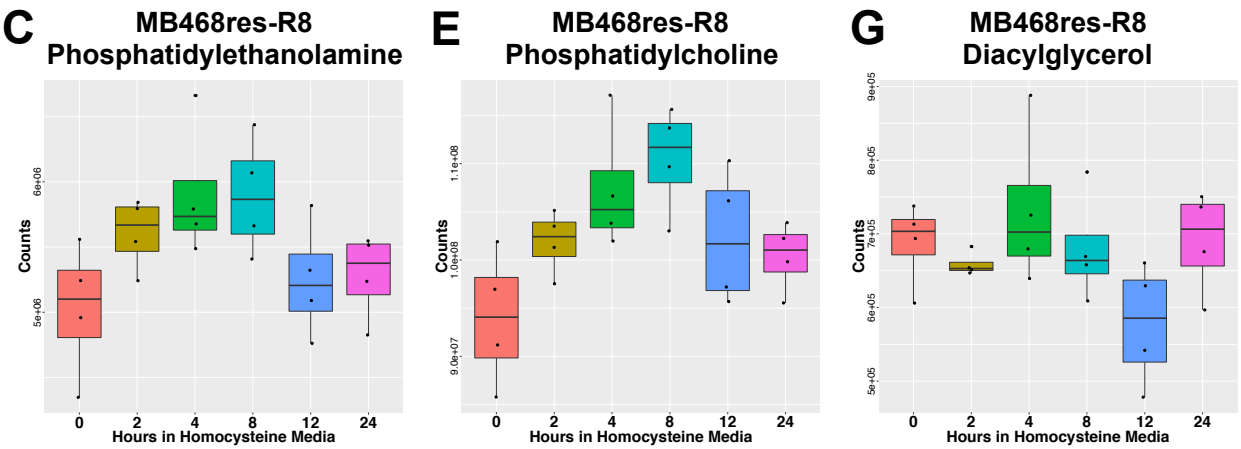
C
MB468res-R8
Phosphatidylethanolamine
E
MB468res-R8
Phosphatidylcholine
G
MB468res-R8
Diacylglycerol
Counts
Hours in Homocysteine Media
0
2
4
8
12
24

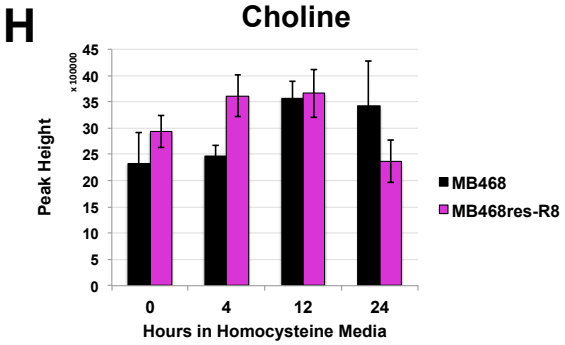
H
Choline
Peak Height
x 100000
Hours in Homocysteine Media
0
4
12
24
MB468
MB468res-R8

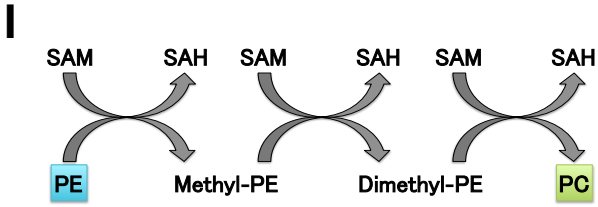
I
SAM
SAH
SAM
SAH
SAM
SAH
PE
Methyl-PE
Dimethyl-PE
PC

Figure 4.4 *Phosphatidylcholine synthesis is dependent on choline and SAM*
A) A schematic of the mammalian Kennedy pathway. B) MB468 and C) MB468res-R8 lipid species in the phosphatidylethanolamine (PE) lipid class were combined and peak height averages for each replicate is plotted for each time point post homocysteine media switch. D) MB468 and E) MB468res-R8 lipid species in the phosphatidylcholine (PC) lipid class and F) MB468 and G) MB468res-R8 lipid species in the diacylglycerol lipid class are presented as described in B) and C). H) Peak height averages are plotted for choline levels for MB468 (*black*) and MB468res-R8 (*magenta*) cells. Error bars represent standard deviation. I) A schematic of PC synthesis via the phosphatidylethanolamine N-methyltransferase (PEMT) pathway. Three methylation events using SAM as a methylation co-factor are necessary for the conversion of PE to PC.

abundances increase after 12 hours post Met-Hcy+ media switch in MB468 and within 4 hours in MB468res-R8. It is possible, that in an attempt to reestablish PC levels after a potential lipid peroxidation chain reaction event, diacylglycerols become depleted. In this scenario, PC levels would show an attempted recovery in abundance until diacylglycerols were no longer available and choline would accumulate.

As a backup for PC synthesis, PE can be processed by phosphatidylethanolamine N-methyltransferase (PEMT) and converted to PC. This route for PC synthesis requires three methylation events on PE using SAM as the methyl donor (FIGURE 4.4I). In our previous report using targeted metabolomics, we observed a steep decrease in SAM in MB468 cells within 2 hours post Met-Hcy+ media switch and little change in SAM levels in MB468res-R8 cells (FIGURE 3.6I) (Borrego et al., 2016). It is important to note that initial SAM levels in MB468 are much higher as compared to MB468res-R8 and may suggest a higher demand for SAM as a methylation co-factor and perhaps a greater sensitivity to reduced levels of this metabolite. This decline in SAM in MB468 may reduce PC synthesis from PE and result in a failed backup method to reestablish PC levels as indicated by the second steep decline in abundance at 24 hours (FIGURE 4.4D). While the reasoning for the trends in lipid behavior in response to Met-Hcy+ media is speculative and requires further study, these hypotheses may be of interest to further investigate considering the connection of phospholipid synthesis and methionine metabolism. The connection between the responses of choline and glutathione in this system is not as clearly linked and will require further study to understand the connection between these two metabolites in the context of lipid metabolism.

In addition to PC and PE, sphingolipids are structural membrane lipids that are interconnected with the Kennedy pathway but are not directly linked to methionine metabolism.

In a non-reversible reaction, small amounts of phosphoethanolamine can be generated through the degradation of the sphingolipid ceramide by sphingosine-1-phosphate lyase. Phosphoethanolamine can then be further processed by the CDP-ethanolamine branch of the Kennedy pathway to produce PE (Gibellini and Smith, 2010; Hannun et al., 2001). In a reversible reaction, ceramide can receive a phosphocholine headgroup from PC, through the action of sphingomyelin synthase, yielding sphingomyelin and diacylglycerol (FIGURE 4.5A) (Tafesse et al., 2006). In our analysis, MB468 ceramide levels decrease in a similar fashion to PC and PE but recover to steady-state levels after 8 hours post media switch (FIGURE 4.5B), whereas MB468res-R8 ceramide levels are unaffected (FIGURE 4.5C). Similar to the PE profile, sphingomyelin levels indicate a partial recovery after 24 hours in MB468 cells (FIGURE 4.5D). In contrast, MB468res-R8 sphingomyelin abundances are unaffected and have similar abundance profiles as ceramide, PE, and PC (FIGURE 4.5E). Despite the connection to the Kennedy pathway, it is unlikely that sphingolipids would play a large part in the response to methionine stress in terms of biosynthesis but rather from a signaling perspective. Recent research has identified the bioactive role of sphingolipids, particularly ceramide, in cell growth, differentiation, senescence, and apoptosis (Hannun and Obeid, 2002). Although we cannot interpret such sphingolipid signaling programs from our data, it is worth taking note for future analyses.

Triglycerides respond to homocysteine media in a cell line specific manner

Triglycerides are esters derived from glycerol and three fatty acid chains and are well known as cellular energy reservoirs. Energy can be harvested from triglycerides by release of the fatty acid chains by lipases and further oxidized in the mitochondria (Santos and Schulze, 2012).

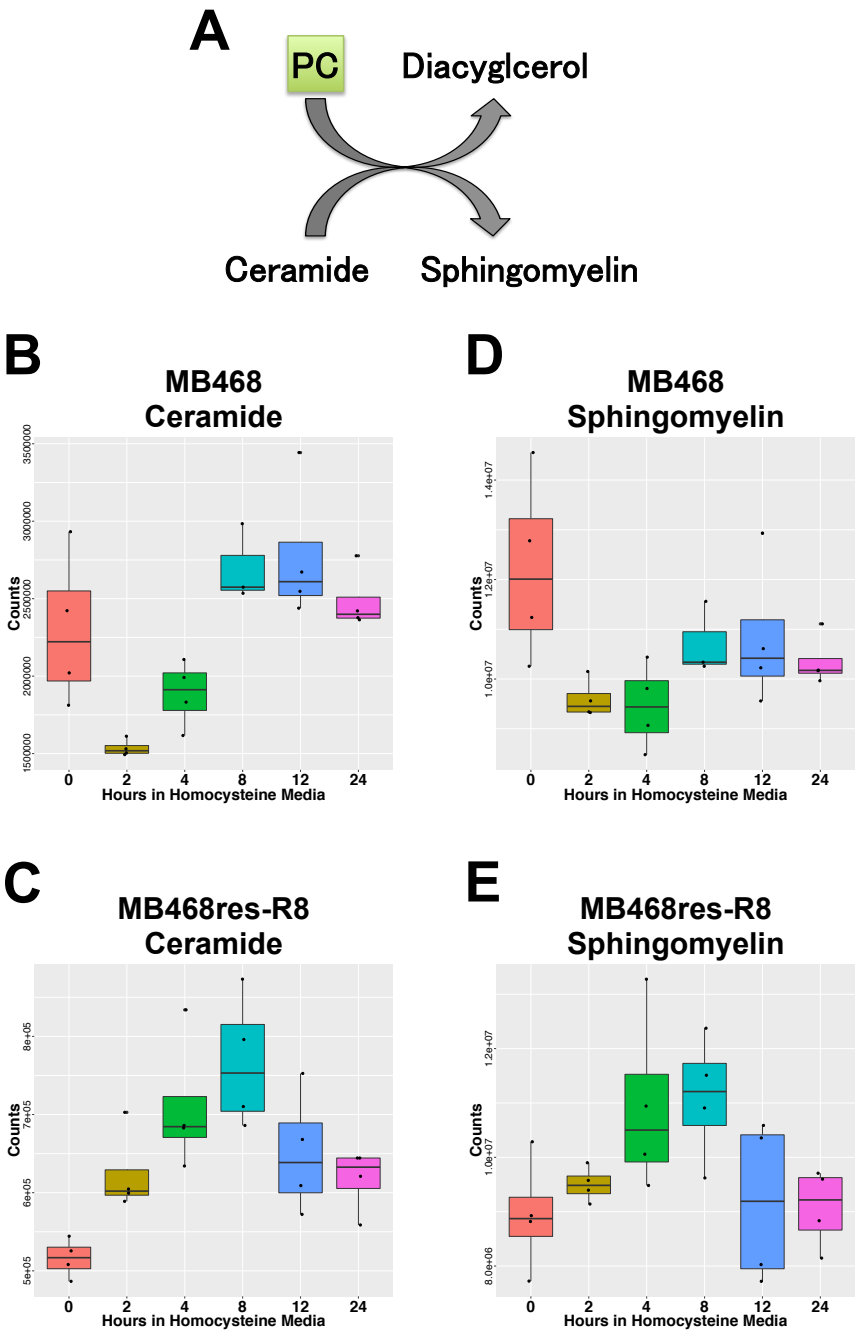

Figure 4.5 *Sphingolipids in response to homocysteine media*
A) A schematic of sphingomyelin synthesis from ceramide and phosphatidylcholine (PC). By way of sphingomyelin synthase (SMS), ceramide takes the phosphocholine head group of PC yielding sphingomyelin and diacylglycerol. B) MB468 and C) MB468res-R8 lipid species in the ceramide lipid class were combined and peak height averages for each replicate is plotted for each time point post homocysteine media switch. D) MB468 and E) MB468res-R8 lipid species in the sphingomyelin lipid class were combined and peak height averages for each replicate is plotted for each time point post homocysteine media switch.

In addition to their use for energy, triglycerides can also be broken down by lipolysis into glycerol and free fatty acids for use as building blocks for other lipids including diacylglycerols. As indicated by our global analysis of lipids in Met-Hcy+ media over time (FIGURE 4.2), it is clear that triglycerides respond to the metabolic stress of Met-Hcy+ in a completely different way from the other lipid classes. In MB468 cells, the same steep drop in abundance is observed at 2 hours post media switch in triglycerides similar to PC and PE's, however, the recovery in abundance within 8 hours is a unique behavior to the class and cell line (FIGURE 4.6A). In contrast, MB468res-R8 triglyceride abundances plummet at 4 hours and show a partial recovery only at 24 hours (FIGURE 4.6B).

Excess citric acid from the citric acid cycle can be transported from the mitochondria to the cytoplasm and converted to acetyl-CoA for use in fatty acid synthesis (Bhaduri and Srere, 1963). Citric acid was measured by untargeted metabolomics in MB468 and MB468res-R8 cells cultured in Met+ or Met-Hcy+ media at 2, 4, 8, 12, and 24 hours (FIGURE 4.6C). In MB468 cells, citric acid levels decrease after 2 hours to approximately three-quarters of the starting abundance as triglycerides increase after the two hour depletion event. In MB468res-R8, citric acid levels almost double with 2 hours post media switch and return to starting levels at 24 hours whereas triglyceride levels decline at 4 hours but approach starting levels at 24 hours. The starting abundance of citric acid in MB468 is more than four times greater than MB468res-R8, which may have an important role in triglyceride synthesis for use as energy storage. As a provider for cellular building blocks, we do not observe a recovery in diacylglycerides that could aide in the reestablishment of PC. In MB468res-R8 cells, triglyceride depletion and recovery could be attributed to cell cycle progression and the synthesis of lipids such as PC and PE for cell membranes.

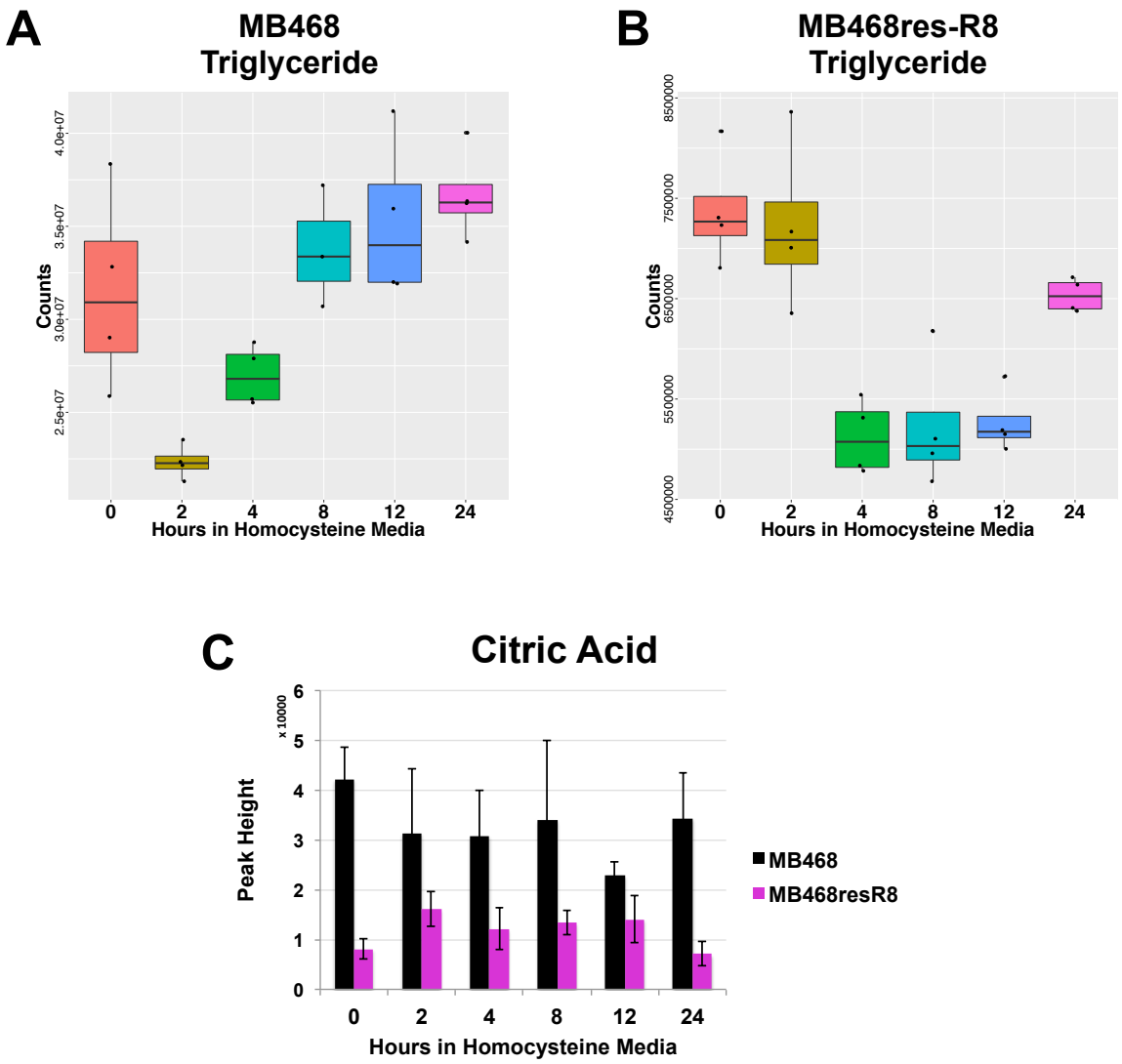

Figure 4.6 *Triglyceride use in MB468 and MB468res-R8 cells cultured in homocysteine media*

A) MB468 and B) MB468res-R8 lipid species in the triglyceride lipid class were combined and peak height averages for each replicate is plotted for each time point post homocysteine media switch. B) Citric acid levels for MB468 (*black*) and MB468res-R8 (*magenta*) cells were measured by GCTOF MS. Error bars represent standard deviation.

DISCUSSION

Understanding the connection between metabolites in the methionine pathway and lipid metabolism is essential for human disease. On a clinical level, high homocysteine levels in the plasma, or hyperhomocysteinemia, is common in patients with heart disease and liver dysfunction (Clarke et al., 1991; García-Tevijano et al., 2001; Gulsen et al., 2005). As a result, patients exhibit hepatic steatosis, or "fatty liver", which is characterized by an accumulation of large lipid droplets (Werstuck et al., 2001). Although this connection with homocysteine and steatosis has been observed and analyzed in patient studies, the molecular mechanism that causes this phenotype is yet to be fully understood.

One way homocysteine has been shown to cause cellular damage and lipid accumulation is by activation of the ER unfolded protein response (UPR) and sterol regulatory element-binding protein 1 (SREBP-1). High homocysteine levels induce protein misfolding and activate the UPR, which results in an upregulation of protein folding chaperones, inhibition of translation, and degradation of misfolded proteins (Basseri and Austin, 2012; Werstuck et al., 2001). In parallel, activation of SREBP-1, an ER-membrane bound transcription factor, increases transcription of key genes in cholesterol and triglyceride biosynthesis and uptake pathways. As a result, cholesterol and triglyceride accumulation is considered a consequence of increased production and defective secretion (Werstuck et al., 2001). Other groups have determined a similar defect in triglyceride accumulation and immobilization when SAM is unavailable (Martinez-Una et al., 2013; Walker et al., 2011). Furthermore, upon SAM depletion in nematodes, methylation-dependent PC biogenesis was reduced while PE levels were unaffected (Walker et al., 2011). Although the enzyme homology differs between nematodes and humans, it

is suggested that SREBP-1 regulates gene expression of enzymes connected to methionine metabolism and phospholipid synthesis.

Other studies have expanded the investigation of lipids and methionine metabolism to various model systems including cancer cells. Beyond homocysteine and SAM, choline has been shown to play a large role in methionine metabolism and lipid synthesis and is associated with cancer malignancy (Glunde et al., 2004, 2011). The difference in choline processing, breakdown and synthesis of phosphatidylcholine, and abundances of these two molecules between normal and cancer cells suggest a reprogrammed lipid metabolism in cancer that encourages metastasis (Cao et al., 2012). In our system, we observe a difference in the homeostatic levels of many metabolites between the triple negative, methionine-dependent breast cancer cell line MB468 and its normal-like, methionine-independent derived clone MB468res-R8. Furthermore, the response to homocysteine media induced methionine stress could not be more dissimilar. To compare the epigenetic, transcriptome, and/or proteome differences that makes these two cell lines unique would allow us to understand why methionine is essential for lipid metabolism in the context of breast cancer.

CHAPTER FIVE

Integration of SAM metabolism and cell cycle regulation by mRNA 5' cap methylation

INTRODUCTION

RNA polymerase II transcripts require multiple modifications to become translationally competent messenger RNAs (mRNA). These modifications include the addition of the 7-methylguanosine cap, exon splicing, and polyadenylation (Bentley, 2005). The addition of the 7-methylguanosine cap at the 5' end is the first RNA modification as it occurs co-transcriptionally by four enzymatic reactions conserved from budding yeast to mammals (Figure 5.1A). The first reaction is performed by an RNA triphosphatase, which prepares the nascent RNA for the guanosine cap by hydrolyzing the 5' triphosphate group to produce a 5' diphosphate group (Figure 5.1B) (Tsukamoto et al., 1997; Yue et al., 1997). The second and third enzymatic reactions are catalyzed by an RNA guanylyltransferase (Shibagaki et al., 1992). GTP is first bound to the guanylyltransferase, forming a GMP intermediate and releasing pyrophosphate (PPi). Subsequently, the enzyme bound GMP is transferred to the 5' diphosphate group on the

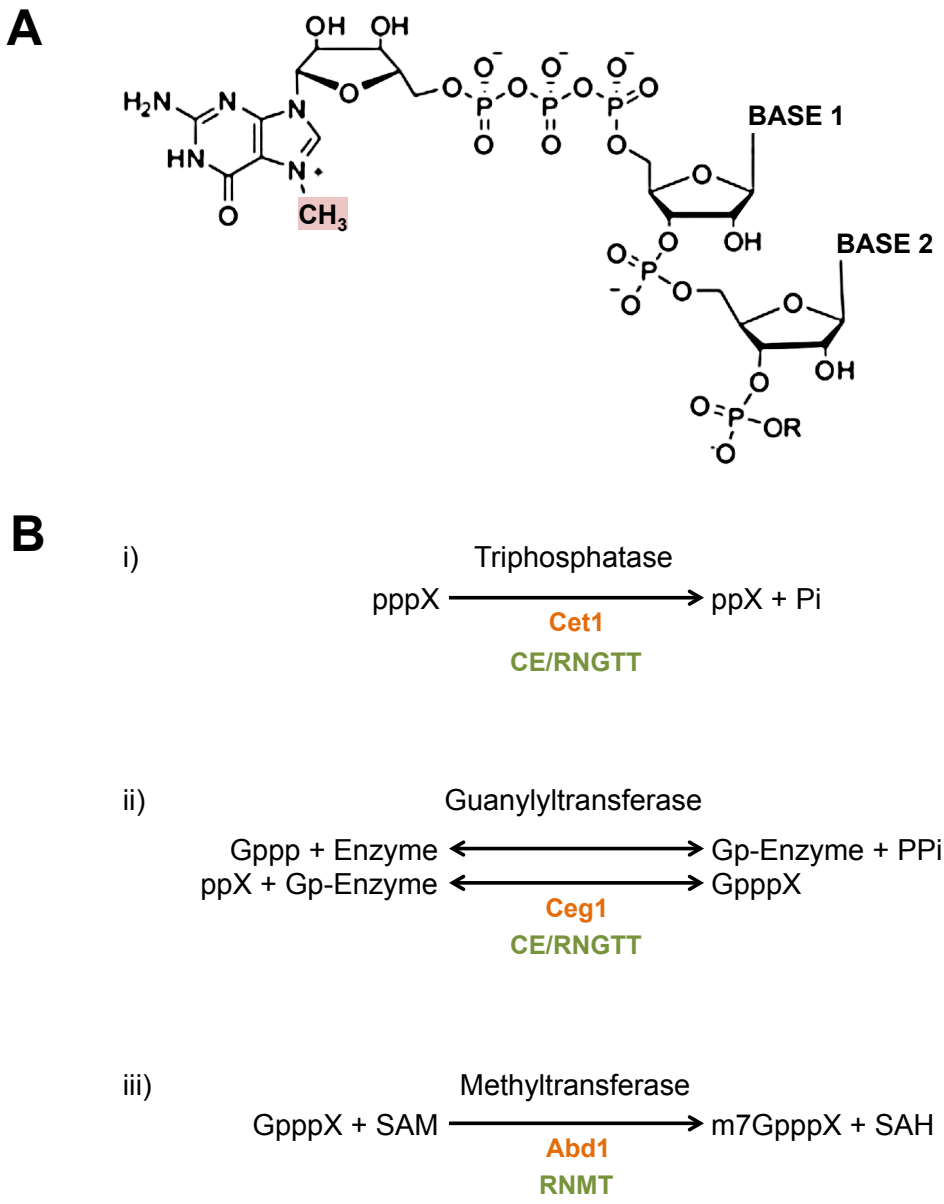

Figure 5.1 *7-methylguanosine mRNA cap*
A) The 7-methylguanosine cap is located at the 5' end of nascent RNA polymerase II transcripts. The structure shown is methylated at the N7 position of the last guanosine nucleotide (highlighted in *red*) and known as cap zero (cap-0). B) The 7-methylguanosine cap is synthesized by four enzymatic reactions carried out by an i) RNA triphosphatase, ii) RNA guanylyltransferase, and iii) RNA (guanine-7-) methyltransferase. The enzyme names are listed below the arrows, *Saccharomyces cerevisae* enzyme s are *orange* and mammalian enzymes are *green*. G = terminal guanosine, m7G = terminal 7-methylguanosine, p = phosphate group, X = the first transcribed base.

nascent RNA and the cap is fully formed. The fourth reaction is the methylation of the 5' cap by an RNA methyltransferase and the methyl donor S-adenosylmethionine (SAM) (Mao et al., 1995). In both yeast and mammals, capping and cap methylation are two independent processes. In *S. cerevisiae*, triphosphatase and guanyltransferase activities are contained within the two enzymes of Cet1 and Ceg1, respectively (Shibagaki et al., 1992; Tsukamoto et al., 1997). In mammals, these two enzymatic activities are found in a single polypeptide called capping enzyme (CE) or RNA guanylyltransferase and 5' triphosphatase (RNGTT) (Yamada-Okabe et al., 1998; Yue et al., 1997). In both species, the RNA methyltransferase is a distinct protein known as Abd1 in yeast and RNA (guanine-7-) methyltransferase (RNMT) in mammals (Mao et al., 1995). The conserved separation of capping and cap methylation activities may suggest differential regulation and important roles for each function.

The 7-methylguanosine cap has an influential role of pre-mRNAs including stability, splicing, nuclear export, and translation. The cap plays an important role in RNA stability as early studies demonstrated a greater stability of capped and methyl capped RNAs to uncapped RNAs with little difference between the two capped forms (Furuichi et al., 1977; Green et al., 1983). However, recent studies have elucidated decapping mechanisms in both yeast and mammalian systems that are selective for incomplete, unmethylated guanosine caps (Chang et al., 2012a; Jiao et al., 2013). Once the cap is removed, the decapping enzyme or associated exoribonuclease degrades the RNA in a processive 5' to 3' manner. Splicing is also dependent on the 7-methylguanosine cap. When substituted with a cap analog or completely removed, splicing defects are observed with a prominent impact at the first intron (Edery and Sonenberg, 1985; Konarska et al., 1984). Although the severity of splicing defects are gene specific *in vivo*, binding of the 7-methylguanosine cap to components of the cap binding complex (CBC) is

essential for efficient recognition of the 5' splice site (Izaurralde et al., 1994; Ohno et al., 1987; Schwer and Shuman, 1996). In mammals, the mRNA 5' methyl cap is also necessary for nuclear export. Binding between the methyl cap and the CBC is required for interactions with mRNA export machinery, which results in exportation to the cytoplasm for protein translation (Cheng et al., 2006). With the exception of mRNAs with an internal ribosome entry site, the presence of a 7-methylguanosine cap is imperative for recognition by the translation initial factor eIF4E and thus protein translation (Muthukrishnan et al., 1975; Schwer et al., 2000). The methylated form of the 5' cap is necessary for efficient binding to protein complexes, which result in a mature mRNA transcript and translated protein (Figure 5.2). Although this modification occurs at the earliest point of transcription, it may not be as constitutive as previously thought and has potential for regulation of protein expression.

In the past decade, investigations of capping and cap methylation have endeavored into the regulation behind these cell functions. While no dedicated 5' methyl cap demethylase has been identified to date, decapping activity on fully capped, unmethylated transcripts have been identified as previously mentioned (Chang et al., 2012b; Jiao et al., 2013). This regulation is suggested to be a means of quality control for transcripts not bound to the CBC or protein translation complexes and thus specifically target "translationally incompetent" transcripts. In contrast, upregulation of mRNA cap methylation has been linked to transcription factor c-Myc expression and RNMT phosphorylation (Aregger et al., 2016; Cole and Cowling, 2009; Cowling and Cole, 2007). In the context of c-Myc, overexpression results in increased transcription and cap methylation of c-Myc target genes with a greater effect on cap methylation (Cole and Cowling, 2009). RNMT phosphorylation by cell cycle regulators aide in coordinating increased cap methylation and protein translation following mitosis (Aregger et al., 2016). Although not a

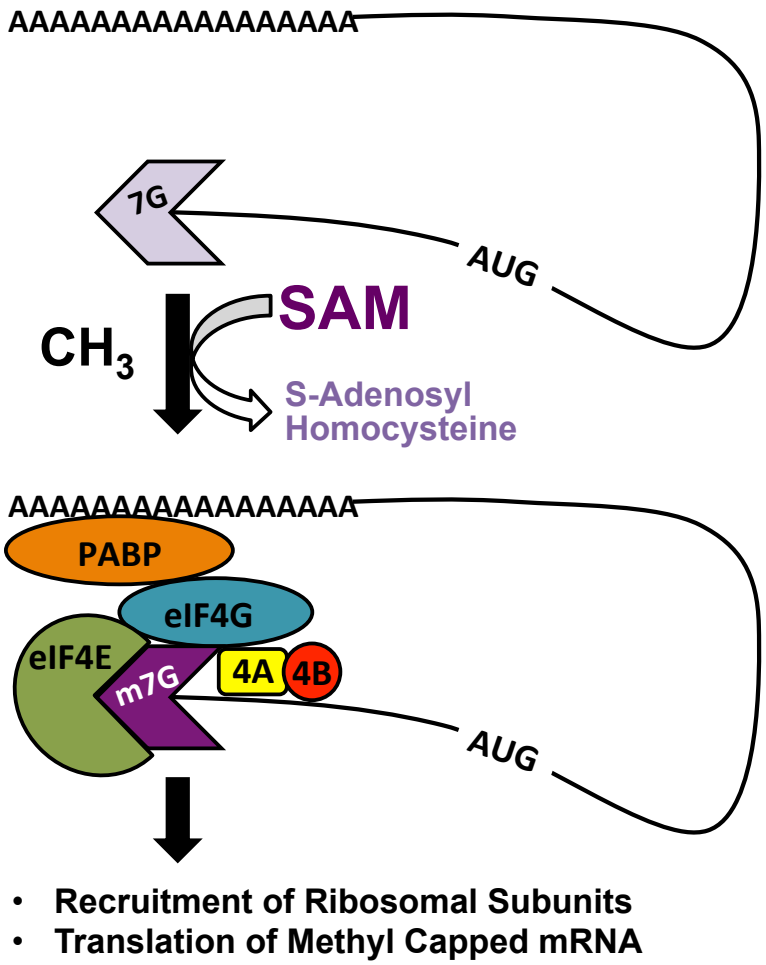

Figure 5.2 *SAM is a co-factor for RNA 5' cap methylation*
S-adenosylmethionine (SAM) is a necessary metabolite for the methylation of the mRNA 5' cap. Once methylated, the cap is recognized by the cap binding complex for export to the cytoplasm and bound by translation initiation factor 4E (eIF4E) which recruits protein translational machinery.

direct methylation on the cap, the mRNA m6A modification in the 5' untranslated region of mRNA (UTR) has been shown to bypass cap dependent translation in response to cellular stresses (Meyer et al., 2015). The discovery that increased m6A methylation in the 5' UTR can upregulate translation of transcripts during stress may suggest that regulated methylation of the 5' cap during cellular and metabolic stress may also exist.

The importance of the 5' methyl cap has been known and characterized for decades. As we delve further into the connections of different cell processes including metabolic pathways and cell cycle machinery, cap methylation seems to be a promising mechanism to serve as a way to communicate within the cell. Our studies use both human cell lines and yeast wild-type and mutant strains to characterize cap methylation during methionine stress and SAM depletion. We use a monoclonal antibody specific for the RNA methyl cap and have identified a transcript dependent response to SAM depletion. We hypothesize that regulation of methylation on the cap may help cells sense nutrient levels once they fall below a specific threshold and induce cell survival mechanisms to prevent use of the limited resources available.

RESULTS

Global protein translation decreases during methionine stress in MB468 breast cancer cells

To investigate the global effect of translation during methionine stress, we employed the methionine-dependent and -independent MDA-MB-468 breast cancer cell line pair (Booher et al., 2012; Borrego et al., 2016). The majority of cancer cell lines exhibit a methionine dependent phenotype and cannot proliferate when methionine (Met+) is replaced with its metabolic precursor, homocysteine (Met-Hcy+). Using the triple negative, methionine-dependent breast cancer cell line MDA-MB-468 (shortened to MB468) we have derived the methionine-

independent derivative, MB468res-R8, that has a similar proliferation rate in Met+ media as the parental line but continues to grow in Met-Hcy+ media unlike MB468 cells.

MB468 cells cultured in Met+ or Met-Hcy+ media for 48 hours were analyzed by polysome profiling to measure global translation. Sucrose density gradient centrifugation was used to separate ribosomal complexes and fractions were measured at 260 nm (Figure 5.3A). As compared to normal Met+ growth media, Met-Hcy+ media reduced polysomes and subsequently increased ribosomal monomers indicating an overall decrease in translation. Similar results were observed during nascent protein labeling of MB468 and MB468res-R8 cells cultured in Met+ and Met-Hcy+ media for 48 hours (Figure 5.3B). Incorporation of the alanine amino acid analog is only reduced in MB468 cells cultured in Met-Hcy+ growth medium. Previous work in this system eliminate altered RNA expression or increased protein degradation as explanations but rather suggest a pre-translation regulation during methionine stress (Keith Booher, personal communication).

7-methylguanosine capped but not unmethyled capped or uncapped mRNA is detected by an anti- 2, 2, 7-trimethylguanosine monoclonal antibody

Many factors from RNA Polymerase II interacting proteins to translation initiation factors are involved in the maturity of pre-RNAs. To identify the factor that is responsible for reduced translation during methionine stress we focused on the cellular metabolite and principal methyl donor S-adenosylmethionine (SAM). SAM is not only the co-factor for RNA 5' cap methyltransferases in both mammalian and yeast, but supplementation of SAM can rescue proliferation defects associated with methionine stress in MB468 cells (Figure 5.2)(Booher et al., 2012). To monitor cap methylation in human cells and yeast, we used a monoclonal antibody

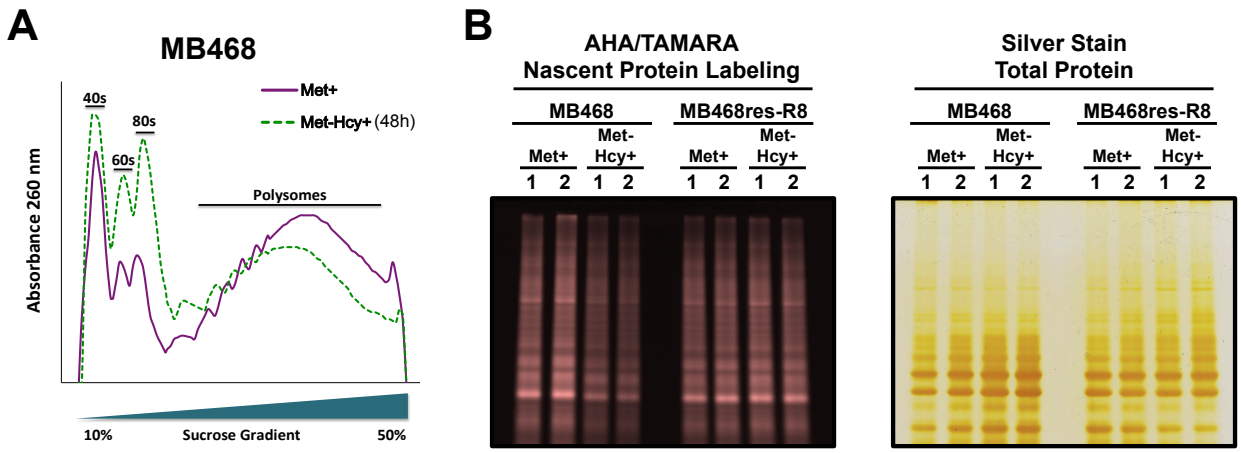

Figure 5.3 *Global protein translation is reduced in the methionine-sensitive breast cancer cell line MB468 when cultured in homocysteine media*

A) Cell extracts from MB468 cells cultured in methionine (Met+, *purple*) or homocysteine (Met-Hcy+, *green*) media for 48 hours were separated on sucrose gradients and absorbance measured at 260 nm. B) Translation rates were measured by L-azidohomoalanine (AHA) labeling for 2 hours after MB468 and MB468res-R8 cells were shifted to homocysteine medium (Met-Hcy+) for 48 hours. Experiment is shown in duplicate.

against the 2, 2, 7–trimethylguanosine RNA cap, which has been shown to detect both trimethylated and 7-methylguanosine caps (Bochnig et al., 1987; Cowling and Cole, 2007; Moteki and Price, 2002). We validated binding to human and yeast capped RNA using total RNA samples and uncapped, *in vitro* transcribed actin transcripts (Figure 5.4A). Human and yeast total RNA samples were combined with uncapped actin transcripts from yeast and human, respectively (Human RNA + scActin, Yeast RNA + hActin), immunopurified with the anti-2, 2, 7-trimethylguanosine cap antibody, and input, supernatant, and elution fractions were analyzed by real-time PCR (Figure 5.4B and 5.4C). In both "Human RNA + scActin" and "Yeast RNA + hActin" mixtures, only the endogenous forms of actin were detected in the elution fraction. These results indicate that the 2, 2, 7-trimethylguanosine antibody is unable to bind uncapped RNAs.

To further validate the specificity of the trimethylguanosine antibody for methyl capped RNAs we used a yeast temperature-sensitive (ts) RNA methyltransferase *ABD1* mutant strain (*abd1-8*) (Figure 5.5A) (Schroeder et al., 2004). When cultured at the permissive temperature (25°C) the enzyme is active and cells are viable but at the non-permissive temperature (37°C) Abd1 activity is reduced and cell growth is inhibited (Figure 5.5B). Cultures collected at both permissive and non-permissive temperatures were immunopurified with the trimethylguanosine antibody and input, supernatant, and elution fractions were analyzed by real-time PCR (Figure 5.5C and 5.5D). U5 splicesomal RNA was included in the analysis as it is a trimethylated RNA that requires Abd1 for the priming methylation of its cap before the second and third methyl groups can be added. Both actin and U5 transcripts are present in the elution fraction of samples cultured at the permissive temperature and both decrease when cultured at the non-permissive temperature, when Abd1 activity has been reduced. These results suggest that the anti-2, 2, 7-

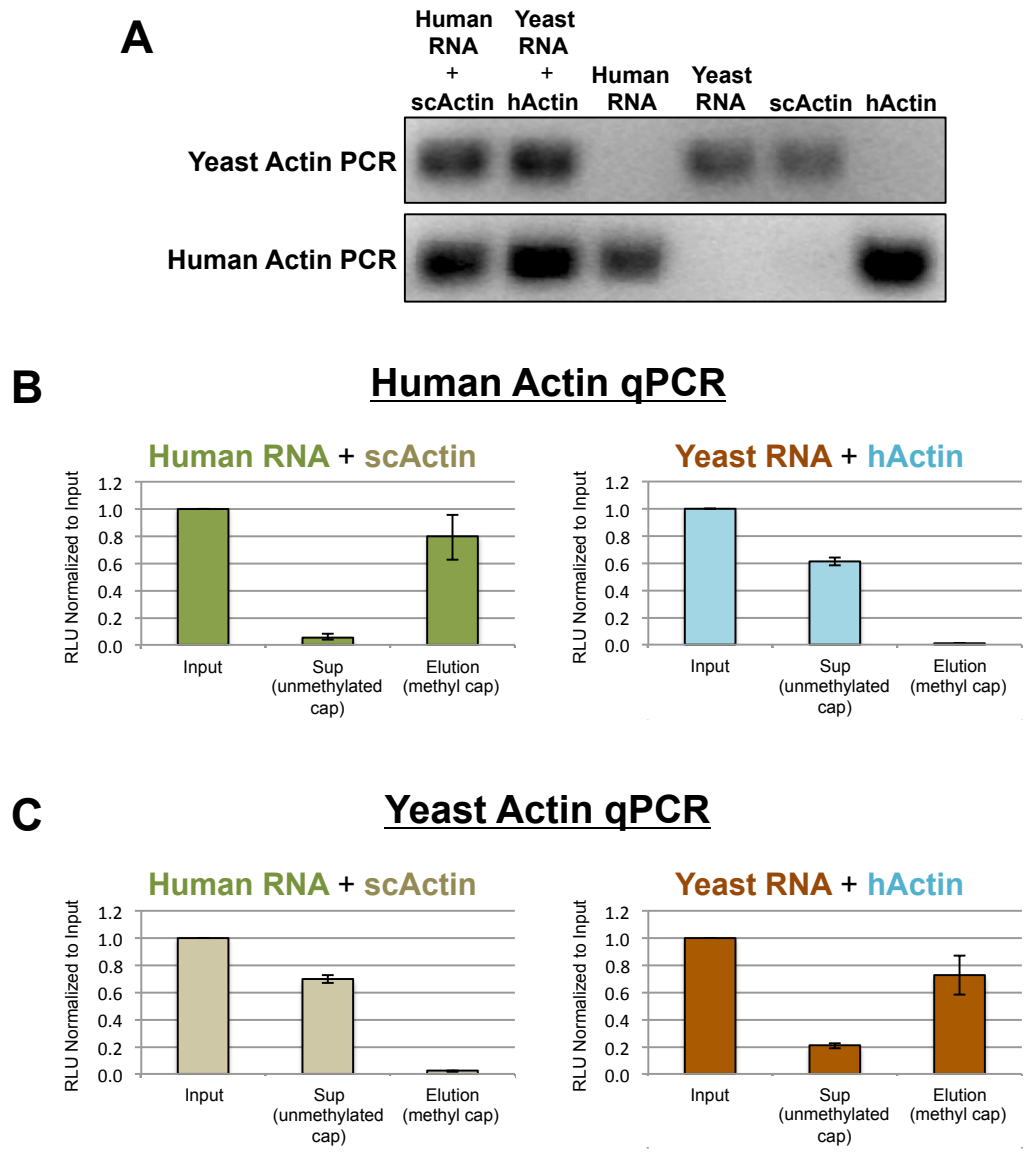

Figure 5.4 *Anti-2,2,7- trimethylguanosine monoclonal antibody specifically detects capped mRNAs*

A) In vitro transcribed, non-capped RNAs were prepared from human ACTB (hActin) and yeast ACT1 (scActin) gene sequences and combined with total RNA from human (Human RNA) and yeast (Yeast RNA) samples to test for primer specificity. Human and yeast ACTB PCRs was performed on the human/yeast mixed samples (Human RNA + scActin, Yeast RNA + hActin), total RNA (Human RNA, Yeast RNA), and in vitro transcribed RNA (scActin, hActin). Samples were run on a 1% agarose gel stained with ethidium bromide.

B) Human/yeast mixed samples (Human RNA + scActin, Yeast RNA + hActin) were immunopurified with anti-2, 2, 7 trimethylguanosine monoclonal antibody and input, supernatant, and elution fractions were analyzed by real-time PCR for human ACTB. C) Same as B except samples were analyzed by real-time PCR for yeast ACT1.

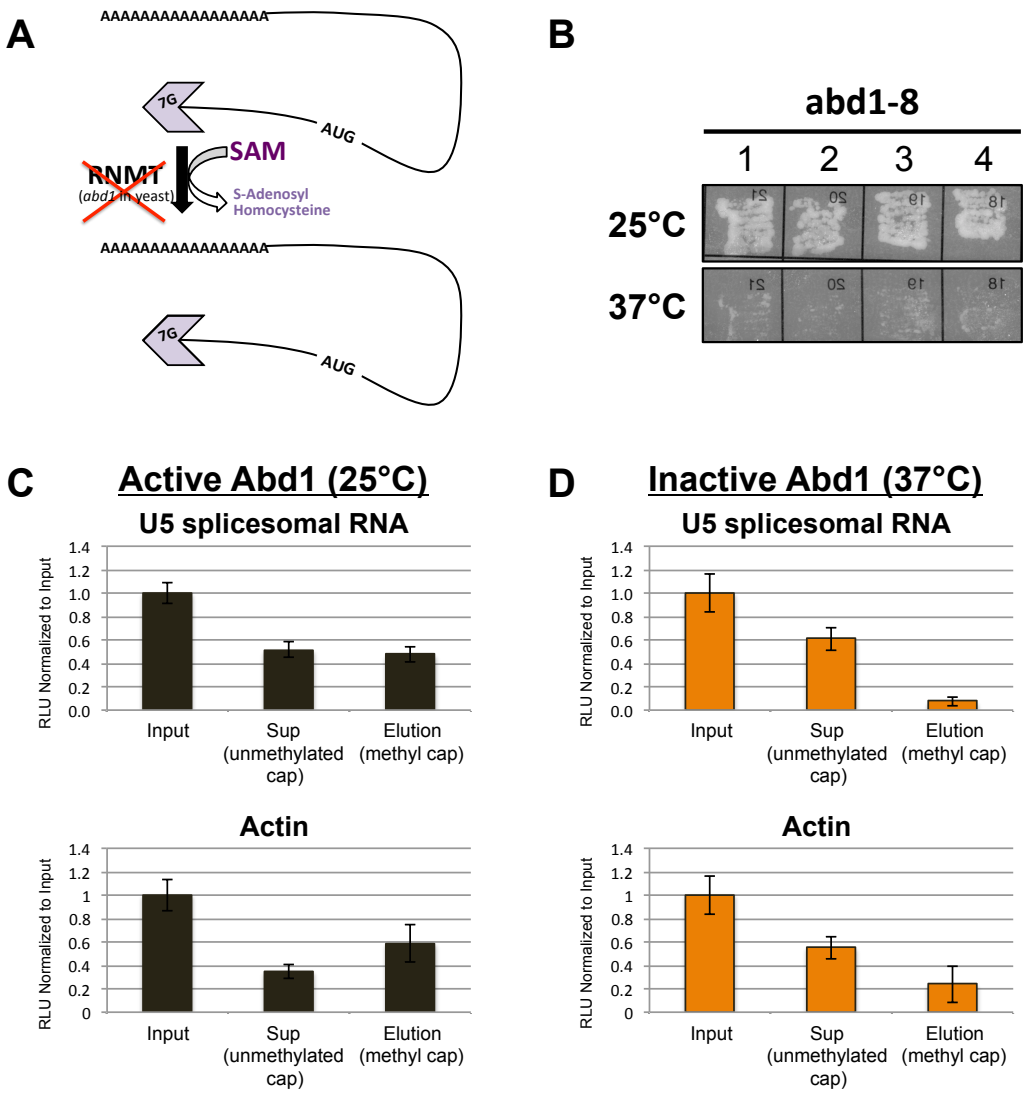

Figure 5.5 *Anti-2, 2, 7-trimethylguanosine monoclonal antibody specifically detects methylated, capped mRNAs*

A) Human (RNMT) and yeast (Abd1) RNA (guanine-7-) methyltransferases use SAM as a co-factor for 5' cap methylation. In the absence of a cap methyltransferase, the 5' guanosine cap is not methylated and cells are not viable. B) *Saccharomyces cerevisiae abd1-8* ts mutants were cultured on YEPD plates and incubated at 25°C (permissive – active Abd1) or 37°C (non-permissive – inactive Abd1) for 48hrs. Four different colonies of *abd1-8* are shown. C) *abd1-8* ts mutant strain were grown in YEPD at 25°C until early log phase, switched to D) 37°C YEPD, and cultured for 3 hours at 180 rpm. RNA samples were immunopurified with anti- 2, 2, 7 trimethylguanosine monoclonal antibody and input, supernatant, and elution fractions were analyzed by real-time PCR for the trimethylated U5 splicesomal snRNA and Actin. Data shown represents the average of three independent studies, error bars indicate standard deviation.

trimethylguanosine antibody is specific for methyl capped RNAs and is an invaluable tool to monitor cap methylation.

SAM depletion alters cap methylation in a transcript dependent manner

Previous work in the Kaiser lab indicates that the substitution of homocysteine for methionine results in reduced SAM levels, pre-replication complex (pre-RC) instability, cell cycle arrest, and ultimately cell death (Booher et al., 2012; Borrego et al., 2016; Lin and Gregory, 2014). In yeast, intracellular SAM depletion activates the transcription activator Met4, which results in cell cycle arrest as well (Kaiser et al., 2006b). The replication factor cell division cycle 6 (Cdc6) was identified as a protein effected by SAM depletion and the responsible factor for pre-RC instability (Booher et al., 2012). In contrast to other pre-RC components, Cdc6 total protein levels decreased during SAM depletion with no change in mRNA expression or rate of degradation. We hypothesize that select proteins, such as Cdc6, are regulated by cap methylation and serve as SAM sensory proteins, preventing the cell from partaking in SAM and other nutrient consuming activities when they are not available.

To test our hypothesis, we used a SAM auxotrophic yeast strain (*Δsam1 Δsam2)* to measure the effects of SAM depletion on cap methylation over time. When cultured on nutrient rich YEPD agar plates, the *Δsam1 Δsam2* double mutant is not viable unless exogenous SAM is provided (Figure 5.6A). In the absence of SAM, methylation reactions cannot take place including RNA 5' cap methylation (Figure 5.6B). To measure cap methylation during SAM depletion, *Δsam1 Δsam2* double mutant cultures were grown in medium supplemented with SAM and then switched to growth medium without SAM. Cells were collected at 0, 5, 10, 20, 30, and 60 minutes post-media switch (Figure 5.6C). Samples were immunopurified with

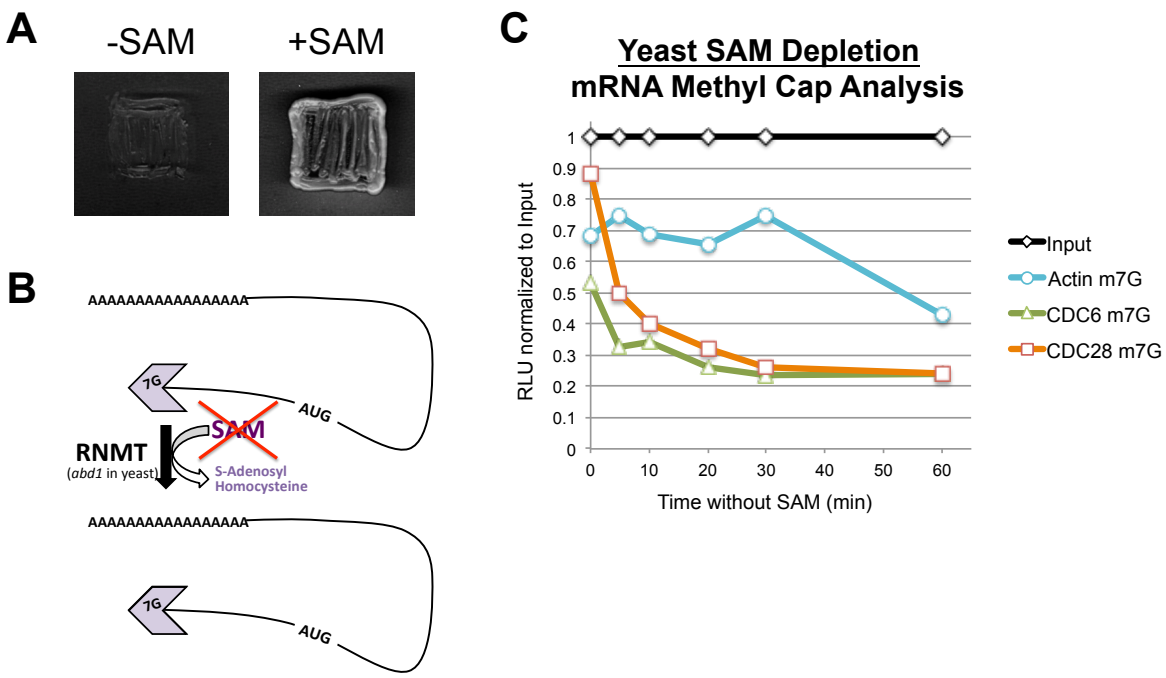

Figure 5.6 *Capped and methyl capped levels respond to SAM depletion in a transcript dependent manner*

A) The *Saccharomyces cerevisiae Δsam1 Δsam2* double mutant (PY852) are SAM auxotrophic and not viable in the absence of SAM. Cells were cultured for 48 hours (30°C) on YEPD plates with or without 0.4 mM SAM supplementation. B) Abd1, the yeast RNA (guanine-7-) methyltransferase, requires SAM as a methylation co-factor. C) *Δsam1 Δsam2* double mutants (PY852) were grown in YEPD supplemented with 0.4 mM SAM until early log-phase, switched to YEPD without SAM, and collected at the times indicted. RNA samples were immunopurified with anti- 2, 2, 7-trimethylguanosine monoclonal antibody and input, supernatant, and elution fractions were analyzed by real-time PCR for ACTIN, CDC6, and CDC28 (cyclin dependent kinase). Samples are normalized to input at each time point.

anti-2, 2, 7-trimethylguanosine antibodies and input, supernatant, and elution fractions were analyzed by real-time PCR for actin, *CDC6*, and cyclin-dependent kinase *CDC28*. A unique, transcript dependent response to SAM depletion was observed in the elution fractions.

It is interesting to note the different steady-state levels of cap methylation as compared to input for each transcript even in the presence of abundant SAM in the growth medium. The majority of *CDC28* (90%) and actin (70%) transcripts are methyl capped whereas only 50% of *CDC6* mRNAs are methyl capped. This difference in methylated mRNA proportions is not only observed in the mutant yeast strains but in wild type yeast as well. Furthermore, the starting level of methyl capped RNAs does not seem to affect the response to SAM depletion. Comparing starting methyl cap levels of *CDC28* and *CDC6*, one might expect that these transcripts would behave very differently. Surprisingly, both transcripts show an immediate reduction of cap methylation within 5 minutes of SAM depletion and reach 50% of starting levels at 10 (*CDC28*) and 20 (*CDC6*) minutes. In contrast, actin cap methylation remains fairly stable until 60 minutes post-media switch, at which time cap methylation levels approach 50% of the starting level.

Taken together, these results suggest that cap methylation may have a transcript dependent effect. With *CDC6* as an example, it seems that cap methylation may be a means of regulation for cellular proteins that have a large impact on cell function in response to SAM depletion (Booher et al., 2012). This reasoning would also explain the delayed reduction observed in actin cap methylation during SAM depletion as reduced actin in the cell could have pleiotropic effects on cell physiology. Transcripts highly sensitized to fluctuations in SAM levels are likely sensors that trigger selective pathways to react to nutrient limitation before overall cell integrity is compromised. We envision such sensors for example in cell cycle control pathways

(*CDC6* and *CDC28*) that trigger checkpoint-type cell cycle arrests and allow cells to modulate metabolic pathways to respond to nutrient limitation.

Cap methylation on a global scale

Our results using the trimethylguanosine antibody indicate that we have developed a robust method to monitor cap methylation in both human and yeast samples. We also obtained that transcripts behave differently in response to SAM depletion. To identify more SAM sensitive transcripts we expanded our analysis using the high-throughput method of RNA sequencing (RNAseq). Although several publications describe RNAseq analysis of the m6A RNA modification, methyl cap analysis at the RNAseq level has yet to be shown (Dominissini et al., 2012; Meyer et al., 2012). Using both human MB468 cells cultured in normal Met+ media and a wild-type yeast strain (PY1) cultured in normal YEPD media conditions, we developed a protocol for RNAseq analysis of samples immunopurified by the trimethylguanosine antibody (Figure 7).

This experimental RNAseq indicated that our approach could be scaled to the transcriptome level and provided information on the pitfalls of our technique. Reads for both species indicate the average ratio of input mRNAs to the elution fraction containing methyl capped mRNAs is approximately 1 (human=0.96, yeast = 1.03)(Figure 7A and 7B). Importantly, due to the nature of this experiment we cannot deduce the actual average fraction of methyl-cap RNAs. However, we can identify transcripts that deviate from the average. These transcripts are either undermethylated or hypermethylated on N7 during standard growth conditions as compared to the population average. We therefore identified transcripts that were increased or decreased in the elution fraction as compared to input with a significance cutoff of $p \leq 0.005$.

Genes identified as significant were then analyzed by DAVID to identify enriched functional categories (Figure 7C and 7D) (Huang et al., 2009a, 2009b). In the human sample, high methyl capped transcripts were categorized into cell maintenance functions and low methyl capped transcripts were included in RNA and metabolism functions (Figure 7C). In contrast, ribosome related functions were enriched in the high methyl capped transcripts in yeast but due to the low number of significant genes with low levels of methyl caps, functional analysis was limited and uninformative (Figure 7D). While we did not attempt to compare a SAM depleted sample in either human or yeast, this first RNAseq analysis of our control samples provided our first insight into the homeostatic status of cap methylation on a global view.

In regard to pitfalls, several issues surfaced during our first attempt to prepare samples and analyze results for this RNAseq experiment. Although not useful for the interpretation of the final result, I believe they are worth noting and discussing in regards to this method. It is common to prepare RNAseq libraries by first enriching the sample for poly-A containing mRNAs using poly-T oligo-attached magnetic beads or a similar method removing ribosomal RNA (rRNA) using rRNA probes. We compared the two methods by first poly-A enriching or rRNA depleting total RNA samples before immunopurifying with the trimethylguanosine antibody and analyzing by real-time PCR. The results of the two methods were incomparable with each other but when compared against samples immunopurified from total RNA the rRNA depleted samples best reproduced the same result. This suggests that poly-A enrichment introduces a bias in the RNA sample, likely based on the poly-A tail lengths of different transcripts. This bias can be reduced using rRNA depletion methods. With respect to data analysis, the difference in sample size between input and elution fractions introduced sample normalization issues. In the elution fraction, we expect to find only methyl capped mRNAs,

A

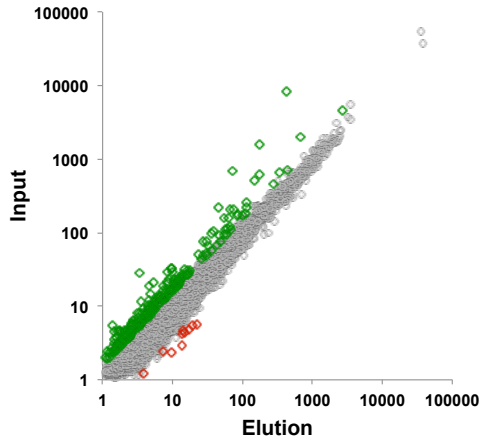

C

MB468 - Increased RNA Methyl Cap

Category	Enrichment Score
Organelle and Mitochondrial Enzymes	2.00
Amino acid biosynthesis	1.58
Kinase/Phosphotransferase	1.46
Gene transcription, Development, and Cytoskeleton	1.34
Protein Transport	1.31
Negative Regulator of Protein Modification	1.29
Membrane Organization	1.20

MB468 - Decreased RNA Methyl Cap

Category	Enrichment Score
RNA binding	3.72
Nucleus	2.67
Glutathione Metabolism	1.74
RNA processing	1.23
FAD and Oxidoreductase	1.21

B

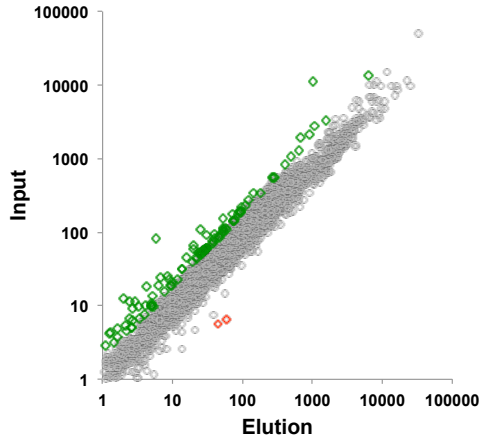

D

Yeast - Increased RNA Methyl Cap

Category	Enrichment Score
Ribosomes	6.10
Cellular Homeostasis	1.29
RNA Processing and Ribosomal biogenesis	1.26

Yeast - Decreased RNA Methyl Cap

Category	Enrichment Score
Membrane Proteins	1.89

Figure 5.7 *RNA cap methylation varies between species and may have a regulatory role for transcripts with similar functions*

Samples from A) human MB468 breast cancer cells and B) *S. cerevisiae* background strain PY1 were cultured in normal culturing conditions, immunopurified with anti- 2, 2, 7-trimethylguanosine monoclonal antibody, and analyzed by RNA sequencing. In homeostatic conditions the majority of RNAs are methyl capped at a ratio of 1 as compared to input (grey points). Transcripts that deviate by two standard deviations above (*red*) and below (*green*) the average ratio are indicated. In C) and D) transcripts with a significant difference in methyl cap ratio ($p \leq 0.005$) were analyzed with DAVID – the Database for Annotation, Visualization, and Integrated Discovery. Categories with an enrichment score above 1 are shown for both increased and decreased fractions of methyl caps.

which results in a smaller sample than the input fraction and thus a normalization factor must be included. In this study, we used statistical normalization methods to address this issue, however, a more effective method will require an RNA control spike-in. The National Institute of Standards and Technology (NIST) has developed an RNA spike-in control of 92 transcripts that can be analyzed with bioinformatics packages available in the programming language R (Jiang et al., 2011). Including this control in future methyl cap RNAseq experiments will be essential to obtain reproducible and valid results.

DISCUSSION

SAM is essential for faithful duplication of epigenetic marks during DNA replication, chromatin methylation and gene expression, and protein function to name a few important roles. It is therefore reasonable to suggest that a regulatory mechanism would be in place to notify the cell when SAM levels are becoming low and unavailable for necessary methylation reactions. The mRNA 5' cap is the perfect opportunity for the cell to control cellular functions in response to SAM levels. The 5' cap has the potential to be a dedicated SAM sensor and it's methylation status may be regulated on genes capable of preventing SAM and other nutrient depleting activities when SAM is unavailable.

Although nutrient sensing pathways such as mTORC1 exist to induce a cell cycle arrest during nutrient limitation, previous work in MB468 cells indicate that SAM depletion does not affect factors involved in this pathway (Booher et al., 2012). In yeast, however, SAM availability can regulate autophagy through the action of specific methyltransferase enzymes (Sutter et al., 2013a). When methionine levels are low, intracellular SAM decreases and methylation of protein phosphatase 2A (PP2A) is eliminated, resulting in an induction of autophagy. In this

system, SAM serves as an amino acid indicator and when unavailable induces a methyltransferase-dependent response outside of the traditional mTORC1 nutrient sensing pathway. Similar to PP2A regulated methylation, the 7-methylguanosine cap has potential for regulation in a transcript-selective manner. As our results indicate, initial methyl cap levels vary between transcripts possibly indicating some level of regulation in the absence of stress and during SAM depletion it is even more conceivable that this regulatory mechanism would be more active. Therefore, regulation of the mRNA 5' cap is an area of biology that warrants further study as it may be a direct means to communicate the metabolic state of the cell to other cellular functions.

CHAPTER SIX

Discussion

The methionine dependency of cancer is a metabolic vulnerability prime for exploitation. For over 50 years this cancer specific phenotype has been investigated with the hope to identify key factors linking metabolism and malignancy for use in cancer therapeutics. With the ability to target a general cancer feature absent in surrounding normal cells, the development of targeted chemotherapeutics and combined therapeutics can be improved at a level we have yet to reach. While we do not completely understand methionine dependency or how cellular abundances of the metabolite S-adenosylmethionine are communicated in cancer, we have started filling in the gaps.

The methionine-dependent and -independent breast cancer cell pair we have developed has dramatically enhanced our ability to study methionine dependency as it simplifies the interpretation of results and easily identifies cancer specific behaviors. We have generated several methionine-independent derivatives from MB468 cells and characterized their morphologies, proliferation rates, and anchorage independent growth. As previously reported,

reversion to a methionine-independent phenotype results in a spectrum of normal-like cells each with varying degrees of transformed and non-transformed properties (Hoffman et al., 1978, 1979). Within our own derivative cell lines (MB468res) we observe differences in proliferation rates and anchorage dependent growth (Booher et al., 2012; Borrego et al., 2016). Although the final phenotypes of these revertant cell lines have been reported, it is still unknown what chromatin differences exist between these cells and the parental cancer cell line. Further exploration of the DNA methylome and gene expression profiles in both cell types would be valuable to identify genes involved in metabolism dependent transformation.

Using the methionine-dependent, MB468, and -independent, MB468res-R8, breast cancer cell pair we were able to investigate early metabolic responses to methionine stress using mass spectroscopy techniques. Both MB468 and MB468res-R8 cells experience an oxidative stress insult resulting in a redirection of homocysteine metabolism from the remethylation pathway toward the transsulfuration pathway and glutathione synthesis. Interestingly, both cell lines experience oxidative stress but each addresses the issue by increasing levels of the antioxidant glutathione at different times. Both reduced and oxidized glutathione increase in MB468 cells after 12 hours in homocysteine media and within 4 hours in MB468res-R8 cells. The different responses to oxidative stress between the two cell lines suggests a defective self-preservation system in cancer. It almost seems that the high reduced to oxidized glutathione ratio of MB468 cells in normal culturing conditions prevents the detection of cell damaging assaults, resulting in a delayed survival response. As a consequence, lipid damage and downregulation of select metabolic pathways such as the remethylation of homocysteine, polyamine synthesis, and purine and pyrimidine pathways reprogram the metabolic state in cancer cells during methionine stress.

With a large effect on global metabolism, these studies require further assessment at a mechanistic level to fully understand their role in the methionine dependency of cancer.

In addition to oxidative stress, methionine stress results in a decrease of S-adenosylmethionine (SAM) in both methionine-dependent and -independent cells. While the biochemical changes associated with methionine stress are broad, focusing on SAM as a methylation co-factor helps narrow down the molecular effects taking place. In many cases, the methylation of substrates is reversible and in recent studies, select substrates lose their methyl group modification in response to reduced SAM levels (Sutter et al., 2013b). Although the mRNA 5' cap does not have a dedicated demethylase, the initial methylation of select nascent transcripts may also be sensitive to the availability of cellular SAM. Using both human and yeast model systems we were able to investigate the SAM sensitivity of the mRNA 5' cap using a specific methyl cap antibody and RNA sequencing. In yeast, we have identified transcript specific differences in cap methylation in normal homeostatic conditions and a unique loss of methyl capped transcripts in response to SAM deprivation. Interestingly, the cell cycle components cyclin-dependent kinase (Cdk) and cell division cycle 6 (Cdc6) have an immediate decrease in cap methylation despite the difference in the proportions of the methyl capped population in normal culturing conditions. In contrast, methyl capped actin transcripts and other cell cycle component encoding RNAs (Cdc53, Cdc47) show only a very slow loss of cap methylation. These preliminary results suggest that low cellular SAM may be communicated to the cell by select downregulation of mRNA cap methylation on transcripts capable of preventing cell cycle progression in suboptimal SAM conditions. In addition to potential methyl cap regulation by SAM, mTORC1 regulation of translational machinery by way of the mRNA 5' cap is a well established mechanism (Hay and Sonenberg, 2004; Ma and Blenis, 2009). As a

dedicated sensor for nutrient availability, cell stress, and energy sufficiency, the mTORC1 signaling pathway prevents cell cycle progression by modulating protein synthesis. Specifically, mTORC1 regulates phosphorylation of the inhibitory 4E-binding protein 1 (4E-BP1), which prevents the assembly of eukaryotic translation initiation factors on the mRNA 5' cap when 4E-BP1 is hypophosphorylated. Although a connection between SAM depletion and mTORC1 signaling seems likely, SAM limitation actually has little to no effect on mTORC1 activity (Booher et al., 2012; Lin et al., 2013). Therefore, regulation of protein translation by engaging the 5' cap with the ribosome may be regulated by two independent nutrient sensing pathways.

Collectively, the work presented in this thesis contributes to our understanding of methionine dependency in breast cancer from both a biochemical and mechanistic perspective. While metabolomics studies can be complicated and difficult to interpret, our results suggest a cancer-specific delayed survival response to methionine stress. Understanding the timeframe of vulnerability in cancer cells and tumors may allow for more effective treatment combinations implementing methionine stress conditions. Furthermore, regulation of translation by mRNA 5' cap methylation is a novel area of nutrient sensing that has yet to be explored. With a higher demand for substrate methylation and therefore SAM, understanding SAM nutrient sensory pathways is essential to specifically target cancer in a metabolically sensitive area. Further exploration of methionine dependency of cancer will yield promising developments in cancer therapeutics by exploiting a general metabolic characteristic of this disease.

METHODS

CHAPTER 2: A methionine dependent and independent breast cancer cell pair

Cell lines and growth conditions

MDA-MB-468 (shortened to MB468) were maintained in DMEM (Sigma-Aldrich, D0422) supplemented with 10% dialyzed FBS (Gemini Bio-Products), 1.5 μM cyanocobalmin (vitamin B12), 4 mM L-glutamine, 100 μM L-cysteine (Fisher Scientific), and 100 μM L-methionine (Sigma-Aldrich). In the case of methionine-free media, 370 μM DL-homocysteine (Sigma-Aldrich) was added in the absence of methionine.

Resistant cell lines were isolated as previously described (Hoffman et al., 1979). Briefly, MDA-MB-468 resistant clones were isolated after prolonged culturing in methionine-free media. The majority of MDA-MB-468 cells detach; however, resistant clones begin to appear after two weeks. Clones were isolated and proliferation rates were measured using CellTiter-Glo luminescent cell viability assay (Promega).

Both MD468 and MB468res-R8 cell lines were tested for authentication via STR profiling in January 2016 by Genetica DNA Laboratories (a LabCorp brand; Burlington, NC) using the commercially available PowerPlex® 16HS amplification kit (Promega Corporation)

and GeneMapper ID v3.2.1 software (Applied Biosystems). Authentication of each cell line was confirmed by a 100% match to the reference STR profile of MDA-MB-468 (ATCC HTB- 132) cells from ATCC.

Anchorage Independence Assay

To detect anchorage independence of transformed cells, MDA-MB-468 and resistant cell lines were cultured in soft agar for 30 days. Each assay was conducted in a 35 mm Petri dish with a 0.5% agar base layer and 0.35% agar top layer prepared using low gelling temperature agarose (Sigma, A9045) in methionine growth media. The top layer of each assay contained 5,000 cells except for control plates. Assays were maintained at 37°C in a humidified incubator and 0.5 ml methionine growth media containing methionine was added to each plate twice weekly. Colonies were stained with 0.005% crystal violet for 1 hour, washed once with PBS, and manually counted.

CHAPTER 3: Metabolic changes associated with methionine stress sensitivity in MDA-MB-468 breast cancer cells

Cell lines and growth conditions

MDA-MB-468 were maintained in DMEM (Sigma-Aldrich, D0422) supplemented with 10% dialyzed FBS (Gemini Bio-Products), 1.5 μM cyanocobalmin (vitamin B12), 4 mM L-glutamine, 100 μM L-cysteine (Fisher Scientific), and 100 μM L-methionine (Sigma-Aldrich). In the case of methionine-free media, 370 μM DL-homocysteine (Sigma-Aldrich) or 370 μM DL-homocysteine-2H4 (13C Molecular, 12714-158) was added in the absence of methionine.

See Chapter 2 methods for additional cell line information

Anchorage Independence Assay

See Chapter 2 methods

Preparing Cells for Metabolite Extraction

Cells were harvested by first washing attached cells with 10 ml PBS before adding 0.5% trypsin (Life Technologies, 25300-054) for 10 minutes and incubating at 37°C. Cells were collected in complete DMEM (4°C) without methionine or homocysteine and centrifuged (300 x g, 5 min, 4°C), from this point on cells were kept on ice during all processing steps. Cell pellets were washed with 10 ml PBS (4°C) and counted. The appropriate number of cells were aliquoted and centrifuged (300 x g, 5 min, 4°C). Cell pellets were resuspended in 1 ml PBS (4°C), transferred to a pre-weighed microcentrifuge tube, and centrifuged (300 x g, 5 min, 4°C). PBS was aspirated and cell pellets were weighed before flash freezing in liquid nitrogen. Samples were stored at -80°C until shipped on dry ice. This protocol was performed as previously described (Fan, 2012).

Immunoblots

MDA-MB-468 and MDA-MB-468res-R8 cells were cultured in methionine or homocysteine media for 24, 48, 72, and 96 hours. Lysates were prepared in urea buffer (8 M urea, 300 mM NaCl, 0.5% NP-40, 50 mM Na_2HPO_4, 50 mM Tris (pH 8.0), 1 mM PMSF, 1 ng/ml aprotinin) and resolved by 10% SDS-PAGE. Protein levels were detected by immunoblot using MAT2A (Abcam, ab77471) and MAT2B (Abcam, ab86506) antibodies.

FLIM Acquisition and Phasor Data Analysis

MDA-MB-468 and MDA-MB-468res-R8 cells were cultured in methionine or homocysteine media. To inhibit oxidative phosphorylation, cells were treated with 4 mM potassium cyanide (KCN) for 5 minutes before imaging.

FLIM was performed on Zeiss LSM 710 microscope (Carl Zeiss, Jena, Germany) using a 40x water immersion objective, 1.2 N.A. (Carl Zeiss, Oberkochen, Germany) coupled with two photon excitation of 740 nm (titanium:sapphire MaiTai laser from Spectra-Physics, Mountain View, CA). Image scan speed was 25.21 µs/pixel and image size is 256 × 256 pixels. The emission signal was collected using a 460/80 nm bandpass filter and photomultiplier tube (H7422P-40, Hamamatsu, Japan) was used for detection. FLIM data was acquired using A320 FastFLIM FLIMbox (ISS, Champaign, IL). SimFCS software, developed at the Laboratory for Fluorescence Dynamics (LFD, UC Irvine) was employed for both FLIM data acquisition and analysis. FLIM-phasor approach was used for phasor analysis, as described previously (Stringari et al., 2011, 2012a). Briefly, lifetime information from every pixel of the image is transformed into a phasor and plotted on a phasor plot. This can be mapped back onto the image to create the FLIM map.

Extracellular Flux (XF) Analyses

All XF analyses were performed on the Seahorse Bioscience XF24 Extracellular Flux Analyzer (Seahorse Bioscience, North Billerica, MA) using the manufacturer's protocol. Cells were plated in 24-well Seahorse XF-24 assay plates at a density of 90, 000 cells per well in Met+ media (as previously described). After 6 hours, 8 wells were washed with pre-warmed PBS before Met+ media and Met-Hcy+ media were added in 4 wells each. This process was repeated for the 8, 4,

and 2 hour time points. One hour before metabolic flux analysis, cells were washed once with un-buffered, serum-free media (Caisson Labs, DMP39-10XLT) containing 100 uM methionine or 370 μM DL-homocysteine and incubated with un-buffered media at 37°C in a non-CO_2 incubator for 1 hour. Four baseline oxygen consumption rate (OCR) and extracellular acidification rate (ECAR) measurements were taken before sequential injection of the following mitochondrial inhibitors: oligomycin (1 μg/ml), FCCP (0.4 μM) and rotenone (0.1 μM). Four measurements were taken after the addition of each inhibitor and OCR and ECAR values were automatically calculated and recorded by the Seahorse XF-24 software. Basal respiration was calculated by averaging the four measurements of OCR before injection of inhibitors. Basal ECAR values were calculated in the same manner. Spare respiration capacity was calculated by subtracting basal OCR values from OCR values after FCCP treatment.

Metabolomics Analysis

The MiniX database was used as a Laboratory Information Management System (LIMS) and for sample randomization prior to all analytical procedures (Scholz and Fiehn, 2007).

GCTOFMS Analysis

For analysis of primary metabolism, cell lysates, stored at −80°C, were thawed on ice, extracted, derivatized and metabolite levels were quantified by gas chromatography time-of-flight (GC-TOF) mass spectrometry (MS) as previously described (Fiehn et al., 2008). Acquired spectra were further processed using the BinBase database (Fiehn et al., 2005; Scholz and Fiehn, 2007). Briefly, output results were filtered based on multiple parameters to exclude noisy or inconsistent peaks (Kind et al., 2007). All entries in BinBase were matched against the Fiehn mass spectral

library of 1,200 authentic metabolite spectra using retention index and mass spectrum information or the NIST14 commercial library. Data, reported as quantitative ion peak heights, were normalized by the sum intensity of all annotated metabolites (*Equation 1*) and used for further statistical analysis.

Equation 1:

$$metabolite\ ij,normalized = metabolite\ ij,\ raw\ /\ mTIC\ j\ *\ mTIC\ average$$

HILIC-UHPLC-qTOFMS Analysis

For analysis of biogenic amines, cell lysates, stored at -80°C, were thawed on ice, and extracted with ice-cold "degassed" 3:3:2 acetonitrile/isopropanol/ultra-pure water. Supernatant containing extracted metabolites were dried to completeness under reduced pressure and re-suspended in 60 µL of 80:20 ACN/H2O containing an internal Val-Tyr-Val (Sigma Aldrich). Resuspended samples were analyzed on an Agilent 1290A Infinity Ultra High Performance Liquid Chromatography system with an Agilent Accurate Mass-6550-QTOF mass spectrometer. The column (45°C) was a Waters Acquity UPLC BEH (150 mm length x 2.1 mm internal diameter; 1.7 µM particles) coupled with a Waters Acquity VanGuard BEH C18 (50 mm length x 2.1 mm internal diameter; 1.7 µM particles) Pre-column. The solvent system included A) 100% water (LCMS grade) containing 10 mM ammonium formate and 0.125% formic acid and B) 95:5 v/v acetonitrile:water containing 10 mM ammonium formate and 0.125% formic acid. The gradient started from 0 min 100% (B), 0-2 min 100% (B), 2-7.7 min 70% (B), 7.7-9.5 min 40% (B), 9.5-10.25 min 30% (B), 10.25-12.75 min 100% (B), and 12.75-16.75 min 100% (B). The flow rate was 0.4 mL/min and with an injection volume of 5 µL. ESI capillary voltage was +3.5 kV with collision energies of 20 eV MSMS collection in positive acquisition mode. Data was collected at a mass range of m/z 60-1700 Da with a spectral acquisition speed of 4 spectra per second.

Data was processed using MZmine 2.10 software. Metabolites were identified by searching against a precursor accurate mass and retention time library in conjunction with matching tandem mass spectra against the LipidBlast virtual MS/MS database (Kind et al., 2013). Data are reported as peak heights for the quantification ion (m/z) at the specific retention time for each annotated and unknown metabolite.

Stable Isotope Tracer Studies

Evaluation of Methionine, Homocysteine, and Cystathionine Enrichment

Cells were extracted with ice-cold 1 ml of 'degassed' 3:3:2 acetonitrile/isopropanol/ultra-pure water, the supernatant removed and solvents evaporated to dryness under reduced pressure. To remove membrane lipids and triacylglycerides, dried samples were reconstituted with acetonitrile/water (1:1), decanted and taken to dryness under reduced pressure. Samples were derivatized with methoxyamine hydrochloride in pyridine and subsequently by MTBSTFA (Sigma-Aldrich) and analyzed by gas chromatography mass spectrometry.

An Agilent 7890A gas chromatograph (Santa Clara, CA) was used with a 30 m x 0.25 mm i.d. (internal diameter) x 0.25 μM HP-5 MS Column (Agilent J&W GC Columns). An Agilent 7693 auto-sampler was used to eliminate cross-contamination during GCMS analysis. One microliter (1 μL) of sample was injected at 60˚C (ramped to 250˚C) in splitless mode with a 30 second purge time. The chromatographic gradient consisted of a constant flow of 1 mL/min, ramping the oven temperature from 60˚C to 350˚C over 37 minutes. Mass spectrometry was done using an Agilent 5977A MSD spectrometer, 290˚C transfer line temperature, electron ionization at -70 eV and an ion source temperate of 230˚C. Mass spectra were acquired at 1555 V at m/z 50-600 with 2.7 spectra/sec.

Acquired spectra were converted to netCDF files using vendor (Agilent) software and submitted for non-targeted enrichment analysis using the Non-targeted Fate Detection Software version 1.1 (Hiller et al., 2010). Spectrum of enriched peaks was manually compared against reference spectrum derived authentic standard and from parallel experiments using non-labeled homocysteine.

Enrichment due to presence of deuterium was validated using a secondary independent Mass Isotopomer Distribution (MID) analyzer developed at the West Coast Metabolomics Center. MID calculations were determined using a modified least-squares linear regression matrix as previously modeled; corrected for natural abundance and reduced isotopic probability with increasing deuterium enrichment (Jennings and Matthews, 2005). MID values are reported as fractional proportions (1=100% enriched) that the respective mass isotopologue contributes to the overall abundance of the respective analyte.

Evaluation of SAM and SAH Enrichment

SAM and SAH levels were determined by HILIC-UHPLC-qTOFMS as described above. Enrichment due to presence of deuterium was determined using the MID Analyzer as described above. Spectrum of enriched peaks was manually compared against reference spectrum derived authentic standard and from parallel experiments using non-labeled homocysteine.

CHAPTER 4: Lipid remodeling associated with methionine stress sensitivity in MDA-MB-468 breast cancer cells

Cell lines and growth conditions

See Chapter 3 methods

Preparing Cells for Metabolite Extraction

See Chapter 3 methods

Analysis of the Lipidome

Cell lysates were extracted as previously described (Fahrmann et al., 2015). Briefly, 225µl of chilled methanol containing an internal standard mixture (PE (17:0/17:0); PG (17:0/17:0); PC (17:0/0:0); C17 Spingosine; C17 Ceramide; SM (d18:0/17:0); Palmitic Acid-d3; PC (12:0/13:0); Cholesterol-d7; TG (17:0/17:1/17:0)-d5; DG (12:0/12:0/0:0); DG (18:1/2:0/0:0); MG (17:0/0:0/0:0); PE (17:1/0:0); LPC (17:0); LPE (17:1)) and 750 µL of chilled MTBE (Methyl Tertiary Butyl Ether, Sigma Aldrich) containing the internal standard 22:1 cholesteryl ester was added to cell lysates. Samples were shaken for 6 minutes at 4°C using an orbital mixing chilling/heating plate (Torrey Pines Scientific Instruments) followed by the addition of 188 µl of room temperature distilled water. Samples were vortexed, centrifuged, the upper layer transferred to a new 1.5 mL microcentrifuge tube and subsequently dried to completeness under reduced pressure.

Upon complete dryness, samples were resuspended in methanol:toluene (90:10) with 50 ng/mL CUDA ((12- [[(cyclohexylamino)carbonyl]amino]- dodecanoic acid, Cayman Chemical).

Lipid extracts were subsequently analyzed on an Agilent 1290A Infinity Ultra High Performance Liquid Chromatography system with an Agilent Accurate Mass-6530-QTOF in both positive and negative mode. The column (65°C) was a Waters Acquity UPLC CSH C18 (100 mm length x 2.1 mm internal diameter; 1.7 µM particles) containing a Waters Acquity VanGuard CSH C18 1.7 µM Pre-column. The solvent system included A) 60:40 v/v acetonitrile:water (LCMS grade) containing 10 mM ammonium formate and 0.1% formic acid and B) 90:10 v/v isopropanol:acetonitrile containing 10 mM ammonium formate and 0.1% formic acid. The gradient started from 0 min 15% (B), 0-2 min 30% (B), 2-2.5 min 48% (B), 2.5-11 min 82% (B), 11-11.5 min 99% (B), 11.5-12 min 99% (B), 12-12.1 min 15% (B), and 12.1-15 min 15% (B). The flow rate was 0.6 mL/min and with an injection volume of 1 µL for ESI (+) and 5µL for ESI (-) mode acquisition. ESI capillary voltage was +3.5 kV and -3.5 kV with collision energies of 25 eV and 40 eV for MSMS collection in positive and negative acquisition modes, respectively. Data was collected at a mass range of m/z 60-1700 Da with a spectral acquisition speed of 2 spectra per second. Method blanks and pooled bioreclamation plasma samples were included to serve as additional quality controls.

Data was processed using MZmine 2.10. All peak intensities are representative of peak heights. Peaks were annotated by matching experimental accurate mass MS/MS spectra to MS/MS libraries including Metlin-MSMS, NIST12, and LipidBlast (Kind et al., 2013). Spectral matching was automated using the MSPepSearch tool, and manually curated using The NIST Mass Spectral Search Program Version 2.0g. Metabolite libraries were created, in positive and negative ionization modes, containing all confirmed identified compounds. MZmine's Custom Database Search tool was used to assign annotations based on accurate mass and retention time matching.

CHAPTER 5: Integration of SAM metabolism and cell cycle regulation by mRNA 5' cap methylation

Cell lines and growth conditions

See Chapter 2 methods

Yeast strains and culturing conditions

Yeast strains used in this study are listed in Table 1 below (Reed et al., 1985; Schwer et al., 2000). All strains were grown in standard culture media and standard yeast genetics were used (Guthrie and Fink, 1991). For SAM depletion studies, yeast were grown in yeast medium containing 2% dextrose and 0.4 mM SAM (Santa Cruz Biotechnology, sc-278677) until early log phase. The cells collected were then collected by filtration, washed with yeast medium containing 2% dextrose without SAM, and transferred to a new flask with pre-warmed yeast medium containing 2% dextrose without SAM.

Table 1. Yeast Strains Used in this Study

Strain	Genotype	Reference
PY1 (15Daub)	a *bar1 ura3 ns, ade1 his2 leu2-3, 112 trp1-1*	Reed et al., 1985
PY852	a *bar1 sam1::ZEO sam2::HYG*	source Dr. Peter Kaiser
PY2236 (ABD1 WT)	MATα leu2 ura3 lys2 trp1 his3 Δabd1::LEU2 p358ABD1 (TRP1, CEN)	Schwer et al., 2000
PY2238 (*abd1-8)*	MATα leu2 ura3 lys2 trp1 his3 Δabd1::LEU2 p358*abd1-8* (TRP1, CEN)	Schwer et al., 2000

Polysome profiling

MB468 cells were cultured either three 150 mm x 25 mm plates in Met+ media or six 150 mm x 25 mm containing Met-Hcy+ for 48 hours (media components described in Chapter 2 methods).

Media was replaced with 15 ml of either Met+ or Met-Hcy+ media containing 0.1 mg/ml cycloheximide (CHX) and rocked at room temperature for 3 minutes. Cells were washed once with 1x PBS - 0.1 mg/ml CHX, scraped off the plates in 10 ml 1x PBS – 0.1 mg/ml CHX with a rubber policeman, and transferred to a 15 ml conical tube. Lysates were centrifuged at 1,500 rpm for 5 minutes at 4°C, the PBS aspirated off the pellet, and four pellet volumes of lysis buffer (10 mM Tris pH 7.5, 15 mM $MgCl_2$, 300 mM NaCl, 1% Triton-X, 0.1 mg/ml cycloheximide) were added to the pellet and incubated for 30 minutes on ice. Lysates were transferred to microcentrifuge tubes and centrifuged for 5 minutes at 14, 000 rpm. Supernatants were transferred to new microcentrifuge tubes, flash frozen with liquid nitrogen, and stored at -80°C until further processed.

Sucrose gradients (10 -50%, w/v) were prepared in polyallomer tubes (Beckman Centrifuge Tubes, 331372) on the same day as centrifugation. Polyallomer tubes were first prepared by washing with a 1% SDS, 1 N NaOH solution and rinsing with DEPC treated water four times. Gradients were established using a two chamber gradient maker with using 10% and 50% sucrose solutions (140 mM NaCl, 15 mM MgCl2, 10 mM Tris pH 7.5, 10% sucrose or 50% sucrose, and 0.1 mg/ml CHX). Gradients were balanced and 1 mg of protein ysates were added to each. Samples were centrifuged for 2 hours at 4°C at 31, 000 rpm in a Beckman ultracentrifuge using a SW41 rotor. Centrifuged gradients were chased with a 60% sucrose solution and fractionated into 25 microcentrifuge tubes while being read by a UV read at 260 nm.

Nascent protein labeling

Nascent protein synthesis was determined using the Invitrogen Click-IT system per manufacturer's instructions (Invitrogen, C10276). L-azidohomoalanine (AHA - Invitrogen, C10102) was used to label nascent proteins for 2 hours at 37°C in cells depleted of methionine for the previous hour. Cell lysates were prepared using Click-IT system reagents and protein concentrations were measured by BCA (Pierce, 23227). AHA labeling nascent proteins were labeled with tetramethylrohodamine-alkyne (TAMARA – Invitrogen, T10183). Samples were resolved by 10% SDS-PAGE, imaged using an excitation of 550 nm and emission of 570 nm, and subsequently silver stained for total protein visualization (Pierce, 24612).

RNA extraction

RNA extraction was performed using the Qiagen RNeasy Mini kit (Qiagen, 74104) per manufacturer's instructions for both mammalian and yeast samples. Samples were DNase treated using the in-tube method and purified per manufacturer's instructions.

***In vitro* transcription**

In vitro transcribed RNAs were prepared from MDA-MB-468 human cells and the background yeast strain PY1. cDNA transcripts were prepared from total mRNA samples and actin transcripts were amplified using primers to incorporate 5' T7 promoter and 3' poly $dT_{(40)}$ sequences (see below) using the following thermocycler program: (1) 95°C, 5 minutes; (2 – repeated 5 times) 95°C, 30 seconds; 55°C, 30 seconds; 72°C, 1:17 minutes; (3 – repeated 20 times) 95°C, 30 seconds; 65°C, 30 seconds; 72°C, 1:17 minutes; (4) 72°C, 10 minutes.

- Human 5' T7 promoter actin sequence

- 5’ - AAT TTA ATA CGA CTC ACT ATA GGG CAC CAT GGA TGA TGA TAT CGC C – 3’

- Human 3’ poly $dT_{(40)}$ actin sequence
  - 5’ – $T_{(40)}$ CT AGA AGC ATT TGC GGT GGA – 3’
- Yeast 5’ T7 promoter actin sequence
  - 5’ – AAT TTA ATA CGA CTC ACT ATA GGG ATG GAT TCT GAG GTT GCT GC – 3’
- Yeast 3’ poly $dT_{(40)}$ actin sequence
  - 5’ – $T_{(40)}$ AG AAA CAC TTG TGG TGA ACG – 3’

PCR products were purified (Qiagen Qiaquick PCR purification kit, 28104), in vitro transcribed per manufacturer’s instructions (Thermo Fisher MAXIscript T7 transcription kit, AM1312), and RNA transcripts were purified (Qiagen RNeasy Mini Kit, 74104).

RNA methyl cap IP

7-methylguanosine capped mRNAs were immunopurified with an anti-2, 2, 7-trimethylguanosine antibody (Calbiochem, NA02A). 15 µL of antibody conjugated beads were washed three times with 200 µL binding buffer (0.025% NP-40 in DEPC treated water) and centrifuged at 1,000 rpm for 10 seconds prior to immunopurification. For each sample, 4 ug of purified, DNase treated RNA was combined with 200 µL binding buffer supplemented with RNase inhibitor and half was transferred to a tube with prepared anti-2, 2, 7-trimethylguanosine beads. Samples were incubated at room temperature for 1 hour, nutating. Supernatants were transferred to a new tube and beads were washed three times with 100 µL binding buffer. Samples were eluted twice with 150 µL elution buffer (7 M Urea, 2% SDS, 350 mM NaCl, 10

mM EDTA, 10 mM Tris pH 7.5) by incubating at 65°C for 5 min followed by centrifugation at 1,000 rpm for 10 seconds and transferring the eluate to a new tube. 200 µL elution buffer was added to input and supernatant and all samples were purified by phenol: chloroform pH 4.3, precipitated with glycogen and isopropanol, and ethanol washed prior to resuspension of all pellets in 20 µL DEPC treated water.

Real time PCR

RNAs were reverse transcribed into cDNA using SuperScript II reverse transcriptase (ThermoFisher Scientific, 18064014). cDNAs were amplified for quantitation using the primers listed below and iTaq Universal SYBR green master mix (BioRad, 172-5122).

- Human actin
    - Forward: 5’ - AGG CCA ACC GCG AGA AGA TG – 3’
    - Reverse: 3’ - GCC AGA GGC GTA CAG GGA TA – 3’
- Human actin
    - Forward: 5’ - AGG CCA ACC GCG AGA AGA TG – 3’
    - Reverse: 3’ - GCC AGA GGC GTA CAG GGA TA – 3’
- S. cerevisiae actin:
    - Forward: 5’ - ATT CTG AGG TTG CTG CTT TGG – 3’
    - Reverse: 5’ - TGT CTT GGT CTA CCG ACG ATA G – 3’
- S. cerevisiae snR7 (U5)
    - Forward: 5’ - ACA TCA AGA ACT GTG GGC CTT – 3’
    - Reverse: 5’ - TCT ATG GAG ACA ACA CCC GGA – 3’
- S. cerevisiae CDC6

- Forward: 5’ - TGG ACG AGA TGG ACA GGC TA – 3’
- Reverse: 5’ - TGC GGT AAC AAC CCT CTG TC – 3’

- S. cerevisiae CDC28
  - Forward: 5’ - CAT ACT GCC ACT CAC ACC GT – 3’
  - Reverse: 5’ - AAC GGA ACA CCA AAA GCA CG – 3’

RNAseq

RNA methyl cap immunopurified samples were prepared as described above with some modifications. Prior to immunopurification, 4 ug total mRNA was depleted of ribosomal RNA using the Ribo-Zero Magnetic Gold kit (Illumina, yeast - MRZY1306, human - MRZG126) per manufacturer’s instructions. Eluate was used to combined with 200 µL binding buffer supplemented with RNase inhibitor and half was transferred to a tube with prepared anti-2, 2, 7-trimethylguanosine beads and immunopurification was performed as described above. RNA sequencing libraries were prepared using the TruSeq RNA Sample Preparation Kit (Illumina, RS-122-2001) per manufacturer’s instructions without poly (A) enrichment. RNA sequencing was performed by the UC Irvine High Throughput Facility.

REFERENCES

Aregger, M., Kaskar, A., Varshney, D., Fernandez-Sanchez, M.E., Inesta-Vaquera, F.A., Weidlich, S., and Cowling, V.H. (2016). CDK1-Cyclin B1 Activates RNMT, Coordinating mRNA Cap Methylation with G1 Phase Transcription. Mol. Cell *61*, 734–746.

Ayala, A., Muñoz, M.F., Argüelles, S., Elles, S., Ayala, A., Oz, M.F., and Elles, S. (2014). Lipid Peroxidation: Production, Metabolism, and Signaling Mechanisms of Malondialdehyde and 4-Hydroxy-2-Nonenal. Oxid. Med. Cell. Longev. *2014*, 1–31.

Baldi, P., and Long, A.D. (2001). A Bayesian framework for the analysis of microarray expression data: regularized t -test and statistical inferences of gene changes. Bioinformatics *17*, 509–519.

Banno, Y. (2002). Regulation and possible role of mammalian phospholipase D in cellular functions. J Biochem *131*, 301–306.

Barak, a J., Beckenhauer, H.C., Junnila, M., and Tuma, D.J. (1993). Dietary betaine promotes generation of hepatic S-adenosylmethionine and protects the liver from ethanol-induced fatty infiltration. Alcohol. Clin. Exp. Res. *17*, 552–555.

Basseri, S., and Austin, R.C. (2012). Endoplasmic reticulum stress and lipid metabolism: Mechanisms and therapeutic potential. Biochem. Res. Int. *2012*.

Bentley, D.L. (2005). Rules of engagement: Co-transcriptional recruitment of pre-mRNA processing factors. Curr. Opin. Cell Biol. *17*, 251–256.

Bhaduri, A., and Srere, P.A. (1963). The incorporation of citrate carbon into fatty acids. Biochim. Biophys. Acta 221–230.

Bird, D.K., Yan, L., Vrotsos, K.M., Eliceiri, K.W., Vaughan, E.M., Keely, P.J., White, J.G., and Ramanujam, N. (2005). Metabolic mapping of MCF10A human breast cells via multiphoton fluorescence lifetime imaging of the coenzyme NADH. Cancer Res. *65*, 8766–8773.

Bochnig, P., Reuter, R., Bringmann, P., and Lührmann, R. (1987). A monoclonal antibody against 2,2,7-trimethylguanosine that reacts with intact, class U, small nuclear ribonucleoproteins as well as with 7-methylguanosine-capped RNAs. Eur. J. Biochem. *168*, 461–467.

Booher, K., Lin, D.W., Borrego, S.L., and Kaiser, P. (2012). Downregulation of Cdc6 and pre-replication complexes in response to methionine stress in breast cancer cells. Cell Cycle *11*, 4414–4423.

Borrego, S.L., Fahrmann, J., Datta, R., Stringari, C., Grapov, D., Zeller, M., Chen, Y., Wang, P., Baldi, P., Gratton, E., et al. (2016). Metabolic changes associated with methionine stress sensitivity in MDA-MB-468 breast cancer cells. Cancer Metab. *4*, 9.

Breillout, F., Antoine, E., and Poupon, M.F. (1990). Methionine Dependency of Malignant Tumors: A Possible Approach for Therapy. J. Natl. Cancer Inst. *82*, 1628–1632.

Cao, M.D., Dopkens, M., and Glunde, K. (2012). Glycerophosphodiester phosphodiesterase domain containing 5 (GDPD5) expression correlates with malignant choine phospholipid metabolite profiles in human breast cancer. *25*, 1022–1042.

Cassingena, R., Lafarge-Frayssinet, C., Painchault, V., Estrade, S., Nardeux, P., and Frayssinet, C. (1990). Methionine-independence, tumorigenicity and oncogene expression of rat hepatocarcinoma cells. Biol. Cell *69*, 113–118.

Caudill, M. a, Wang, J.C., Melnyk, S., Pogribny, I.P., Jernigan, S., Collins, M.D., Santos-Guzman, J., Swendseid, M.E., Cogger, E. a, and James, S.J. (2001). Intracellular S-adenosylhomocysteine concentrations predict global DNA hypomethylation in tissues of methyl-deficient cystathionine beta-synthase heterozygous mice. J. Nutr. *131*, 2811–2818.

Cavuoto, P., and Fenech, M.F. (2012). A review of methionine dependency and the role of methionine restriction in cancer growth control and life-span extension. Cancer Treat. Rev. *38*, 726–736.

Chagoyen, M., and Pazos, F. (2011). MBRole: Enrichment analysis of metabolomic data. Bioinformatics *27*, 730–731.

Chang, J.H., Jiao, X., Chiba, K., Oh, C., Martin, C.E., Kiledjian, M., and Tong, L. (2012a). Dxo1 is a new type of eukaryotic enzyme with both decapping and 5′-3′ exoribonuclease activity. Nat. Struct. Mol. Biol. *19*, 1011–1017.

Chang, J.H., Jiao, X., Chiba, K., Oh, C., Martin, C.E., Kiledjian, M., and Tong, L. (2012b). Dxo1 is a new type of eukaryotic enzyme with both decapping and 5′-3′ exoribonuclease activity. Nat. Struct. Mol. Biol. *19*, 1011–1017.

Chello, P.L., and Bertino, J.R. (1973). Dependence of 5 methyltetrahydrofolate utilization by L5178Y murine leukemia cells in vitro on the presence of hydroxycobalamin and transcobalamin II. Cancer Res. *33*, 1898–1904.

Cheng, H., Dufu, K., Lee, C.S., Hsu, J.L., Dias, A., and Reed, R. (2006). Human mRNA Export Machinery Recruited to the 5' End of mRNA. Cell *127*, 1389–1400.

Clarke, R., Daly, L., Robinson, K., Naughten, E., Cahalane, S., Fowler, B., and Graham, I. (1991). Hyperhomocysteinemia: an independent risk factor for vascular disease. N. Engl. J. Med. *324*, 1149–1155.

Coalson, D.W., Mecham, J.O., Stern, P.H., and Hoffman, R.M. (1982). Reduced availability of endogenously synthesized methionine for S-adenosylmethionine formation in methionine-dependent cancer cells. Proc. Natl. Acad. Sci. U. S. A. *79*, 4248–4251.

Cole, M.D., and Cowling, V.H. (2009). Specific regulation of mRNA cap methylation by the c-Myc and E2F1 transcription factors. Oncogene *28*, 1169–1175.

Cowling, V.H., and Cole, M.D. (2007). The Myc transactivation domain promotes global phosphorylation of the RNA polymerase II carboxy-terminal domain independently of direct DNA binding. Mol. Cell. Biol. *27*, 2059–2073.

Datta, R., Alfonso-García, A., Cinco, R., and Gratton, E. (2015). Fluorescence lifetime imaging of endogenous biomarker of oxidative stress. Sci. Rep. *5*, 9848.

Daum, G., Lees, N.D., Bard, M., and Dickson, R. (1998). Biochemistry, cell biology and molecular biology of lipids of Saccharomyces cerevisiae. Yeast *14*, 1471–1510.

DeLong, C.J., Shen, Y.J., Thomas, M.J., and Cui, Z. (1999). Molecular distinction of phosphatidylcholine synthesis between the CDP- choline pathway and phosphatidylethanolamine methylation pathway. J. Biol. Chem. *274*, 29683–29688.

Dominissini, D., Moshitch-Moshkovitz, S., Schwartz, S., Salmon-Divon, M., Ungar, L., Osenberg, S., Cesarkas, K., Jacob-Hirsch, J., Amariglio, N., Kupiec, M., et al. (2012). Topology of the human and mouse m6A RNA methylomes revealed by m6A-seq. Nature *485*, 201–206.

Durando, X., Farges, M., Buc, E., Abrial, C., Petorin-Lesens, C., Gillet, B., Vasson, M.-P., Pezet, D., Chollet, P., and Thivat, E. (2010). Dietary methionine restriction with FOLFOX regimen as first line therapy of metastatic colorectal cancer: a feasibility study. Oncology *78*, 205–209.

Edery, I., and Sonenberg, N. (1985). Cap-dependent RNA splicing in a HeLa nuclear extract. Proc. Natl. Acad. Sci. U. S. A. *82*, 7590–7594.

Epner, D.E., Morrow, S., Wilcox, M., and Houghton, J.L. (2002). Nutrient intake and nutritional indexes in adults with metastatic cancer on a phase I clinical trial of dietary methionine restriction. Nutr. Cancer *42*, 158–166.

Fahrmann, J., Grapov, D., Yang, J., Hammock, B., Fiehn, O., Bell, G.I., and Hara, M. (2015). Systemic alterations in the metabolome of diabetic NOD mice delineate increased oxidative

stress accompanied by reduced inflammation and hypertriglyceremia. Am. J. Physiol. Endocrinol. Metab. *308*, E978–E989.

Fan, T.W. (2012). The Handbook of Metabolomics. *17*.

Fiehn, O., Wohlgemuth, G., and Sholz, M. (2005). Setup and annotation of metabolomic experiments by integrating biological and mass spectrometric metadata. Dils *LNBI 3615*, 224–239.

Fiehn, O., Wohlgemuth, G., Scholz, M., Kind, T., Lee, D.Y., Lu, Y., Moon, S., and Nikolau, B. (2008). Quality control for plant metabolomics: reporting MSI-compliant studies. Plant J. *53*, 691–704.

Finkelstein, J.D., and Martin, J.J. (1984). Methionine Metabolism in Mammals. *259*, 9508–9513.

Finkelstein, J.D., and Mudd, S.H. (1967). Trans-sulfuration in Mammals. 873–880.

Furuichi, Y., LaFiandra, A., and Shatkin, A.J. (1977). 5'-Terminal structure and mRNA stability. Nature *266*, 235–239.

García-Tevijano, E.R., Berasain, C., Rodríguez, J. a, Corrales, F.J., Arias, R., Martín-Duce, a, Caballería, J., Mato, J.M., and Avila, M. a (2001). Hyperhomocysteinemia in liver cirrhosis: mechanisms and role in vascular and hepatic fibrosis. Hypertension *38*, 1217–1221.

Giardiello, F.M., Hamilton, S.R., Hylind, L.M., Yang, V.W., Tamez, P., and Jr, Casero, R.A. (1998). Ornithine decarboxylase and polyamines in familial adenomatous polyposis. Clin. Cancer Res. *4*, 1597–1602.

Gibellini, F., and Smith, T.K. (2010). The Kennedy pathway-De novo synthesis of phosphatidylethanolamine and phosphatidylcholine. IUBMB Life *62*, 414–428.

Glunde, K., Jie, C., and Bhujwalla, Z.M. (2004). Molecular causes of the aberrant choline phospholipid metabolism in breast cancer. Cancer Res. *64*, 4270–4276.

Glunde, K., Bhujwalla, Z.M., and Ronen, S.M. (2011). Choline metabolism in malignant transformation. Nat. Rev. Cancer *11*, 835–848.

Green, M.R., Maniatis, T., and Melton, D. a. (1983). Human Beta-globin pre-mRNA synthesized in vitro is accurately spliced in xenopus oocyte nuclei. Cell *32*, 681–694.

Grzelakowska-sztabert, B., and Balinska, M. (1980). Induction of betaine: homocysteine methyltransferase in some murine cells cultured in vitro. Biochim. Biophys. Acta *632*, 164–172.

Gulsen, M., Yesilova, Z., Bagci, S., Uygun, A., Ozcan, A., Ercin, C.N., Erdil, A., Sanisoglu, S.Y., Cakir, E., Ates, Y., et al. (2005). Elevated plasma homocysteine concentrations as a

predictor of steatohepatitis in patients with non-alcoholic fatty liver disease. J. Gastroenterol. Hepatol. *20*, 1448–1455.

Guthrie, C., and Fink, G.R. (1991). Guide to yeast genetics and molecular biology. Methods Enzymol. *194*.

Halliwell, B., and Chirico, S. (1993). Lipid peroxidation : and significanc & 3 its mechanism ,. Am. J. Clin. Nutr. *57*, 715S – 725S.

Halpern, B.C., Clark, B.R., Hardy, D.N., Halpern, R.M., and Smith, R. a (1974). The effect of replacement of methionine by homocystine on survival of malignant and normal adult mammalian cells in culture. Proc. Natl. Acad. Sci. U. S. A. *71*, 1133–1136.

Hanahan, D., and Weinberg, R.A. (2011a). Hallmarks of cancer: The next generation. Cell *144*, 646–674.

Hanahan, D., and Weinberg, R.A. (2011b). Hallmarks of cancer: the next generation. Cell *144*, 646–674.

Hannun, Y. a., and Obeid, L.M. (2002). The ceramide-centric universe of lipid-mediated cell regulation: Stress encounters of the lipid kind. J. Biol. Chem. *277*, 25847–25850.

Hannun, Y. a., Luberto, C., and Argraves, K.M. (2001). Enzymes of sphingolipid metabolism: From modular to integrative signaling. Biochemistry *40*, 4893–4903.

Hay, N., and Sonenberg, N. (2004). Upstream and downstream of mTOR. Genes Dev. *18*, 1926–1945.

Vander Heiden, M.G., Cantley, L.C., and Thompson, C.B. (2009). Understanding the Warburg effect: the metabolic requirements of cell proliferation. Science *324*, 1029–1033.

Heikal, A.A. (2010). Intracellular coenzymes as natural biomarkers for metabolic activities and mitochondrial anomalies. Biomark. Med. *4*, 241–263.

Hiller, K., Metallo, C.M., Kelleher, J.K., and Stephanopoulos, G. (2010). Nontargeted elucidation of metabolic pathways using stable-isotope tracers and mass spectrometry. Anal. Chem. *82*, 6621–6628.

Hoffman, R.M., and Erbe, R.W. (1976). High in vivo rates of methionine biosynthesis in transformed human and malignant rat cells auxotrophic for methionine. Proc. Natl. Acad. Sci. U. S. A. *73*, 1523–1527.

Hoffman, D.R., Marion, D.W., Cornatzer, W.E., and Duerre, J.A. (1980). S-Adenosylmethionine and S-Adenosylhomocysteine Metabolism in Isolated Rat Liver. J. Biol. Chem. *255*, 10822–10827.

Hoffman, R.M., Jacobsen, S.J., and Erbe, R.W. (1978). Reversion to methionine independence by malignant rat and SV40-transformed human fibroblasts. Biochem. Biophys. Res. Commun. *82*, 228–234.

Hoffman, R.M., Jacobsen, S.J., and Erbe, R.W. (1979). Reversion to methionine independence in simian virus 40-transformed human and malignant rat fibroblasts is associated with altered ploidy and altered properties of transformation. Proc. Natl. Acad. Sci. U. S. A. *76*, 1313–1317.

Hsu, P.P., and Sabatini, D.M. (2008). Cancer cell metabolism: Warburg and beyond. Cell *134*, 703–707.

Hu, X., Washington, S., Verderame, M.F., Demers, L.M., Mauger, D., and Manni, A. (2004). BIological activity of the S-adenosylmethionine decarboxylase inhibitor SAM486A in human breast cancer cells in vitro and in vivo. Int. J. Oncol. *25*, 1831–1838.

Huang, D.W., Sherman, B.T., and Lempicki, R. a. (2009a). Bioinformatics enrichment tools: Paths toward the comprehensive functional analysis of large gene lists. Nucleic Acids Res. *37*, 1–13.

Huang, D.W., Sherman, B.T., and Lempicki, R.A. (2009b). Systematic and integrative anlaysis of large gene lists using DAVID bioinformatics resources. Nautre Protoc. *4*, 44–57.

Izaurralde, E., Lewis, J., McGuigan, C., Jankowska, M., Darzynkiewicz, E., and Mattaj, I.W. (1994). A nuclear cap binding protein complex involved in pre-mRNA splicing. Cell *78*, 657–668.

Jennings, M.E., and Matthews, D.E. (2005). Determination of complex isotopomer patterns in isotopically labeled compounds by mass spectrometry. Anal. Chem. *77*, 6435–6444.

Jiang, L., Schlesinger, F., Davis, C.A., Zhang, Y., Li, R., Salit, M., Gingeras, T.R., and Oliver, B. (2011). Synthetic spike-in standards for RNA-seq experiments. Genome Res. *21*, 1543–1551.

Jiao, X., Chang, J.H., Kilic, T., Tong, L., and Kiledjian, M. (2013). A Mammalian Pre-mRNA 5′ End Capping Quality Control Mechanism and an Unexpected Link of Capping to Pre-mRNA Processing. Mol. Cell *50*, 104–115.

Johnson, C.H., Dejea, C.M., Edler, D., Hoang, L.T., Santidrian, A.F., Felding, B.H., Ivanisevic, J., Cho, K., Wick, E.C., Hechenbleikner, E.M., et al. (2015). Metabolism Links Bacterial Biofilms and Colon Carcinogenesis. Cell Metab. *21*, 891–897.

Kaiser, P., Su, N., Yen, J.L., Ouni, I., and Flick, K. (2006a). The yeast ubiquitin ligase SCFMet30: connecting environmental and intracellular conditions to cell division. Cell Div. *1*, 16.

Kaiser, P., Su, N.-Y., Yen, J.L., Ouni, I., and Flick, K. (2006b). The yeast ubiquitin ligase SCFMet30: connecting environmental and intracellular conditions to cell division. Cell Div. *1*, 16.

Kamely, D., Littlefield, J.W., and Erbe, R.W. (1973). Regulation of 5-methyltetrahydrofolate: homocysteine methyltransferase activity by methionine, vitamin B12, and folate in cultured baby hamster kidney cells. Proc. Natl. Acad. Sci. U. S. A. *70*, 2585–2589.

Kayala, M.A., and Baldi, P. (2012). Cyber-T web server: Differential analysis of high-throughput data. Nucleic Acids Res. *40*, 553–559.

Kind, T., Tolstikov, V., Fiehn, O., and Weiss, R.H. (2007). A comprehensive urinary metabolomic approach for identifying kidney cancer. Anal. Biochem. *363*, 185–195.

Kind, T., Liu, K.-H., Lee, D.Y., DeFelice, B., Meissen, J.K., and Fiehn, O. (2013). LipidBlast in silico tandem mass spectrometry database for lipid identification. Nat. Methods *10*, 755–758.

Kokkinakis, D.M., Liu, X., Chada, S., Ahmed, M.M., Shareef, M.M., Singha, U.K., Yang, S., and Luo, J. (2004). Modulation of gene expression in human central nervous system tumors under methionine deprivation-induced stress. Cancer Res *64*, 7513–7525.

Konarska, M.M., Padgett, R. a., and Sharp, P. a. (1984). Recognition of cap structure in splicing in vitro of mRNA precursors. Cell *38*, 731–736.

Kreis, W., and Goodenow, M. (1978). Methionine requirement and replacement by homocysteine in tissue cultures of selected rodent and human malignant and normal cells. Cancer Res. *38*, 2259–2262.

De la Haba, G., and Cantoni, G.L. (1958). The Enzymatic Synthesis of S-Adenosyl-L-homocysteine and Homocysteine*. Enzyme *234*, 603–608.

Lakowicz, J.R., Szmacinski, H., Nowaczyk, K., and Johnson, M.L. (1992). Fluorescence lifetime imaging of free and protein-bound NADH. Proc. Natl. Acad. Sci. U. S. A. *89*, 1271–1275.

Lee, T.A., Jorgensen, P., Bognar, A.L., Peyraud, C., Thomas, D., and Tyers, M. (2010). Dissection of Combinatorial Control by the Met4 Transcriptional Complex. Mol. Biol. Cell *21*, 456–469.

Lin, S., and Gregory, R.I. (2014). Methyltransferases modulate RNA stability in embryonic stem cells. Nat. Cell Biol. *16*, 129–131.

Lin, D.W., Chung, B.P., and Kaiser, P. (2013). S-adenosylmethionine limitation induces p38 mitogen-activated protein kinase and triggers cell cycle arrest in G1. J. Cell Sci. *127*, 50–59.

Liou, G.-Y., and Storz, P. (2010). Reactive oxygen species in cancer. Free Radic. Res. *44*, 479–496.

Locasale, J.W. (2013). Serine, glycine and one-carbon units: cancer metabolism in full circle. Nat. Rev. Cancer *13*, 572–583.

Ma, X.M., and Blenis, J. (2009). Molecular mechanisms of mTOR-mediated translational control. Nat. Rev. Mol. Cell Biol. *10*, 307–318.

Malanovic, N., Streith, I., Wolinski, H., Rechberger, G., Kohlwein, S.D., and Tehlivets, O. (2008). S-adenosyl-L-homocysteine hydrolase, key enzyme of methylation metabolism, regulates phosphatidylcholine synthesis and triacylglycerol homeostasis in yeast: Implications for homocysteine as a risk factor of atherosclerosis. J. Biol. Chem. *283*, 23989–23999.

Mao, X., Schwer, B., and Shuman, S. (1995). Yeast mRNA cap methyltransferase is a 50-kilodalton protein encoded by an essential gene. Mol. Cell. Biol. *15*, 4167–4174.

Martinez-Una, M., Varela-Rey, M., Cano, A., Fernandez-Ares, L., Beraza, N., Aurrekoetxea, I., Martinez-Arranz, I., Garcia-Rodriguez, J.L., Xabier, B., Mestre, D., et al. (2013). Excess S-adenosylmethionine reroutes phosphatidylethanolamine towards phosphatidylcholine and triglyceride synthesis. Hepatology *58*, 1296–1305.

McCully, K.S. (2009). Chemical pathology of homocysteine. IV. Excitotoxicity, oxidative stress, endothelial dysfunction, and inflammation. Ann. Clin. Lab. Sci. *39*, 219–232.

Mecham, J.O., Rowitch, D., Wallace, C.D., Stern, P.H., and Hoffman, R.M. (1983). The metabolic defect of methionine dependence occurs frequently in human tumor cell lines. Biochem. Biophys. Res. Commun. *117*, 429–434.

Meyer, K.D., Saletore, Y., Zumbo, P., Elemento, O., Mason, C.E., and Jaffrey, S.R. (2012). Comprehensive Analysis of mRNA Methylation Reveals Enrichment in 3′ UTRs and near Stop Codons. Cell *149*, 1635–1646.

Meyer, K.D., Patil, D.P., Zhou, J., Zinoviev, A., Skabkin, M. a., Elemento, O., Pestova, T. V., Qian, S.B., and Jaffrey, S.R. (2015). 5’ UTR m6A Promotes Cap-Independent Translation. Cell *163*, 999–1010.

Moteki, S., and Price, D. (2002). Functional coupling of capping and transcription of mRNA. Mol. Cell *10*, 599–609.

Muthukrishnan, S., Both, G.W., Furuichi, Y., and Shatkin, A.J. (1975). 5’-terminal 7-methylguanosine in eukaryotic mRNA is required for translation. Nature *255*, 33–37.

North, W.G., Gao, G., Jensen, A., Memoli, V. a., and Du, J. (2010a). NMDA receptors are expressed by small-cell lung cancer and are potential targets for effective treatment. Clin. Pharmacol. Adv. Appl. *2*, 31–40.

North, W.G., Gao, G., Memoli, V. a., Pang, R.H., and Lynch, L. (2010b). Breast cancer expresses functional NMDA receptors. Breast Cancer Res. Treat. *122*, 307–314.

Obeid, R., and Herrmann, W. (2009). Homocysteine and lipids: S-Adenosyl methionine as a key intermediate. FEBS Lett. *583*, 1215–1225.

Ohno, M., Sakamoto, H., and Shimura, Y. (1987). Preferential excision of the 5' proximal intron from mRNA precursors with two introns as mediated by the cap structure. Proc. Natl. Acad. Sci. U. S. A. *84*, 5187–5191.

Olszewski, A.J., and S., M.K. (1993). Homocysteine metabolism adn the oxidative modification of proteins and lipids. Free Radic. Biol. Med. *14*, 683–693.

Ouni, I., Flick, K., and Kaiser, P. (2010). A Transcriptional Activator Is Part of an SCF Ubiquitin Ligase to Control Degradation of Its Cofactors. Mol. Cell *40*, 954–964.

Pardee, a B. (1974). A restriction point for control of normal animal cell proliferation. Proc. Natl. Acad. Sci. U. S. A. *71*, 1286–1290.

Pate, K.T., Stringari, C., Sprowl-Tanio, S., Wang, K., TeSlaa, T., Hoverter, N.P., McQuade, M.M., Garner, C., Digman, M.A., Teitell, M.A., et al. (2014). Wnt signaling directs a metabolic program of glycolysis and angiogenesis in colon cancer. EMBO J.

Pegg, a E., Pegg, a E., McCann, P.P., and McCann, P.P. (1982). Polyamine metabolism and function. Am. J. Physiol. *243*, C212–C221.

Reed, S.I., Hadwiger, J. a, and Lörincz, a T. (1985). Protein kinase activity associated with the product of the yeast cell division cycle gene CDC28. Proc. Natl. Acad. Sci. U. S. A. *82*, 4055–4059.

Santos, C.R., and Schulze, A. (2012). Lipid metabolism in cancer. FEBS J. *279*, 2610–2623.

Scholz, M., and Fiehn, O. (2007). Setup X - A public study design database for metabolomic projects. Biocomput. 2007 - Proc. Pacific Symp. *180*, 169–180.

Schroeder, S.C., Zorio, D.A.R., Schwer, B., Shuman, S., and Bentley, D. (2004). A function of yeast mRNA cap methyltransferase, Abd1, in transcription by RNA polymerase II. Mol. Cell *13*, 377–387.

Schwer, B., and Shuman, S. (1996). Conditional inactivation of mRNA capping enzyme affects yeast pre-mRNA splicing in vivo. Rna *2*, 574–583.

Schwer, B., Saha, N., Mao, X., Chen, H.W., and Shuman, S. (2000). Structure-function analysis of yeast mRNA cap methyltransferase and high-copy suppression of conditional mutants by AdoMet synthase and the ubiquitin conjugating enzyme Cdc34p. Genetics *155*, 1561–1576.

Seidenfeld, J., Block, a. L., Komar, K. a., and Naujokas, M.F. (1986). Altered cell cycle phase distributions in cultured human carcinoma cells partially depleted of polyamines by treatment with difluoromethylornithine. Cancer Res. *46*, 47–53.

Shibagaki, Y., Itoh, N., Yamada, H., Nagata, S., and Mizumoto, K. (1992). mRNA capping enzyme. Isolation and characterization of the gene encoding mRNA guanylytransferase subunit from Saccharomyces cerevisiae. J. Biol. Chem. *267*, 9521–9528.

Shyh-Chang, N., Locasale, J.W., Lyssiotis, C.A., Zheng, Y., Teo, R.Y., Ratanasirintrawoot, S., Zhang, J., Onder, T., Unternaehrer, J.J., Zhu, H., et al. (2013). Influence of threonine metabolism on S-adenosylmethionine and histone methylation. Science (80-.). *339*, 222–226.

Sperber, H., Mathieu, J., Wang, Y., Ferreccio, A., Hesson, J., Xu, Z., Fisher, K.A., Devi, A., Detraux, D., Gu, H., et al. (2015). The metabolome regulates the epigenetic landscape during naive to primed human embryonic stem cell transition. Nat. Cell Biol.

Stern, P.H., Mecham, J.O., Wallace, C.D., and Hoffman, R.M. (1983). Reduced free-methionine in methionine-dependent SV40-transformed human fibroblasts synthesizing apparently normal amounts of methionine. J Cell Physiol *117*, 9–14.

Stern, P.H., Wallace, C.D., and Hoffman, R.M. (1984). Altered methionine metabolism occurs in all members of a set of diverse human tumor cell lines. J. Cell. Physiol. *119*, 29–34.

Storch, K.J., Wagner, D. a, Burke, J.F., and Young, V.R. (1990). [1-13C; methyl-2H3]methionine kinetics in humans: methionine conservation and cystine sparing. Am. J. Physiol. *258*, E790–E798.

Stringari, C., Cinquin, A., Cinquin, O., Digman, M. a, Donovan, P.J., and Gratton, E. (2011). Phasor approach to fluorescence lifetime microscopy distinguishes different metabolic states of germ cells in a live tissue. Proc. Natl. Acad. Sci. U. S. A. *108*, 13582–13587.

Stringari, C., Nourse, J.L., Flanagan, L.A., and Gratton, E. (2012a). Phasor fluorescence lifetime microscopy of free and protein-bound NADH reveals neural stem cell differentiation potential. PLoS One *7*, e48014.

Stringari, C., Edwards, R. a., Pate, K.T., Waterman, M.L., Donovan, P.J., and Gratton, E. (2012b). Metabolic trajectory of cellular differentiation in small intestine by Phasor Fluorescence Lifetime Microscopy of NADH. Sci. Rep. *2*.

Sugimura, T., Birnbaum, S.M., Winitz, M., and Greenstein, J.P. (1959). Quantitative nutritional studies with water-soluble, chemically defined diets. VIII. The forced feeding of diets each lacking in one essential amino acid. Arch. Biochem. Biophys. *81*, 448–455.

Sutter, B.M., Wu, X., Laxman, S., and Tu, B.P. (2013a). Methionine Inhibits Autophagy and Promotes Growth by Inducing the SAM-Responsive Methylation of PP2A. Cell *154*, 403–415.

Sutter, B.M., Wu, X., Laxman, S., and Tu, B.P. (2013b). Methionine Inhibits Autophagy and Promotes Growth by Inducing the SAM-Responsive Methylation of PP2A. Cell *154*, 403–415.

Tafesse, F.G., Ternes, P., and Holthuis, J.C.M. (2006). The multigenic sphingomyelin synthase family. J. Biol. Chem. *281*, 29421–29425.

Tang, B., Li, Y.N., and Kruger, W.D. (2000). Defects in methylthioadenosine phosphorylase are associated with but not responsible for methionine-dependent tumor cell growth. Cancer Res. *60*, 5543–5547.

Tehlivets, O., Malanovic, N., Visram, M., Pavkov-Keller, T., and Keller, W. (2013). S-adenosyl-L-homocysteine hydrolase and methylation disorders: Yeast as a model system. Biochim. Biophys. Acta - Mol. Basis Dis. *1832*, 204–215.

Thivat, E., Farges, M.C., Bacin, F., D'Incan, M., Mouret-Reynier, M.A., Cellarier, E., Madelmont, J.C., Vasson, M.P., Chollet, P., and Durando, X. (2009). Phase II trial of the association of a methionine-free diet with cystemustine therapy in melanoma and glioma. Anticancer Res. *29*, 5235–5240.

Tsukamoto, T., Shibagaki, Y., Imajoh-Ohmi, S., Murakoshi, T., Suzuki, M., Nakamura, a, Gotoh, H., and Mizumoto, K. (1997). Isolation and characterization of the yeast mRNA capping enzyme beta subunit gene encoding RNA 5'-triphosphatase, which is essential for cell viability. Biochem. Biophys. Res. Commun. *239*, 116–122.

Turner, M.A., Yang, X., Yin, D., Kuczera, K., Borchardt, R.T., and Howell, P.L. (2000). Structure and Function of S-Adenosylhomocysteine Hydrolase. Cell Biochem. Biophys. *33*, 101–125.

Walker, A.K., Jacobs, R.L., Watts, J.L., Rottiers, V., Jiang, K., Finnegan, D.M., Shioda, T., Hansen, M., Yang, F., Niebergall, L.J., et al. (2011). A conserved SREBP-1/phosphatidylcholine feedback circuit regulates lipogenesis in metazoans. Cell *147*, 840–852.

Warburg, O. (1956). On the Origin of Cancer Cells. Science (80-.). *123*, 309–314.

Watkins, S.M., Zhu, X., and Zeisel, S.H. (2003). Phosphatidylethanolamine-N-methyltransferase activity and dietary choline regulate liver-plasma lipid flux and essential fatty acid metabolism in mice. J. Nutr. *133*, 3386–3391.

Werstuck, G.H., Lentz, S.R., Dayal, S., Hossain, G.S., Sood, S.K., Shi, Y.Y., Zhou, J., Maeda, N., Krisans, S.K., Malinow, M.R., et al. (2001). Homocysteine-induced endoplasmic reticulum stress causes dysregulation of the cholesterol and triglyceride biosynthetic pathways. J. Clin. Invest. *107*, 1263–1273.

Wheeler, G.L., Quinn, K. a, Perrone, G., Dawes, I.W., and Grant, C.M. (2002). Glutathione regulates the expression of gamma-glutamylcysteine synthetase via the Met4 transcription factor. Mol. Microbiol. *46*, 545–556.

Wheeler, G.L., Trotter, E.W., Dawes, I.W., and Grant, C.M. (2003). Coupling of the Transcriptional Regulation of Glutathione Biosynthesis to the Availability of Glutathione and Methionine via the Met4 and Yap1 Transcription Factors. J. Biol. Chem. *278*, 49920–49928.

Wikoff, W.R., Hanash, S., DeFelice, B., Miyamoto, S., Barnett, M., Zhao, Y., Goodman, G., Feng, Z., Gandara, D., Fiehn, O., et al. (2015). Diacetylspermine Is a Novel Prediagnostic Serum Biomarker for Non-Small-Cell Lung Cancer and Has Additive Performance With Pro-Surfactant Protein B. J. Clin. Oncol. 1–8.

Xu, X., Gammon, M.D., Zeisel, S.H., Lee, Y.L., Wetmur, J.G., Teitelbaum, S.L., Bradshaw, P.T., Neugut, A.I., Santella, R.M., and Chen, J. (2008). Choline metabolism and risk of breast cancer in a population-based study. FASEB J. *22*, 2045–2052.

Yamada-Okabe, T., Doi, R., Shimmi, O., Arisawa, M., and Yamada-Okabe, H. (1998). Isolation and characterization of a human cDNA for mRNA 5'-capping enzyme. Nucleic Acids Res. *26*, 1700–1706.

Yen, J.L., Flick, K., Papagiannis, C. V., Mathur, R., Tyrrell, A., Ouni, I., Kaake, R.M., Huang, L., and Kaiser, P. (2012). Signal-induced disassembly of the scf ubiquitin ligase complex by cdc48/p97. Mol. Cell *48*, 288–297.

Yue, Z., Maldonado, E., Pillutla, R., Cho, H., Reinberg, D., and Shatkin, a J. (1997). Mammalian capping enzyme complements mutant Saccharomyces cerevisiae lacking mRNA guanylyltransferase and selectively binds the elongating form of RNA polymerase II. Proc. Natl. Acad. Sci. U. S. A. *94*, 12898–12903.